LBNL-45436

Creep of SiC Hot-Pressed with Al, B, and C

Mark Sixta
(Ph.D. Thesis)

Department of Materials Science and Mineral Engineering
University of California, Berkeley

and

Materials Sciences Division
Ernest Orlando Lawrence Berkeley National Laboratory
University of California
Berkeley, California 94720

March 2000

This work was supported by the Director, Office of Science, Office of Basic Energy Sciences, Materials Sciences Division, of the U.S. Department of Energy under Contract No. DE-AC03-76SF00098.

DISCLAIMER

Creep of SiC Hot-Pressed with Al, B, and C

by

Mark Eldon Sixta

B.S. (University of California, Berkeley) 1994
M.S. (University of California, Berkeley) 1997

A dissertation submitted in partial satisfaction of the

requirements for the degree of

Doctor of Philosophy

in

Engineering: Materials Science and Mineral Engineering

in the

GRADUATE DIVISION

of the

UNIVERSITY OF CALIFORNIA, BERKELEY

Committee in charge:

Professor Lutgard C. De Jonghe, Chair
Professor Robert O. Ritchie
Professor Peter Yu

Spring 2000

Abstract

Creep of SiC Hot-Pressed with Al, B, and C

by

Mark Eldon Sixta

Doctor of Philosophy in Materials Science and Mineral Engineering

University of California, Berkeley

Professor Lutgard C. De Jonghe, Chair

The creep of a high strength, high toughness SiC, sintered with Al, B, and C (ABC-SiC), was investigated. For elevated temperature applications, the time-dependent deformation, creep response, must be fully characterized for candidate materials. The mechanisms responsible for high temperature deformation in ABC-SiC were evaluated. The creep response was compared to materials that have glassy grain boundary phases but do not have interlocked grains.

The creep mechanisms were assessed by calculating the stress exponent and apparent activation energy. For creep tests conducted between 1200-1500°C, 50-200 MPa, the stress exponent, n, was ~ 1. The activation energy for the same temperature and stress range was E_a ~ 225 kJ/mol. This data was utilized in conjunction with microstructural features to determine the operative creep mechanisms. Characterization revealed isolated grains containing dislocations after creep. However, these dislocations were not the controlling creep mechanism, as evidenced by the low stress exponent and lack of dislocation slip and climb. Grain boundary analysis revealed that the boundaries

changed upon exposure at creep temperatures. The initial amorphous grain boundaries exhibited crystalline features after the heat treatments.

The controlling creep mechanism was determined to be grain boundary sliding accommodated by diffusion along the grain boundary interlayer/SiC interface. Parallel mechanisms of solution-precipitation and cavitation were also operative in ABC-SiC. Additionally, the dislocations were likely introduced at regions of grain-to-grain contact where the local stresses were high.

The high temperature strength and long exposure oxidation resistance were assessed. The four-point bend strength of ABC-SiC decreased by a factor of 5, from ~ 515 MPa to 100 MPa, as the temperature was increased from room temperature to 1300°C. However, long heat treatments in Ar improved the high temperature strength at 1300°C from ~100 MPa to almost 400 MPa, while also improving the room temperature strength. Crystallization of the grain boundary phase during annealing limited softening of the grain boundary glass and thus minimized subcritical crack growth. Little degradation was observed for ABC-SiC after oxidation at 1200°C for ~ 9.5 days.

TABLE OF CONTENTS

Acknowledgements

I am extremely grateful to Professor De Jonghe for providing the opportunity to work in his group. I owe him many thanks for supporting this project and providing numerous valuable discussions. Dr. Xiao Feng Zhang provided guidance, discussion, and characterization to help facilitate this work. Many thanks are in order for the numerous high-resolution micrographs that Dr. Zhang provided. Dr. Jim McNaney was instrumental in setting up and providing training on the creep apparatus. Additionally, his discussions on mechanical properties were most valuable.

The friendships and advice from the various members of the De Jonghe research group, both past and present, are much appreciated. I am especially grateful for the friendships with Dr. Mani Gopal, Tim Perham, Qing Yang, Caroline Lee, and Abraham Anapolsky.

My wife, Helen, deserves so much credit for being patient and supportive during this work. Finally, I wish to thank my parents, Eldon and Lynn, who sacrificed to ensure that I always had the best opportunities.

CHAPTER 1: Introduction

1.1 SiC Properties

The physical properties of SiC that make it appealing for high temperature structural applications are: high melting temperature, high elastic modulus, oxidation resistance, creep resistance, and hardness and wear resistance. In addition to the advantageous mechanical properties at elevated temperatures, SiC is desirable because of its low density and low thermal expansion coefficient. The origin of most of these desirable properties is in the highly covalent bonding that occurs between these two group IV elements. Table 1.1 lists some physical properties of a hot-pressed SiC and a commercially available pressureless sintered SiC, Hexoloy SA.

Property	Sintered SiC Hexoloy SA	Hot-Pressed SiC
Density (g/cc)	3.10	3.21
Hardness (km/mm^2)	3100	3100
Flexural Strength (MPa)	460	930
Young's Modulus (GPa)	410	440
Poisson's ratio	0.14	~ 0.17
Coefficient of thermal expansion (x 10^{-6}/°C)	4.02	4.8
Themal conductivity at room temperature (w/m°K)	126	79
Toughness (MPa$\sqrt{m}$)	2.5	not available

Table 1: Physical Properties of SiC.[1]

1.2 Motivation for High Temperature Applications

The dominant driving force for structural ceramics research is the necessity to operate at higher temperatures. Basic thermodynamics elucidates the importance of increasing the operating temperature for energy producing operations. The efficiency of an engine can be improved by increasing the high temperature reservoir, the operating temperature, or decreasing the low temperature reservoir, the environment, as can be seen by Equation 1.1,

$$\eta = \frac{T_2 - T_1}{T_2} \times 100\% \tag{1.1}$$

where η is the efficiency of the process, T_2 is the high temperature reservoir, and T_1 is the low temperature reservoir. Obviously, it is not feasible to alter the temperature of the environment, thus the motivation for increasing the operating temperature of engines.

As the temperature requirement of materials is raised to enhance performance, ceramic materials gain more interest for structural applications. In general, ceramic materials exhibit better thermal stability than metals. Since SiC exhibits high thermal stability, it is a candidate for components in gas turbines, piston engines, and heat exchangers.[2,3] Such applications require load bearing components to be subjected to high temperatures (1200-1500°C) for extended periods of time. Therefore, the creep response is a critical parameter that must be evaluated prior to subjecting a material to a stress at elevated temperatures.

1.3 Toughness in Ceramics

Historically, the materials selected for high temperature applications were metals, and more recently intermetallic materials have been increasingly utilized for high temperature components. These materials systems were implemented in components because they demonstrate high fracture toughness compared to ceramic materials. The toughness of a material, to a first approximation, is its ability to resist crack propagation. A typical nickel-based superalloy like Inconel 718 exhibits a fracture tougheness of ~ 100 MPa$\sqrt{m}$,[4] whereas intermetallic materials like Ti_3Al have a toughness on the order of ~ 30 MPa$\sqrt{m}$.[5] In contrast, the inherent toughness of most ceramics is on the order of ~ 2 MPa$\sqrt{m}$. This is true for all of the most commonly utilized structural ceramics, such as Al_2O_3, Si_3N_4, and SiC.

The low inherent toughness of ceramics can be improved through several processing and composite routes. Composite systems are of considerable interest due to the high flaw tolerance exhibited by many of these systems. The improved toughness of these materials is typically accomplished by adding continuous fibers, whiskers or platelets, or secondary phase particles; the demonstrated toughness for these materials is 30 MPa$\sqrt{m}$, 15 MPa$\sqrt{m}$, and 10 MPa$\sqrt{m}$, respectively.[6] For the examples of fibers and whiskers, the toughness is improved by crack propagation along the interface between the reinforcing phase and the matrix. Subsequent elastic bridging and frictional pullout of the delaminated portions of the fibers/and or whiskers increases the toughness of the material.[7] Platelets have been implemented and have increased the toughness of SiC by greater than a factor of 3 by a crack deflection process.[8] In the ZrO_2 system, a toughness of greater than 20 MPa$\sqrt{m}$ was achieved by incorporating particles of tetragonal ZrO_2,

which transform to a monoclinic phase with the energy of the propagating crack.[9] This results in a 6% volume increase that leaves a compressive region around the crack tip and effectively shields the crack tip from the applied stress.

The difficulties with fibers, whiskers, and platelets is generally in tailoring the interface to be weak enough to provide pullout, without being too weak to provide adequate strength. In the ZrO_2 system the tetragonal to monoclinic phase transformation spontaneously occurs at $T > 625°C$, thus precluding its use in high temperature applications.[6] Therefore, while impressive toughness results were achieved through the aforementioned processing techniques, extensive research continues on monolithic ceramic systems.

In monolithic ceramics the most common method for improving the toughness is by *in-situ* toughening, as has been demonstrated in the silicon nitride system with tremendous success. To achieve a high toughness in these inherently brittle materials, the grains are purposely elongated during processing utilizing a liquid phase. The resultant microstructure exhibits grains covered with a residual glass phase and pockets of glass at multi-grain junctions. Toughness values of greater than 10 MPa$\sqrt{m}$ have been achieved for Si_3N_4 processed in this fashion.[10] The toughness derived from these microstructures is generally attributed to elastic bridging and frictional pullout. The enhanced toughness in *in-situ* toughened ceramics should be contrasted with the toughness in metals where phenomena ahead of the crack tip, like plastic yielding and crack tip blunting, are responsible for the high toughness. The tradeoff for monolithic ceramics is that the glassy phase typically limits the high temperature properties, such as oxidation, creep, and high temperature strength.

1.4 Sintering Additives

As previously mentioned, the physical characteristics of SiC that make it most desirable originate in the covalent bonding. However, the presence of such strong bonding makes densification in these systems extremely difficult without the presence of sintering additives. Densification of SiC has been achieved without the presence of sintering additives by hot-pressing at 2600°C.[11] Sintering additives are added to promote mass transport either in the solid state or by promoting the formation of a liquid phase, which provides higher diffusivities and hence faster densification. Some of the common sintering additives in SiC are B and C, which were used by Prochaska and Scanlan[12] to obtain the first free sintered SiC. The role of B and C is not completely understood, but the C is believed to reduce the native SiO_2 on the surface of the starting powder and the B may alter the surface energy, both processes resulting in enhanced mass transport. While many additives have been employed in SiC, the more common materials are B and C, Al_2O_3, Al metal, Al_2O_3 and Y_2O_3. The common feature of the latter three components is that they promote densification through liquid phase formation.

The sintering additives function in several capacities in these *in-situ* toughened silicon carbides. In addition to promoting densification, they also accelerate the β (cubic) to α (hexagonal) phase transformation and the resultant microstructure has grains with high aspect ratios. Several additives have demonstrated improved resistance to crack growth in the SiC system. These include Al_2O_3[13] and yttrium aluminum garnet (YAG).[14,15,16]

1.5 ABC-SiC

Recent research at Lawrence Berkeley National Laboratory produced a SiC, hot-pressed with Al, B, and C (ABC-SiC), with a maximum toughness of 9.1 MPa$\sqrt{m}$, while exhibiting a strength of 650 MPa.[17] These mechanical properties are among the highest reported for SiC. The increased toughness, compared to a commercial SiC that exhibited a toughness of ~2.5 MPa$\sqrt{m}$, was attributed to various crack bridging processes in the wake of the crack.[18] Both elastic bridging and frictional pullout are contributing to the increased toughness, with the frictional pullout component likely to be the most potent toughening mechanism in ABC-SiC.

The toughening of monolithic SiC (*in-situ* toughened) is derived from a microstructure possessing large, elongated, plate-like grains, that is produced by utilizing the β-SiC (cubic) to α-SiC (hexagonal) phase transformation. This toughening is akin to the mechanisms in the Si_3N_4 system where acicular, needle-like, grains are obtained under appropriate processing conditions. The microstructure of ABC-SiC consists of large grains possessing an aspect ratio of ~5-7. These plate-like grains exhibit some interlocking and are surrounded by a thin amorphous grain boundary phase that permits intergranular fracture.

1.6 SiC Polytypes

SiC exists in numerous crystallographic forms. The common unit in all forms of SiC is a tetrahedron of Si and C atoms. It is easily visualized with C atoms at the corners of the tetrahedron and a Si atom in the middle. The starting powder used to produce ABC-SiC is the cubic phase, 3C, which has an FCC lattice. The 3C denotes the three

layers in the stacking sequence of the {111} close packed planes, which comprise an FCC lattice. The various polytypes of SiC are denoted by the number of layers in the stacking sequence, followed by a letter representative of the crystal lattice. For example, 3C represents the three layers, ...ABCABC..., and the C represents the cubic lattice. By comparison, the hexagonal and rhombohedral structures are denoted by H and R, respectively. While the nature of the alpha phase provides for an unlimited number of polytypes, more than 200 polytypes have been identified for SiC. The polytypes that are the most prominent in ABC-SiC are 3C, 4H, and 6H. The stacking sequence of 4H SiC follows ...ABAC.., and the stacking sequence in 6H SiC is ...ABCACB... . Figure 1-1 shows the stacking sequence and lattice parameters for the most common polytypes of SiC.[19] The non-cubic phases are collectively referred to as α-SiC, while the cubic phase is referred to as β-SiC.

The beta phase is generally considered to be the low temperature phase, as β-SiC transforms to one of the various α-SiC phases upon sufficiently high processing temperatures, typically greater than 1700°C. Upon subsequent cooling, the microstructure does not revert back to the cubic phase, but this is believed to be a kinetically limited process as opposed to be thermodynamically unfavorable. The presence of sintering additives alters the phase transformation by decreasing the temperature necessary for transformation. For SiC sintered with B and C the phase transformation does not occur below 2000°C.[20] The transformation temperature is reduced by utilizing sintering additives such as Al.[17] The microstructure of silicon carbides often exhibits a high degree of stacking faults and microtwinning after processing. This is manifested since the energy difference between the various stacking

sequences is very small. The layers of close-packed planes are the same, just the stacking sequence and hence long range order is different between the various alpha phases.

1.7 High Temperature Material Selection

Current applications utilizing high temperature conditions generally employ Ni-based superalloys. However, these materials are nearing fundamental limits as some applications are operating at greater than 0.85 of the melting temperature, T_m.[5] This is accomplished by implementing design advancements such as air cooling in turbine blades. Since creep, which is time-dependant deformation, becomes pronounced at temperatures greater than 0.5 T_m, materials with high melting temperatures possess an inherent resistance to creep deformation. Thus, the high melting temperature of many ceramic materials make them desirable for high temperature applications.

Evaluation of prospective high temperature structural materials begins with assessment of the basic mechanical properties such as strength and toughness. At high temperatures the most critical parameters, provided adequate strength and toughness are maintained, are environmental stability and creep resistance. For many applications materials will be subjected to an oxygen environment, so oxidation resistance is necessary. However, applications such as gas turbines result in an atmosphere that is rich in combustion gases CO_2 and H_2O.[3] Figure 1-2 shows a plot of the respective oxidation and creep resistance for numerous materials. Since the brittle nature of ceramics is an obvious limitation for these materials, it seems like a metal with a high melting temperature, such as W or Ta, both with $T_m > 3000°C$, would be ideal candidate materials since creep resistance generally scales with increasing T_m. However, evaluation of

Figure 1-2 reveals that W readily oxidizes and this precludes its use at high temperatures. The cost of the precious metals that have a high T_m clearly eliminate them as candidate materials. Many intermetallic systems exhibit toughness vales that are intermediate between metals and ceramics, but certain intermetallics, such as $MoSi_2$, have a toughness on the same order at ceramics. The intermetallic materials, such as Ni_3Al, that exhibit better toughness generally oxidize and/or the creep resistance is low. It is clear from Figure 1-2 that metal alloys will not be sufficient for future applications if the operating temperature is to be raised. Likewise, intermetallic systems suffer the same problems as metals since they do not simultaneously exhibit oxidation and creep resistance.

Oxide ceramics systems, such as Al_2O_3, clearly are more refractory in nature than metals and intermetallics since the oxide is the thermodynamically favorable phase. High thermal stability in oxidizing environments is also obtained from Si-based ceramics such as Si_3N_4 and SiC. These materials are both thermodynamically unstable in oxidizing environments; however, the formation of an SiO_2 passivating scale makes the kinetics of subsequent oxidation, whereby oxygen must diffuse through the SiO_2 scale for additional reactions to occur, extremely slow. The each of the aforementioned ceramics possesses a $T_m > 2000°C$, and thus the creep response is expected to be high.

While the desirability of ceramic materials is obvious based on the refractory nature of these materials, the implementation of components with ceramics historically has been precluded by the exceeding low fracture toughness. However, the development of *in-situ* toughned ceramics such as Si_3N_4 and SiC produced materials with rising R-curve behavior.[21] This increased flaw tolerance, where it becomes more difficult to propagate the crack as it extends, is the result of developing a bridging zone in the wake

of the crack tip. As the crack extends more bridging ligaments are formed and ultimately a plateau toughness is achieved; when the distance between the adjacent crack faces exceeds the dimension of the bridging ligaments no additional toughening is derived by further crack extension. There is a maximum number of elements that can bridge the crack at any given time and this corresponds to the plateau, or steady-state, toughness. Flaw tolerance is a parameter that is critical for a material in any engineering application.

Increased toughness was discussed in section 1.3 and can be achieved by composite materials as well as *in-situ* toughening. However, the limitations on composite materials tend to be cost and stability of the interfaces at high temperatures. *In-situ* toughened ceramics are generally limited by the nature of the residual glass that results from liquid phase sintering routes.

Thus, ABC-SiC, having demonstrated excellent strength and toughness, was selected for high temperature testing. The properties of the microstructure provide a unique opportunity to conduct creep experiments. The elongated, plate-like grains, are similar to the elongated, needle-like grains of many silicon nitrides upon which creep experiments have been performed. Both materials are processed by a liquid phase sintering route, and the resultant microstructure has an intergranular phase between the grains that tends to be amorphous. The unique feature of ABC-SiC is the presence of some interlocking between the grains. The plate-like nature of these grains is anticipated to effectively provide fewer degrees of freedom, thus limiting grain boundary sliding, which is required by many creep mechanisms in ceramics.

1.8 Previous SiC Creep Studies

The first creep studies were performed over 30 years ago on SiC with no sintering additives.[11] Since the first studies, numerous silicon carbides have been tested for creep response: single crystal SiC,[22] CVD-SiC,[23] SiC with B_4C and C additives,[24] and SiC with Al.[25,26,27] No consensus has been reached as to the controlling creep mechanism in SiC. The most commonly identified deformation mode is grain boundary sliding accommodated by a diffusional process. At lower test temperatures the creep mechanism was attributed to grain boundary diffusion, Coble creep,[28] with the contribution of bulk diffusion, Nabarro-Herring creep,[29,30]becoming more pronounced at higher temperatures. For tests conducted at high stresses dislocation glide has been identified as a significant component of creep at high temperatures. Alternative mechanisms of deformation such as Harper-Dorn creep,[31] where creep is governed by dislocation climb under saturated conditions, have been suggested for SiC.[32]

1.9 Objectives

While the additives or processing of the materials for the respective studies are different, the common feature of every SiC tested to date is low fracture toughness. The purpose of this work is to evaluate the high temperature properties, especially the creep behavior, of a SiC exhibiting high strength and high toughness while possessing an amorphous grain boundary phase.

The current work is focused on assessing the creep rates and controlling creep mechanism of SiC, sintered with Al, B, and C. The appropriate constitutive relationship for the time dependant deformation of ABC-SiC will be developed. Understanding the

property/processing/microstructure relationship is a vital component of materials science. Identification of the creep mechanism(s) will allow future materials to be processed to obtain a microstructure that is more conducive to creep resistance. Characterization of these materials is devoted to identifying microstructural features that are critical in the creep process.

Additional high temperature properties, such as high temperature strength, microstructural stability, and long-term oxidation resistance, will be evaluated. The high temperature toughness and fatigue behavior of ABC-SiC was evaluated by Chen et al.[33] Long term thermal anneals are employed to asses microstructural stability and the effects of altering the grain boundaries on creep response and high temperature strength.

1.10 References

[1] M. Srinivasan, "The Silicon Carbide Family of Structural Ceramics," in Structural Ceramics, Edited by J. B. Wachtman, Jr., Treatise on Materials Science and Technology, **29**, 99-159, Academic Press, Inc., (1989).

[2] H. E. Helms and P. J. Haley, " Emerging Ceramic Components for Automotive Gas Turbines," Third International Symposium on Ceramic Materials and components for Engines, Edited by V. J. Tennery, 1347-64, 1988.

[3] N. S. Jacobson, "Corrosion of Silicon-Based Ceramics in Combustion Environments," *J. Am. Ceram. Soc.*, **76** [1] 3-28 (1993).

[4] S. D. Antolovich and J. E. Campbell, in Superalloy Source Book, Edited by M. J. Donachie, Jr., American Society For Metals, 156 (1984).

[5] ASM Specialty Handbook: Heat-Resistant Materials, Edited by J. R. Davis, ASM International, 403 (1997).

[6] A. G. Evans, "Perspective on the Development of High-Toughness Ceramics," *J. Am. Ceram. Soc.*, **73** [2] 187-206 (1990).

[7] A. G. Evans, "High Toughness Ceramics," *Materials Science and Engineering, A*105/106 65-75 (1988).

[8] T.D. Mitchell, L.C. De Jonghe, W.J. MoberlyChan, and R.O. Ritchie, "Silicon Carbide Platelet/Silicon Carbide Composites," *J. Am. Ceram. Soc.*, **78** [1] 97-103 (1995).

[9] R. Garvie, R. Hannink, and R. Pascoe, "Ceramic Steel?," Nature, **258**, 703 (1975).

[10] P. F. Becher, "Microstructural Design of Toughened Ceramics," *J. Am. Ceram. Soc.*, **74**[2] 255-69 (1991).

[11] P. L. Farnsworth and R. L. Coble, "Deformation Behavior of Dense Polycrystalline SiC," *J. Am. Ceram. Soc.*, **49** [5] 264-68 (1966).

[12] S. Prochazka and R. M. Scanlan, "Effect of Boron and Carbon on Sintering of SiC," *J. Am. Ceram. Soc.*, **58**[1-2] 72 (1975).

[13] M.A. Mulla and V.D. Krstic, "Low-Temperature Pressureless Sintering of β-Silicon Carbide with Aluminum Oxide and Yttrium Oxide Additives," *Ceramic Bulletin*, **70** [3] 439-43 (1991).

[14] D. -H. Kim and C. H. Kim, "Toughening Behavior of Silicon Carbide with Additions of Yttria and Alumina," *J. Am. Ceram. Soc.*, **73**[5] 1431-34 (1990).

[15] S. K. Lee and C. H. Kim, "Effects of α-SiC versus β-SiC Starting Powders on Microstructure and Fracture Toughness of SiC Sintered with Al_2O_3-Y_2O_3 Additives," *J. Am. Ceram. Soc.*, **77** [6] 1655-58 (1994).

[16] N. P. Padture, "*In Situ*-Toughened Silicon Carbide," *J. Am. Ceram. Soc.*, **77**[2] 519-23 (1994).

[17] J.J. Cao, W.J. MoberlyChan, L.C. De Jonghe, C.J. Gilbert, and R.O. Ritchie, "*In Situ* Toughened Silicon Carbide with Al-B-C Additions," *J. Am. Ceram. Soc.*, **79**[2] 461-69 (1996).

[18] C.J. Gilbert, J.J. Cao, W.J. MoberlyChan, L.C. De Jonghe, and R.O. Ritchie, "Cyclic fatigue and resistance-curve behavior of an in situ toughened silicon carbide with Al-B-C additions," *Acta Materialia*, **44** [8] 3199-214 (1996).

[19] W. J. Choyke and G. Pensl, "Physical Properties of SiC," *MRS Bulletin*, 25-29 (March 1997).

[20] A. H. Heuer, G. A. Fryburg, L. U. Ogbuji, T. E. Mitchell, and S. Shinozaki, "β→α Transformation in Polycrystalline SiC: I, Microstructural Aspects," *J. Am. Ceram. Soc.*, **61** [9-10] 406-12 (1978).

[21] C. W. Li, D. J. Lee, and S. C. Lui, "R-Curve Behavior and Strength for *In-Situ* Reinforced Silicon Nitrides with Different Microstructures," ," *J. Am. Ceram. Soc.*, **75** [7] 1777-85 (1992).

[22] G. S. Corman, "Creep of 6H α-Silicon Carbide Single Crystals," *J. Am. Ceram. Soc.*, **75** [12] 3421-24 (1992).

[23] C. H. Carter, Jr., R. F. Davis, and J. Bentley, "Kinetics and Mechanisms of High Temperature Creep in Silicon Carbide: II, Chemically Vapor Deposited," *J. Am. Ceram. Soc.*, **67** [11] 732-40 (1984).

[24] J. E. Lane, C.H. Carter, and R. F. Davis, "Kinetics and Mechanisms of High Temperature Creep in Silicon Carbide: III, Sintered α-Silicon Carbide," *J. Am. Ceram. Soc.*, **71** [4] 281-95 (1988).

[25] G. Grathwohl, T. H. Reets, "Creep of Hot-Pressed and Sintered SiC with different Sintering Additives," *Sci. Ceram.*, **11**, 425-31 (1981).

[26] R. Moussa, J. L. Chermant, and F. Osterstock, "Creep and Creep Rupture of HP-SiC Containing an Amorphous Intergranular Phase";pp. 617-630 in Materials Science Research, Vol. 18, Deformation of Ceramic Materials II. Edited by R. E. Tressler and R. C. Bradt. Plenum Press, New York, 1984.

[27] J. L. Chermant and F. Osterstock, "Creep Behavior of SiC-Al Materials," *Mater. Sci. Eng.*, **71** 147-58 (1985).

[28] R.L. Coble, "A Model for Boundary Diffusion Controlled Creep in Polycrystalline Materials," *J. Appl. Phys.*, **34** [6], 1679-82 (1963).

[29] F.R.N. Nabarro, "Deformation of Crystals by the Motion of Single Ions," pp. 75-90 in *Report of a Conference on Strength of Solids* (H.H. Wills Physical Laboratory, University of Bristol, July 7-9, 1947). Physical Society, London, U.K., 1948.

[30] C. Herring, "Diffusional Viscosity of a Polycrystalline Solid," *J. Appl. Phys.*, **21**, 437-45 (1950).

[31] Harper and J. Dorn, "Viscous Creep of Aluminum Near its Melting Temperature," *Acta Metallurgica*, **5** 654-665 (1957).

[32] J. N. Wang, "Newtonian Flow Process in Polycrystalline Silicon Carbides: Diffusional Creep or Harper-Dorn Creep?" *J. Mat. Sci.*, **29** 6139-46 (1994).

[33] D. Chen, C. J. Gilbert, and R. O. Ritchie, submitted to *J. Am. Ceram. Soc.*, 1999.

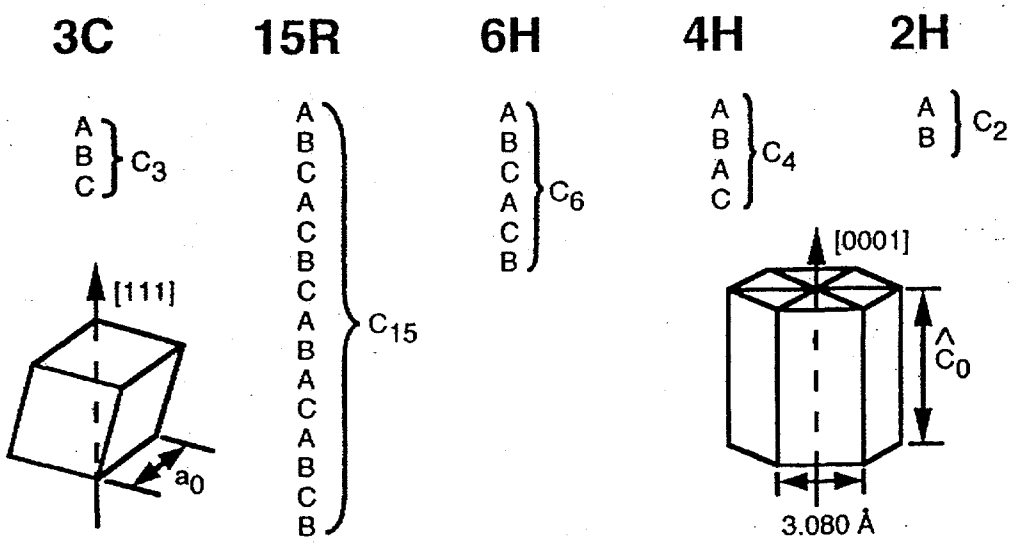

Figure 1-1: Crystal structures and stacking sequence for various SiC polytypes.[1]

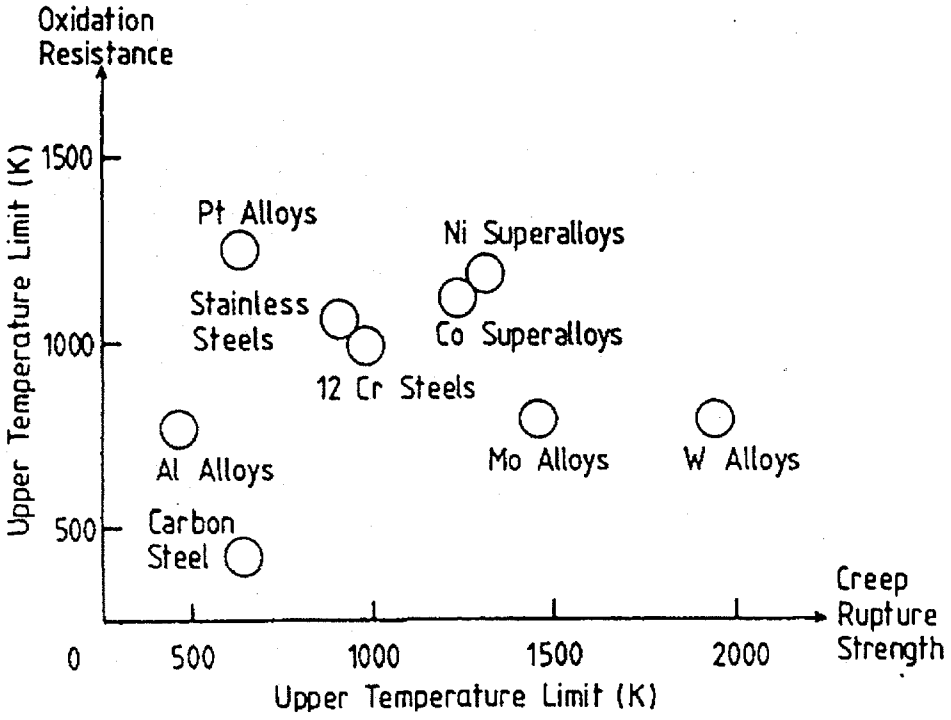

Figure 1-2: Creep and oxidation resistance for numerous materials.
(from Evans and Wilshire, *Introduction to Creep*, 1993)

CHAPTER 2: High Temperature Strength and Long-Term Oxidation

2.1 Introduction

The highly covalent bonding in SiC results from the small electronegativity difference between Si and C atoms. These strong bonds provide a material with desirable mechanical properties, but densification in these materials is difficult without sintering additives. Densification can be achieved without sintering additives by hot-pressing at 2600°C,[1] but this results in a low toughness material. The densification process can be facilitated by adding components that promote the formation of a liquid phase. In the Si_3N_4 system, which also exhibits a high degree of covalent bonding, sintering additives such as Al_2O_3,Y_2O_3, and rare-earth oxides are utilized to enhance densification rates.[2] At the sintering temperature the additives form a eutectic liquid with Si_3N_4. The sintering process can thus proceed by a solution-diffusion-reprecipitation process where the liquid dramatically increases the mass transport in the system. In SiC sintered with Al, B, and C (ABC-SiC), a liquid phase sintering route is also employed, but the mechanism of liquid formation is likely to be different than in Si_3N_4. ABC-SiC is processed by mixing Al metal powder with the SiC powder, B, and C. Thus, at temperatures as low as 660°C a liquid phase is expected to be present because of the melting of Al (details of ABC-SiC processing are provided in Chapter 3).

The sintering additives in both of these materials are effective densification aids, but the liquid tends to remain as glassy phases at the grain boundaries and multi-grain junctions.[3,4] The presence of impurities and amorphous regions degrades the high temperature properties. Strength degradation in silicon nitride is generally attributed to softening of the grain boundary phase.[5] Similarly, the creep rates of ceramics possessing

a glassy grain-boundary phase are degraded when compared to the inherent creep resistance.[6] The presence of impurities, introduced as sintering additives, also reduces the oxidation resistance of silicon nitride and silicon carbide.[7] The impurities tend to migrate to the growing oxide scale and thus diffusion rates are accelerated.

Since the deleterious effects of the grain boundary and secondary phases on the high temperature properties is well documented, several approaches have been developed to improve the high temperature properties without compromising the fracture toughness: (1) crystallization of the grain boundary phase,[8,9] (2) changing the chemistry of the secondary phase,[10] and (3) reducing the amount of sintering additives to minimize the volume of glass present in the final microstructure.[11] The most important parameter governing the high temperature strength is the viscosity of the grain boundary phase. As previously mentioned, the softening of the grain boundary phase is chiefly responsible for reduced flexural strengths at high temperature for ceramics with a glassy phase. By increasing the viscosity of the grain boundary phase, either by crystallization or altering the addtivies to produce a more refractory phase, the high temperature properties can be enhanced.

The differences between several types of grain boundaries must be distinguished for ceramic materials. The grain boundaries discussed thus far are interfaces where the two adjacent grains are clearly separated by a secondary phase. This phase may be crystalline or amorphous. Alternatively, the grain boundaries may be regions where adjacent grains meet with intimate contact being made along the interface. This is a traditional grain boundary, and these boundaries have been studied extensively in metals and semiconductors. Numerous high temperature bend tests have been conducted on

silicon nitrides exhibiting high toughness and grain boundary interlayers.[12] In contrast, the high temperature strengths reported for SiC tend to be for materials with no grain boundary interlayer.[13,14] The absence of a grain boundary phase typically results in very low toughness silicon carbides since the deflection and crack bridging mechanisms necessary for high toughness are absent. Consequently, the resultant fracture mode is predominantly transgranular.

In-situ toughened SiC, which involves intergranular fracture, has been developed using Al_2O_3 and Y_2O_3 sintering additives.[15,16] Liu et al.[17] report the high temperature flexural strength of such an *in-situ* toughened SiC, which possesses a grain boundary interlayer. With the exception of this less than complete work, the high temperature strength of a high toughness silicon carbide has not been reported. ABC-SiC also exhibits amorphous grain boundaries after hot-pressing,[18] but these grain boundary interlayers crystallize upon extended heat treatments.[19] The bend strength of ABC-SiC is evaluated as a function of temperature and annealing. A possible mechanism for the respective flexural strength changes is presented, both as a temperature and annealing are varied.

The high temperature thermal stability of Si-based ceramics is predicated on the ability to form a passivating scale during oxidation. A pure SiO_2 passivating scale provides an excellent diffusion barrier to oxygen. However, incorporation of impurities into the growing layer alters the viscosity of the scale and diffusion rates are accelerated. The viscosity of the silica passiving scale is high dependent on chemisty; thus, the approach of increasing the refractoriness of the glassy phase can also improve the oxidation resistance.

In the current work, creep studies were evaluated in an Ar atmosphere since a tungsten mesh furnace was utilized for the experiments, Chapter 3. The goal of the long term oxidation study is to ensure that excessive oxidation and large compositional changes were not occurring during the creep test. For silicon nitride, altering the composition of the grain boundary phase by oxidation altered the creep response.[20] The aforementioned dependence of the mechanical properties on the composition of the grain boundary phase elucidates the necessity of verifying compositional stability for times scales consistent with the creep tests that were performed.

2.2 Experimental Procedure

2.2.1 Material Processing

Submicron β-SiC powder (H. C. Starck) was ultrasonically wet-mixed with 3 wt% Al, 0.6 wt% B, and 2 wt% C. The slurry was stir dried and sieved through a 200 mesh screen (maximum particle size is ~ 75 μm). The sieved powder was cold pressed and loaded into a graphite die. The die was subsequently placed in a hot-press equipped with graphite heating elements. The samples were hot-pressed at 1900°C, 50 MPa, for 1 hour in flowing Ar. The ~ 4 mm x 38 mm disks were surface ground and polished to a ~ 1 μm finish. The disks were sectioned into beams with approximate dimensions of 3 mm x 3 mm x 3 cm. The edges of the beams were chamfered with a 6 μm diamond wheel to eliminate large surface flaws.

2.2.2 Annealing Experiments

Once creep experiments started, it became obvious that the microstructure, and hence the mechanical properties, were altered during the extended heat treatments of the creep experiments. As some of the first creep experiments were conducted at stresses up to 85 MPa at 1300°C, with negligible creep rates (the strength was expected to be ~ 100 MPa) it became apparent that the strength was changing with time during the test. Therefore, after creep at 85 MPa for 10 days, a bend test was performed at 1300°C and the retained strength was ~ 335 MPa. It is necessary to ensure the stability of the microstructure for creep experiments. Otherwise, unnecessary convolution of the results will occur and make interpretation extremely difficult. Therefore, an annealing procedure was developed to stabilize the microstructure prior to creep experiments. The annealing temperature chosen was 1500°C, and the time was varied from 1 day to 7 days. The annealing was performed in a furnace equipped with graphite heating elements and a flowing Ar atmosphere. The SiC disk was placed inside a graphite sleeve on graphite foil. The surface was ground by ~100 μm to eliminate any surface flaws introduced by thermal etching. The bend strength was evaluated at 1300°C for each of the annealing times to assess when the microstrucuture stabilized. An annealing temperature of 1500°C was selected since this is the highest temperature creep experiments were conducted, and a general rule in ceramic processing is to process at temperatures above the operation, or in this case, test temperature.

2.2.3 Mechanical Tests

Four-point bend tests were performed with a high density graphite bend jig possessing an outer span and inner span of 1 inch and 0.375 inches, respectively. The strength was tested at room temperature and up to 1300°C. A minimum of 8 samples were tested at room temperature and at least 4 samples were tested at high temperature. If the bend strengths were within 5% of each other, additional samples were not tested at high temperature. The four-point bend strength (MOR) was calculated by Equation 2.1,

$$\sigma = \frac{3Pa}{bh^2} \tag{2.1}$$

where P is the fracture load, a is one-half of the difference between the inner and outer span, b is the width of the beam, and h is the beam height.

A Centorr furnace with tungsten mesh heating elements was utilized for the high temperature bend tests. This is the same furnace utilized for the creep experiments and more details of the equipment are provided in Chapter 3. The samples were heated at a rate of 10°C/minute from room temperature to test temperature with a nominal applied load. This heating rate ensured that microcracks were not introduced during heating due to temperature gradients in the material. The samples were held at the test temperature for 15-20 minutes to allow equilibration of the system. The four-point bend tests were performed in displacement control at a cross-head rate of 0.05 mm/minute.

2.2.4 Oxidation Experiment

A long oxidation study was performed at 1200°C for 9.5 days in a Lindberg tube furnace equipped with a mullite tube and SiC heating elements. A notch was placed in the ABC-SiC prior to oxidation to allow fracture of the sample for cross-sectional

evaluation. The sample was placed in an Al_2O_3 crucible and inserted into the furnace. Since the SiC heating elements precluded turning off the furnace without excessive degradation of the heating elements, the samples were introduced at 500°C. The furnace was manually increased to 600, 700, and finally 800°C by hand, with a 30 minute soak at each temperature. Then the controller was set to 1200°C for the oxidation experiment. Since the kinetics are strongly dependent on temperature, and the test ran for better than 9 days, the oxidation during the ramping steps can be considered negligible. The temperature of the furnace was calibrated using a Pt-Pt + 10% Rh thermocouple.

2.2.5 Characterization

The mechanical tests were performed according to section 2.2.3. Samples were evaluated in a scanning electron microscope (SEM) after bend tests at room temperature and high temperature. The fracture surfaces were evaluated to assess the fracture mode. These surfaces were examined with special attention given to determining if intergranular or transgranular fracture was more prevalent. Other features that were explicitly searched for were the presence of any viscous features for samples fractured at high temperature.

Transmission electron microscopy (TEM) was performed on the hot-pressed and annealed ABC-SiC. High resolution TEM (HR-TEM) in conjunction with EDS was performed on the grain boundary phases to ascertain structural and chemical changes during annealing. The details of TEM specimen preparation and evaluation are provided in Chapter 4.

Characterization of the oxidation sample included SEM and energy dispersive spectrometry (EDS). The oxide thickness was evaluated from the cross section samples

detailed above. An additional sample was placed with the oxide surface up to evaluate the chemistry of the oxide. The SEM samples were coated with C to minimize the charging effects of the oxide. Since C is a light element it did not mask chemical features assessed by EDS. The fracture morphology was also evaluated for the oxidation sample since a change is fracture mode is evidence of oxidation induced chemistry changes from the bulk of the sample, as observed in the oxidation of Si_3N_4.[21]

2.3 Results and Discussion

2.3.1 High Temperature Bend Strength of ABC-SiC

Four-point bend tests were performed from room temperature to 1300°C for ABC-SiC, Figure 2-1. The room temperature strength of ~ 515 MPa was reduced by ~ 20% at 800°C, and decreased to ~100 MPa at 1300°C. A reduction in the high temperature strength was observed in numerous studies on Si_3N_4.[4] The strength degradation in these materials was attributed to softening of the amorphous grain boundary phase.[5,8] Strength degradation usually follows creep resistance, hence the materials with the largest drop in high temperature strength are those exhibiting amorphous grain boundaries. The apparent load vs. displacement curve is shown in Figure 2-2 for fracture at 1300°C. The main feature of this curve, which is representative of all tests before and after annealing, is the absence of any plasticity; the curve exhibits very little strain to failure. Plasticity is typically observed in ceramics as the grain boundary layer softens at higher test temperatures.[22] The grain boundary phase in ABC-SiC is also amorphous, Figure 2-3, thus the reduction in strength at high temperatures is not unanticipated.

A fracture surface of ABC-SiC at room temperature is shown in Figure 2-4. To illustrate the nature of the crack path, a crack introduced by a Vickers indent is shown in Figure 2-5. The intergranular nature of the crack path is critical for providing a microstructure with good toughness. Fracture at high temperature did not alter the fracture surface, Figure 2-6. There is no discernable difference between fracture surfaces at room and high temperature. The higher magnification SEM micrograph in Figure 2-7 shows a grain where the triple-junction material was left on the face of a SiC grain. Again, these are the same features as observed at room temperature. For a SiC sintered with yttria and alumina the high temperature fracture surfaces exhibited rounded features from viscous deformation.[17] However, there was no evidence of viscous features on any ABC-SiC fracture surface.

The effect of annealing at 1500°C on the strength at 1300°C is shown in Figure 2-8. Annealing ABC-SiC for 1 day increased the strength from 100 MPa to ~ 200 MPa. The strength tripled to 300 MPa after annealing for 2 days. After a 7 day hold at 1500°C the strength increaed to 385 MPa. Annealing ABC-SiC improved the high temperature strength by almost a factor of 4. Since the 7 day hold yielded the highest strengths, this condition was employed as the standard annealing condition. It should be noted that while the curve in Figure 2-8 did not appear to reach a maximum, this condition is already of such an extended duration that it is impractical for processing a real component. Additional annealing tests at higher temperatures should produce an optimized processing condition that is not so high that the grain boundaries remain amorphous upon cooling, but allows for realistic heat-treatment times. However, optimization of the annealing temperature was not a focus of the current work.

Figure 2-9 shows the variation of strength with temperature for annealed ABC-SiC. The room temperature strength was enhanced from 515 MPa to 685 MPa following the long anneal. The strength decreased with increasing temperature and the retained strength was 385 MPa at 1300°C. The strength decreased less than a factor of 2 for annealed ABC-SiC. In contrast, the strength drops by a factor of 5 for hot-pressed ABC-SiC at the temperature is increased from room temperature to 1300°C.

The strength degradation in ceramics is often attributed to softening of the amorphous grain boundary phase.[5,8] The softening of the grain boundary interlayer permits accelerated grain boundary sliding. Accommodation of grain boundary is achieved by forming cavities. As deformation continues, the cavities grow and new cavities are initiated. Growth and linkage of cavities results in cracks extending from microscopic scales to macroscopic scales. Ultimately, the strength is reduced since the load bearing area is reduced or the size of the flaw is enlarged.[23]

The grain boundary phase crystallized after the long heat treatments, Figure 2-10. The amorphous grain boundaries were ~1-5 nm thick after hot-pressing, with 1 nm thick interlayers being observed with the highest frequency. After heat treatments, the thickness decreased to 1 nm or less, with the majority of the boundaries exhibiting a crystalline nature. However, at the interface between the SiC grains and the grain boundary phase was disordered. In Si_3N_4, crystallization of the grain boundaries was never complete.[24] EDS spectra of the grain boundaries, using a 8 nm probe, revealed an increase in the Al concentration at the grain boundaries after long heat treatments.[19] This phenomenon is described in detail in Chapter 4.

2.3.2 Mechanisms of Strength Change at High Temperature

There are several mechanisms that may be responsible for the changes in strength observed for ABC-SiC: (1) slow crack growth, (2) creep crack growth, (3) toughness changes, (4) crack blunting, and (5) flaw healing. A subtle distinction is often made between slow crack growth and creep crack growth. Both processes are associated with subcritical crack growth, but the former is a function of extension of a preexisting flaw, whereas the latter occurs by the formation of cavities and cracks either by grain boundary sliding or diffusional mechanisms.[4] The net effect of each mechanism is a reduction in the load bearing area; in essence a larger flaw is present and the subsequent strength decreases. These various mechanisms will be addressed in turn in the following sections to evaluate the dominant mechanism for strength changes in ABC-SiC.

2.3.2.1 Slow Crack Growth

Slow crack growth refers to the extension of preexisting flaws upon loading at high temperatures. Several mechanisms are responsible for extension in this situation. Obviously, the applied load provides the driving force for crack extension. Thus, the stress at a preexisting flaw can be relieved by crack extension. Also, stress corrosion crack propagation is present in many materials. Under an applied load, the extension of a flaw is facilitated by the presence of air or oxygen. The chemical attack at the crack tip enhances subcritical crack growth, and thus the effective flaw size increases. The strength and toughness of a material are related by Equation 2.2,

$$K = Y \cdot \sigma \sqrt{\pi \cdot a} \qquad (2.2)$$

where K is the toughness (MPa$\sqrt{m}$), Y is a factor based on the geometry of the flaw, σ is the strength, and a is the crack length. For a case where the toughness does not change as the temperature increases, the strength of a material will decrease as the crack size increases by slow crack growth. The toughness of ABC-SiC changes as the temperature increases, and since the tests were conducted in Ar, this mechanism alone is not responsible for the decrease in strength at high temperature for ABC-SiC. However, it does not preclude slow crack growth from occurring in the current tests.

2.3.2.2 Creep Crack Growth

Creep crack growth can be manifested by several routes. The first is cavity formation by grain boundary sliding, and the second is cavity formation through a diffusional mechanism. Both reduce the effective cross-section and lead to an increased stress and lower strength.

Grain boundary sliding may occur at elevated temperatures as a sample is loaded. In brittle ceramics, triple-point cracks frequently are nucleated by the internal stress as the grain boundaries slide.[23,25] Sliding of the grain boundaries is exacerbated by the presence of an amorphous grain boundary phase. As the temperature is increased, softening of the grain boundary interlayer occurs. Softening refers to a decrease in the viscosity. Since viscosity is a measure of the degree of shearing that can occur, or similarly the resistance to shear, as the viscosity of the grain boundaries decreases grain boundary sliding is enhanced. Since the glass softening temperature will scale with melting temperature, it is desirable to utilize sintering additives that could result in a more refractory grain boundary phase when crystalline.[26]

A second cavity formation mechanism is nucleation and growth of cavities by a diffusional mechanism, as opposed to the triple-point cracking as previously discussed. Formation of these cavities originates in the glassy grain boundary. As the load is increased additional cavities form while existing cracks extend. The cavitation mechanism takes place by the coalescence and growth of the cracks, which is a thermally activated process.[27] This is consistent with the strength degradation increasing for higher temperatures.

Creep crack growth, as a mechanism for subcritical crack growth during bend tests, corresponds to tertiary creep. While various strain rates were not employed in the current tests, increasing the strain rate during strength tests can eliminate creep crack growth.[28] As strain rates decreased, more subcritical crack growth was observed.

2.3.2.3 Effects of Toughness Changes on Bend Strength

Examination of Equation 2.1 shows that the toughness, K, and the strength are directly proportional. For a case where the flaw size is not altered, the toughness and strength should scale together. In other words, if the toughness at high temperature varies from the room temperature value, the strength can be expected to change.

The toughness was evaluated at room temperature and 1300°C, Figure 2-11.[29] The room temperature toughness of ABC-SiC for the current study is 6.2 MPa$\sqrt{m}$. By comparison, the toughness decreased to 4.3 MPa$\sqrt{m}$ at 1300°C. This is an ~ 33% decrease in the toughness at high temperature. Assuming the flaw size does not change, a similar drop in strength would be expected. However, the rapid fracture strength dropped by a factor of 5 compared to the room temperature strength when the temperature was

increased to 1300°C, Figure 2-1. After annealing experiments were performed, 1300°C for 85 hours, the toughness was also evaluated, Figure 2-11.[29] Surprisingly, now the strength of ABC-SiC at 1300°C had recovered by almost a factor of 4, Figure 2-9. Again, this is far more than the ~ 25% increase in the toughness after annealing.

The toughness may be altered by one or more of several mechanisms, which can operate in parallel. The possible mechanisms for changes in toughness at high temperature are: (1) relieving residual stress, (2) changing viscosity of the grain boundary interlayer, (3) changes in the R-curve, and (4) grain boundary softening.

The toughness in ABC-SiC is derived from extensive crack bridging, with the most important component being frictional pullout.[30] The bridging traction is dependent upon the residual stress that results from the difference in the tests temperature and the processing temperature. The bridging traction can be represented by the grain bridging stress function,[30,31]

$$p(u) = \mu \cdot \sigma_n \left(1 - \frac{u}{u_f}\right)^n \tag{2.3}$$

where p(u) is the bridging stress function, μ is the coefficient of friction, σ_n is the normal stress acting on the interface, 2u is the crack opening displacement, and $2u_f$ is the critical crack opening when the bridge fails. The normal stress is manifested by the crystallographic and temperature dependence of the thermal expansion coefficient and elastic modulus. An additional component to the stress may be the thermal expansion mismatch between SiC and the bulk secondary phases such as Al_2O_3 and $Al_8B_4C_7$.[18] The normal stress can be estimated by equation 2.4,[30,32]

$$\sigma_n = -\frac{\Delta(\alpha E) \cdot \Delta T}{2(1-\upsilon^2)} \tag{2.4}$$

where σ_n is the normal stress, α is the thermal expansion coefficient, ΔT is the temperature difference between the test and processing conditions, and ν is the Poisson ratio. Grain to grain variation of stress from thermal mistmatch has been measured for ABC-SiC.[33]

Two critical parameters in Equations 2.3 and 2.4 can be responsible for the changes in toughness. The first is the coefficient of friction, μ, in Equation 2.3. As the temperature is increased the amorphous grain boundaries soften, thus lowering the effective coefficient of friction. Alternatively, the normal stress on the interface is expected to decrease as the bend test temperature rises since ΔT decreases. It is likely that both processes occur in tandem and cause the toughness to decrease at high temperatures.

Another mechanism, which can cause strength changes, is if the toughness is altered by a change in the R-curve shape. The case of toughness decreasing at high temperature is illustrated in Figure 2-13. Fracture instability occurs when the energy balance, Equation 2.5, and tangency conditions, Equation 2.6, are satisfied.[34]

$$G_A = G_R \tag{2.5}$$

$$\frac{\partial G_A}{\partial a} = \frac{\partial G_R}{\partial a} \tag{2.6}$$

G_A and G_R represent the applied driving force and inherent resistance to crack growth (R-curve), respectively. G is related to the toughness, K, through Equation 2.7,

$$G = \frac{K^2}{E} \tag{2.7}$$

where E is the elastic modulus. The blue R-curve in Figure 2-13 is representative of room temperature, and applying the tangency condition for an initial crack size of a_o

provides a toughness of K_{RT}. By comparison, the black R-curve represents the change at high temperature (lower toughness), and applying the tangency condition yields a toughness of K_{HT} at high temperature. Since $K_{HT} < K_{RT}$, this illustrates how the toughness can change for a given flaw size, a_o, by changing the shape of the R-curve.

It is also possible for grain boundary softening to increase toughness at high temperature. If the amorphous grain boundaries soften it is possible to provide an additional bridging traction, which would increase the toughness. However, this event is more plausible in an oxidizing system where viscous ligaments can form to provide the additional traction.[35] The fracture surfaces at high temperature, Figure 2-4, showed no evidence of viscous ligaments as has been observed for other ceramics when grain boundary sliding occurs as a result of softening of the grain boundary interlayer.[36]

Of the possible mechanisms responsible for changes in the toughness, and hence changes in strength, the most plausible mechanisms are changes in the bridging traction as a result of the viscosity of the grain boundary phase changing and a reduction in the residual stress from thermal expansion differences as the temperature increases. The R-curve has not been measured at high temperature, but the former two phenomena are definitely present and may account for the variations in toughness with temperature.

2.3.2.4 Crack Blunting

For the case of crack tip blunting, the strength of a material can be increased by decreasing the stress concentration factor (SCF) at the crack tip. By softening of the grain boundary phase or creep processes, the crack tip may be blunted at high temperatures. For example, the SCF for an elliptical crack is > 3, while the SCF for a

circular crack is 3. Increasing the radius of curvature decreases the SCF. If plastic deformation at the crack tip occurs, either by viscous flow of the grain boundary phase or other creep mechanisms, the SCF can be reduced and thus the strength of a material can be increased at high temperatures.

2.3.2.5 Flaw Healing

As was demonstrated with Equation 2.1, for a constant toughness and strength, varying the crack size will alter the strength. In ceramics, the strength at room temperature is generally governed by the size of the largest flaw, which is on the order of the grain size. As the temperature is increased, if the flaw size is decreased the strength will exhibit a corresponding increase. Healing of flaws may occur by several mechanisms, the most common being additional sintering of the sample and growth of oxides to remove surface defects. Even high density ceramics exhibit residual porosity, and if sintering of a compact occurs at high temperatures the effective flaw size can be reduced. Since surface flaws, which typically are introduced by machining processes, generally dictate the strength of a ceramic, the presence of an oxidizing atmosphere generally enhances the high temperature strength.[37]

2.3.3 Strength Changes Resulting from High Temperature and Annealing

The initial 5 fold decrease in the strength of ABC-SiC as the temperature was raised to 1300°C was likely caused by grain boundary sliding and contaminant cavity formation. The decrease in the toughness also reduced the strength, but this accounts for only a small fraction of the decrease. It appears that the strength of ABC-SiC at room

temperature is governed by flaws, while the high temperature behavior is governed by subcritical crack growth resulting from softening of the grain boundary phase. This is consistent with Si_3N_4 possessing an amorphous grain boundary phase.[26]

After annealing ABC-SiC for 7 days at 1500°C the strength increased almost a factor of 4, Figure 2-9. Since the toughness only increased by ~ 25 %, after an anneal at 1300°C for more than 3 days, it is difficult to image a toughness increase alone could be responsible for the improved high temperature strength after annealing. Even if the R-curve was altered or the grain bridging stress was increased by increasing the viscosity of the grain boundary during annealing, a four-fold increase in the toughness would not be expected by employing an anneal of 1500°C for 7 days. Crystallization of the grain boundary phase with the heat treatment, Figure 2-10, increases the viscosity of the grain boundary. An increase in viscosity will minimize the grain boundary sliding and reduce subcritical crack growth. Therefore, during the extended hold at 1500°C flaw healing and changes in the grain boundary phase properties can account for the dramatic improvement in high temperature strength after annealing. One concern with crystallizing the grain boundaries is a reduction in the room temperature strength, as demonstrated in Si_3N_4,[38] However, the room temperature strength also increases for ABC-SiC.

2.3.4 Long Oxidation Experiment

The main purpose of the long oxidation study was to assess microstructural stability of ABC-SiC in an oxidizing environment since the creep studies were performed in Ar. Large compositional changes were observed for Si_3N_4 with Al_2O_3

after oxidation at 1200°C for ~ 400 hours.[39] Cross-section samples revealed a light-colored border as a result of long heat treatments in oxygen and Ar. In some samples this region extended from the surface to 1 mm into the bulk of the specimen. Since such drastic chemical changes will alter the creep behavior,[20] ABC-SiC was evaluated after exposure to similar conditions. The sample oxidized at 1200°C for 9.5 days is shown in Figure 2-14. The oxide that developed was ~ 2 μm thick. The parabolic kinetics observed for ABC-SiC, Figure 2-15, shows that the growing SiO_2 scale passivates the surface and the rate of oxidation continually decreases.

Of critical importance is the absence of any compositional or morphology contrast in the cross-section of the oxide, Figure 2-14. In the aforementioned Si_3N_4, a white region revealed the variation of the composition that resulted from the heat treatments. No regions of this nature were observed in ABC-SiC after oxidation at 1200°C for 9.5 days. Special attention was given to comparing the area just below the oxide and in the center of the sample. In addition to no chemically induced contrast changes, there was no evidence of the fracture mode changing as a result of oxidation. The predominantly intergranular fracture mode is the same as that observed after fracture of ABC-SiC. Since the fracture path is dependent on the strength of the glass/SiC grain bonding, and hence the glass chemistry, this further supports minimal chemistry changes in ABC-SiC in oxidizing environments. This test result does not prove that at higher temperatures large compositional changes will not occur, but for the temperatures employed is suggests that the creep behavior of ABC-SiC tested in Ar might well be extended to oxidizing atmospheres without introducing a large error.

Oxidation of SiC typically proceeds according to the reaction shown in Equation 2.8, and schematically in Figure 2-16.

$$SiC(s) + \frac{3}{2}O_2(g) = SiO_2(s) + CO(g) \qquad (2.8)$$

The fundamental steps in the oxidation process are: (1) transport of oxygen to the surface of the oxide, (2) diffusion of oxygen to the SiC/SiO_2 interface, (3) chemical reaction, (4) diffusion of CO(g) from interface to oxide surface, and (5) diffusion of gas away from surface. The oxidation reaction was observed to take place at the SiC/SiO_2 interface, thus Si and C diffusion are not fundamental steps in the oxidation reaction.[40] The presence of bubbles in the oxide, as observed with other silicon carbides[41,42] and ABC-SiC[43] at higher oxidation temperatures, were not observed along the entire interface of the cross-section sample.

EDS spectra collected from a polished sample prior to oxidation is compared to the spectra obtained from the oxidized sample, Figure 2-17. An Al enrichment in the oxide, compared to the Al content of ABC-SiC, was observed. Also present were Na impurities in the SiO_2 scale. Contamination of Na is documented to reduce the oxidation resistance of Si-based ceramics by reducing the viscosity of the oxide, hence accelerating mass transport through the protective scale.[44] The presence of Na and Al together is expected since Al has a valence of +3 and Si has a valence of +4. Therefore, incorporation of Al_2O_3 tetrahedra into the growing oxide requires the addition of a positive charge to maintain charge neutrality. Evaluation of the Na_2O-SiO_2-Al_2O_3 phase diagram reveals that the melting temperature of SiO_2 is lowered by these impurities. Since the melting temperature is lowered by impurities, the viscosity will exhibit a

similar decreased when impurities are present. The relationship between viscosity, η, and diffusivity, D, is given by the Stokes-Einstein equation,

$$D = \frac{k_B T}{4\pi R \eta} \tag{2.9}$$

where k_B is Boltzmann's constant, R is the effective molecular radius of the spheres, and T is the temperature. From Equation 2.9, the role of impurities on oxidation is clear. Incorporation of impurities that reduce the viscosity enhances mass transport through the protective oxide scale. A common effect of impurities, typically introduced as sintering additives, is to reduce the oxidation resistance of SiC.[45]

2.3.5 Role of Impurties and Temperature on the Viscosity of Glass

Since the viscosity of glass is a critical parameter in the high temperature strength, creep response, and oxidation, it is valuable to discuss the role of impurities and temperature on the viscosity of glass and the mechanism responsible for the changes. Whether the silica passivating scale or the grain boundary glass is being addressed, understanding how the viscosity changes with chemisty, temperature, and strain rate is of paramount importance in understanding the high temperature behavior of a ceramic like ABC-SiC that contains an amorphous grain boundary phase.

The oxides of Si-based ceramics and the grain boundaries in hot-pressed ABC-SiC tend to be amorphous. The grain boundary phase in ABC-SiC has been identified as an aluminosilicate, Chapter 5, but the following principles on the variation of the structure of silica still holds for the grain boundary phase. Glasses can be viewed as a three-dimensional network or array that lack long range order and symmetry. For the current system, the network is composed of silicon and oxygen tetrahedra. Following the

hypothesis of Zachariasen,[46] the oxygen tetrahedra will share corners and not edges or faces. Also, each polyhedra must share at least three corners. Figure 2-18 shows a schematic representation of a crystalline and amorphous form of silica. Incorporation of impurities can have dramatic effects on the silica structure and properties. Vitreous (amorphous) silica has a much more open structure than the crystalline form. Figure 2-19 shows the effect of adding impurities to the structure. In the presence of impurities fewer bonds between tetrahedra are present and this causes the reduction in viscosity. The network is effectively broken down, and shearing of the glass becomes easier when impurities are incorporated into silica. The viscosity of pure SiO_2 is extremely high to very high temperatures, which accounts for the excellent passivating qualities of silica, but the incorporation of impurities, even is low quantities, can have profound effects on the viscosity, Figure 2-20. Addition of only 10% drops the viscosity by 5 orders of magnitude. Similarly, increasing temperature shows a strong decrease in viscosity, Figure 2-21.

Crystallization of SiO_2, or devitrification, can also alter the high temperature properties. Since the viscosity of pure silica is so high, the presence of impurities enhances crystallization by increasing the mobility, and hence increasing the ability to rearrange the network into a crystalline form.[47] The open structure of amorphous silica allows a higher solubility of impurities than the crystalline form. Consequently, as crystallization proceeds is can be expected that impurities will be expelled ahead of the crystallization front, as with solidification processes. The resultant crystalline phase is anticipated to be higher purity as a result of crystallization. It follows that the viscosity of a crystalline oxide or grain boundary phase will be greater than the amorphous state.

Again, examination of the Stokes-Einstein relation, Equation 2.9, shows that the diffusivity of the SiO_2 is lowered by crystallization. For air atmospheres, this would slow the kinetics of the oxidation reaction by reducing the amount of oxygen that diffuses through the passivating scale.

Pertinent to the creep study, the altered diffusion rates will have an effect if grain boundary diffusion or solution-precipitation mechanisms are operative, in addition to the aforementioned grain boundary sliding mechanisms. Details of the creep mechanisms, and the effects of crystallization on creep rates, are provided in Chapter 3.

As shown in previous oxidation studies,[43] the growing oxide of ABC-SiC starts out amorphous, but a thin layers of crystalline oxide is observed at the SiC/SiO_2 interface. This suggests that while the early stages of oxidation are accelerated by the presence of impurities the crystalline silica that subsequently forms provides excellent oxidation reistance. Since an oxide of only ~ 2 μm was observed for ABC-SiC after better than 9 days, it further supports the notion that the sintering additives decrease the oxidation resistance but do not result in a dramatic reduction in material stability in oxidizing environments. Additional evidence for this assertion comes from the long oxidation studies performed by Becher, where the initial oxidation rates of SiC containing impurities is enhanced, but long oxidation resulted in approximately the same oxide thickness independent of sintering additives.[48]

2.4 Conclusions

For ABC-SiC, a 5 fold decrease in the flexure strength was observed as the temperature was raised from room temperature to 1300°C. This reduction in strength is attributed to a subcritical crack growth, most likely by cavity formation and coalescence introduced by grain boundary sliding, and a decrease in the toughness at higher temperatures. The toughness only played a minimal role in altering the strength. Softening of the grain boundary phase is responsible for the enhanced grain boundary sliding at higher temperatures.

Annealing ABC-SiC at 1500°C for 7 days increased the strength, both at room temperature and up to 1300°C. The room temperature strength improved by ~ 20% and the strength at 1300°C increased by a factor of 4 after annealing ABC-SiC. The improved strength is likely caused by flaw healing and increasing the viscosity of the grain boundary phase, thus minimizing subcritical crack growth.

Oxidation of ABC-SiC performed at 1200°C for 9.5 days revealed that this materials exhibits good oxidation resistance, even for prolonged exposures. This should be contrasted with some silicon nitrides, which exhibit large compositional changes in oxidizing environments. Since only minimal compositional changes occur during oxidation, and these are confined to the surface region, the creep response of ABC-SiC is not anticipated to be dramatically different in oxidizing and inert atmospheres for the temperature utilized in the current experiments.

2.5 References

[1] P. L. Farnsworth and R. L. Coble, "Deformation Behavior of Dense Polycrystalline SiC," *J. Am. Ceram. Soc.*, **49** [5] 264-68 (1966).

[2] C. Greskovich and J. H. Rosolowski, "Sintering of Covalent Solids," *J. Am. Ceram. Soc.*, **59** [7-8] 336-43 (1976).

[3] D. R. Clarke and G. Thomas, "Grain boundary Phases in a Hot-Pressed MgO Fluxed Silicon Nitride," *J. Am. Ceram. Soc.*, **60** [11-12] 491-95 (1977).

[4] M. K. Ferber and M. G. Jenkins, "Evaluation of the Strength and Creep Fatigue Behavior of Hot Isostatically Pressed Silicon Nitride," *J. Am. Ceram. Soc.*, **75** [9] 2453-62 (1992).

[5] D. E. Lloyd; pp. 165-72 in Special Ceramics 4. Edited by P. Popper. British Ceramics Research Association, Stoke-on-Trent, 1968.

[6] R. F. Davis and C. H. Carter, Jr., "A Review of Creep in Silicon Nitride and Silicon Carbide," in Advanced Ceramics, Edited by S. Saito, 95-125 (1988).

[7] S.C. Singhal and F.F. Lange, "Effect of Alumina Content on the Oxidation of Hot-Pressed Silicon Carbide," *J. Am. Ceram. Soc.*, **58** [9-10] 433-35 (1975).

[8] A. Tsuge, K. Nishida, and M. Komatsu, "Effect of Crystallizing the Grain-Boundary Glass Phase on the High-Temperature Strength of Hot-Pressed Si_3N_4 Containing Y_2O_3," *J. Am. Ceram. Soc.*, **58** [7-8] 323-26 (1975).

[9] D. R. Clarke, F. F. Lange, and G. D. Schnittgrund, "Strengthening of a Sintered Silicon Nitride by a Post-Fabrication Heat Treatments," *J. Am. Ceram. Soc.*, **65** [4] C-51-C-53 (1982).

[10] S. M. Wiederhorn, B. A. Fields, B. J. Hockey, "Fracture of Silicon Nitride and Silicon Carbide at Elevated Temperatures," *Materials Science & Engineering A* (Structural Materials: Properties, Microstructure and Processing), **A176** [1-2] 51-60 (1994).

[11] H. Park, H.-E. Kim, and K. Niihara, "Microstructural Evolution and Mechanical Properties of Si_3N_4 with Yb_2O_3 as a Sintering Additive," *J. Am. Ceram. Soc.*, **80** [3] 750-56 (1997).

[12] M. K. Cinibulk, G. Thomas, and S. M. Johnson, "Strength and Creep Behavior of Rare-Earth Dislicate-Silicon Nitride Ceramics," *J. Am. Ceram. Soc.*, **75** [8] 2050-55 (1992).

[13] T. Kinoshita, S. Munekawa, and S.-I. Tanaka, "Effect of Grain boundary Segregation on High-Temperature Strength of Hot-Pressed Silicon Carbide," *Acta Mater.*, **45** [2] 801-09 (1997).

[14] R. K. Govila, "High Temperature Uniaxial Tensile Stress Rupture Strength of Sintered Alpha SiC," *J. Mater. Sci.*, **18**, 1967-76 (1983).

[15] D. -H. Kim and C. H. Kim, "Toughening Behavior of Silicon Carbide with Additions of Yttria and Alumina," *J. Am. Ceram. Soc.*, **73**[5] 1431-34 (1990).

[16] N. P. Pature and B. R. Lawn, "Toughness Properties of a Silicon Carbide with an In Situ Induced Heterogeneous Grain Structure," *J. Am. Ceram. Soc.*, **77** [10] 2518-22 (1994).

[17] D. -M. Liu, Z. -C. Jou, B. -W. Lin, and C. -T. Fu, "Microstructure and High-Temperature Strength of Pressureless-Sintered Silicon Carbide," *J. Mater. Sci. Lett.*, **14**, 1327-28 (1995).

[18] J.J. Cao, W.J. MoberlyChan, L.C. De Jonghe, C.J. Gilbert, and R.O. Ritchie, "*In Situ* Toughened Silicon Carbide with Al-B-C Additions," *J. Am. Ceram. Soc.*, **79** [2] 461-69 (1996).

[19] X.F. Zhang, M.E. Sixta, and L.C. De Jonghe, "The Evolution of Grain Boundaries in SiC," submitted to *J. Am. Ceram. Soc.*, 1999.

[20] F. F. Lange, B. I. Davis, and D. R. Clarke, "Compressive Creep of Si_3N_4/MgO Alloys, Part 3: Effects of Oxidation Induced Compositional Change," *J. Mater. Sci.*, **15**, 616-18 (1980).

[21] D.R. Clarke and F.F. Lange, "Oxidation of Si_3N_4 Alloys: Relations to Phase Equilibria in the System Si_3N_4-SiO_2-MgO," *J. Am. Ceram. Soc.*,**63** [9-10] 586-93 (1980).

[22] D. -S. Cheong, K. -T. Hwang, and C. -S. Kim, "High-Temperature Strength and Microstructural Analysis in Si_3N_4/20-vol%-SiC Nanocomposites," *J. Am. Ceram. Soc.*, **82** [4] 981-86 (1999).

[23] R. L. Tsai and R. Raj, "The Role of Grain-Boundary Sliding in Fracture of Hot-Pressed Si_3N_4 at High Temperatures," *J. Am. Ceram. Soc.*,**63** [9-10] 513-17 (1980).

[24] S. M. Wiederhorn, B. J. Hockey, D. C. Cranmer, and R. Yeckley, "Transient Creep Behaviour of Hot Isostatically Pressed Silicon Nitride," *J. Mat. Sci.*, **28** [2] 445-53 (1993).

[25] T. Vasilos and E. M. Passmore, "Effect of Microstructure on Deformation of Ceramics," pp. 406-40 in *Ceramic Microstructures.* Edited by R. M. Fulrath and J. A. Pask. Wiley, New York, 1968.

[26] Z. -K. Huang, A. Rosenflanz, and I. -W. Chen, "Pressureless Sintering of Si_3N_4 Ceramic Using AlN and Rare-Earth Oxides," *J. Am. Ceram. Soc.*, **80** [5] 1256-62 (1997).

[27] J. L. Chermant and F. Osterstock, "Creep Hehaviour of SiC-Al Materials," M*aterials Science and Engineering*, **71** 147-57 (1985).

[28] I. Tanaka, K. Igashira, H. -J. Kleebe, and M. Ruhle, "High-Temperature Strength of Fluorine-Doped Silicon Nitride," *J. Am. Ceram. Soc.*, **77** [1] 275-77 (1994).

[29] D. Chen, C. J. Gilbert, and R. O. Ritchie, submitted to *J. Am. Ceram. Soc.*, 1999

[30] C. J. Gilbert, J. J. Cao, W. J. MoberlyChan, L. C. De Jonghe, and R. O. Ritchie, "Cyclic Fatigue and Resistance-Curve Behavior of an *In-Situ* Toughened Silicon Carbide with Al-B-C Additions," *Acta Metall. Mater.*, **44** [8] 3199-214 (1996).

[31] R. M. L. Foote, Y. -W. Mai, and B. Cotterell, *J. Mech. Phys. Solids*, **34** 593 (1986).

[32] J. D. Eshelby, *Proc. R. Soc. Lond.*, **A241** 376 (1957).

[33] C. J. Gilbert, J. W. Auger, III, and R. O. Ritchie, "Raman Spectroscopy Measurements of Internal Residual Stresses in Polycrystalline Silicon Carbide," Submitted to *J. Am. Ceram. Soc.*, 1998.

[34] B. Lawn, *Fracture of Brittle Solids*, 2nd ed. Cambridge University Press, New York (1993).

[35] J. M. McNaney, C. J. Gilbert, R.O. Ritchie, "Effect of viscous grain bridging on cyclic fatigue-crack growth in monolithic ceramics at elevated temperatures." *Acta Materialia*, **47** [9] 2809-19 (1999).

[36] H. Peterlik and K. Kromp, "Viscoelastic Effects in Testing of an Al_2O_3 Ceramic Containing a Glassy Phase," ," *J. Mater. Sci.*, **28** [16] 4341-6 (1993).

[37] F. F. Lange,"Healing of Surface Cracks in SiC by Oxidation," *J. Am. Ceram. Soc.*, **53** [5] 290 (1970).

[38] T. Nishimura, M. Mitomo, and H. Suematsu, "High Temperature Strength of Silicon Nitride Ceramics with Ytterbium Silicon Oxynitride," *J. Mater. Res.*, **12** [1] 203-09 (1997).

[39] M. M. Chadwick and D. S. Wilkinson, "Microstructural Evolution in Annealed and Crept Silicon Nitride," *J. Am. Ceram. Soc.*, **76** [2] 376-84 (1993).

[40] J.A. Costello and R.E. Tressler, "Oxidation Kinetics of Hot-Pressed and Sintered α-SiC," *J. Am. Ceram. Soc.*, **64** [6] 327-31 (1981).

[41] D.M. Mieskowski, T. E. Mitchell, and A.H Heuer, "Bubble Formation in Oxide Scales on SiC," *J. Am. Ceram. Soc.*, **67** [1] C-17-C-18 (1984).

[42] K.L. Luthra, "Some New Perspectives on Oxidation of Silicon Carbide and Silicon Nitride," *J. Am. Ceram. Soc.*, **74** [5] 1095-1103 (1991).

[43] M. E. Sixta, 'The Oxidation Behavior of SiC Sintered with Al-B-C and Improved Oxidation Resistance via Heat Treatments," M.S. Thesis, University of California, Berkeley, (1997).

[44] E.J. Opila,"Influence of Alumina Reaction Tube Impurities on the Oxidation of Chemically-Vapor-Deposited Silicon Carbide," *J. Am. Ceram. Soc.*,**78** [4] 1107-10 (1995).

[45] J.W. Fergus and W.L. Worrell, "Effect of Carbon and Boron on the High-Temperature Oxidation of Silicon Carbide," *J. Am. Ceram. Soc.*, **78** [7] 1961-64 (1995).

[46] W.H. Zachariasen, *J. Am. Ceram. Soc.*, **54**, 3841 (1932).

[47] J.A. Costello and R.E. Tressler, "Oxidation Kinetics of Silicon Carbide Crystals and Ceramics: I, in Dry Oxygen," *J. Am. Ceram. Soc.*,**69**[9] 674-81 (1986).

[48] P. F. Becher, "Strength Retention in SiC Ceramics After Long-Term Oxidation," *J. Am. Ceram. Soc.*, **66** [8] C-120-1 (1983).

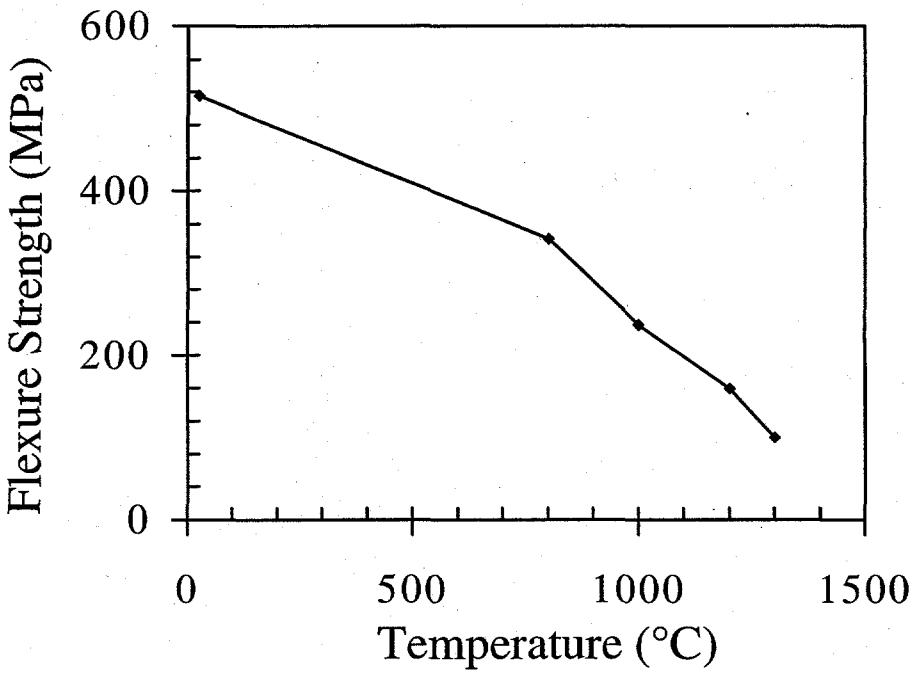

Figure 2-1: High temperature strength of ABC-SiC.

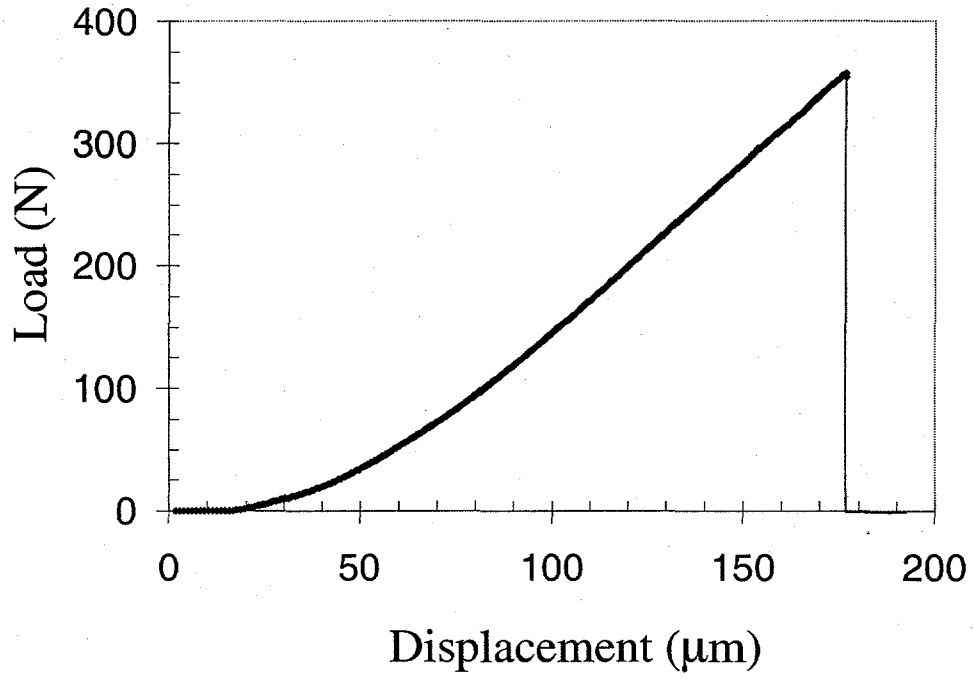

Figure 2-2: Apparent load vs. displacement curve for ABC-SiC fractured at 1300°C. Despite a decrease in the strength at high temperature, no plasticity was observed from these curves.

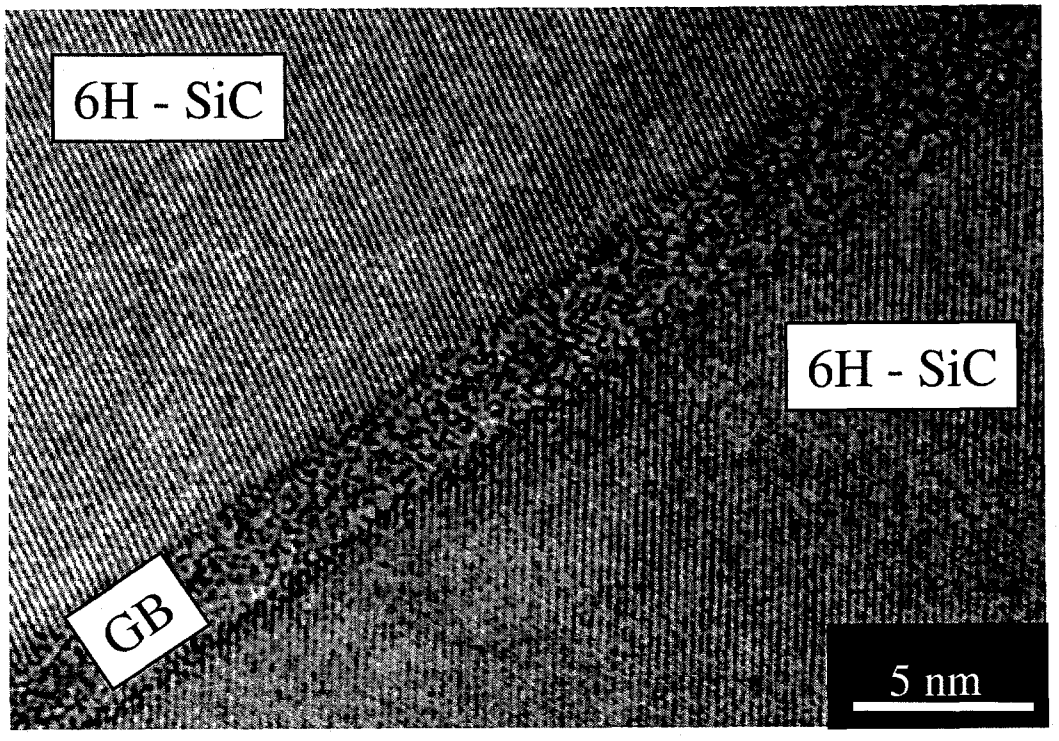

Figure 2-3: Atomic resolution TEM micrograph of a grain boundary in ABC-SiC prior to creep. This boundary is thicker than most of the interlayers. Most grain boundaries are ~ 1 nm thick. Courtesy of Dr. X. F. Zhang.

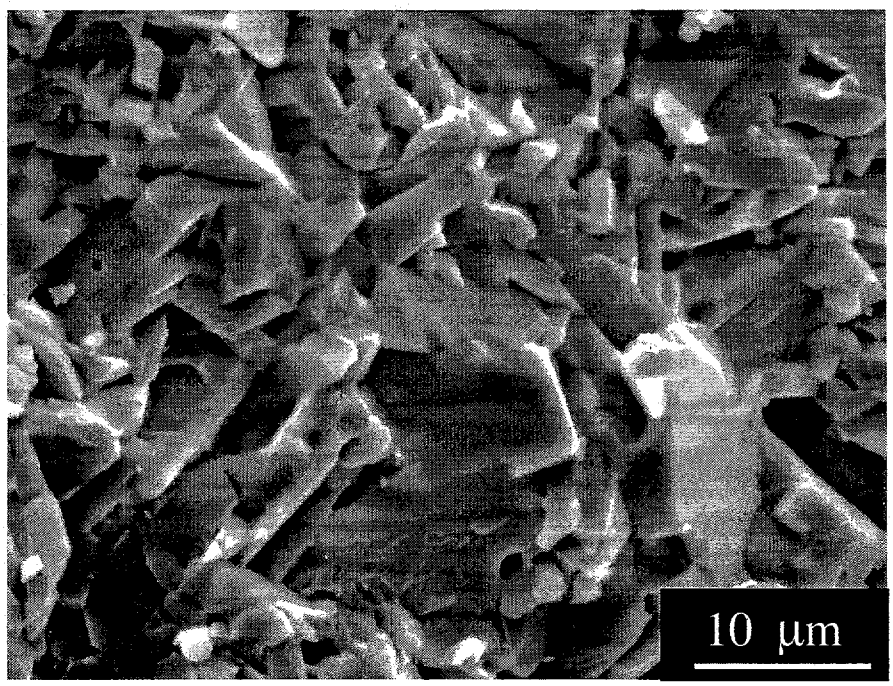

Figure 2-4: SEM micrograph of room temperature fracture surface of ABC-SiC.

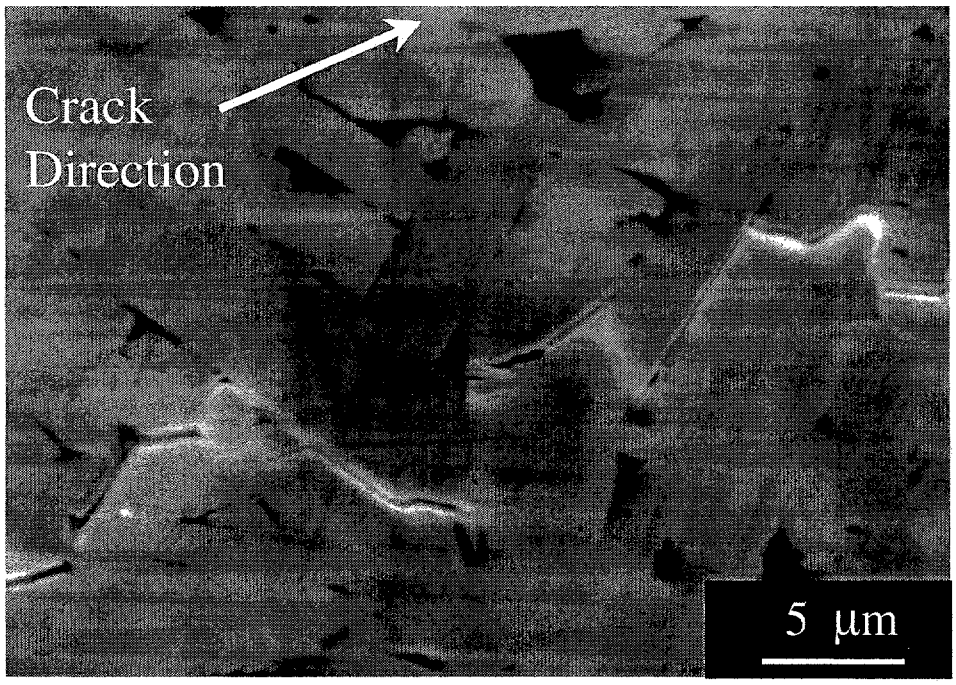

Figure 2-5: SEM micrograph of crack path from a Vickers indent on a polished ABC-SiC surface.

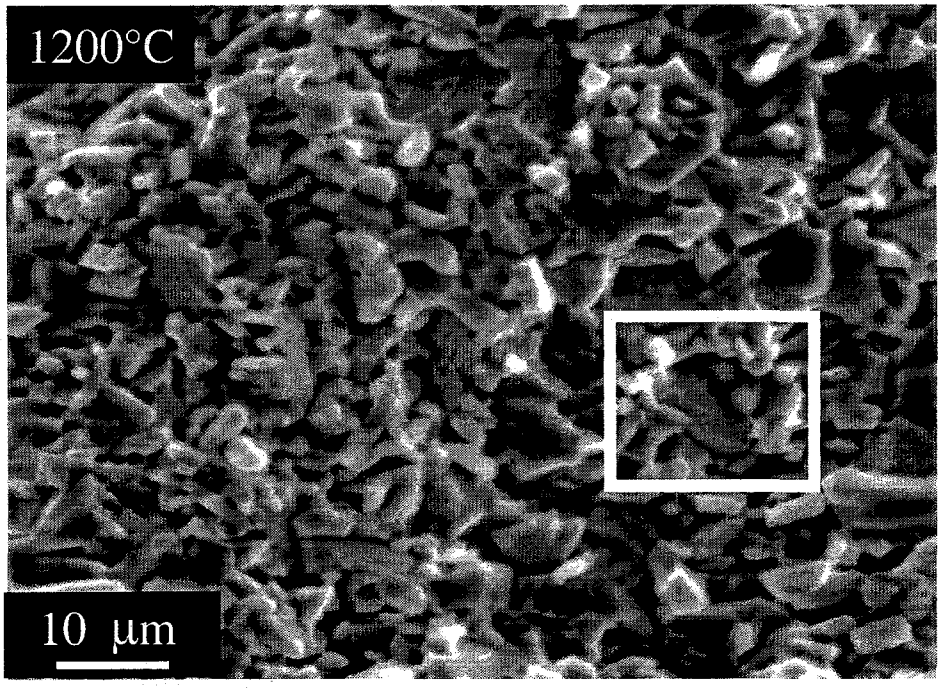

Figure 2-6: Low magnification SEM micrograph of fracture surface at 1200°C.

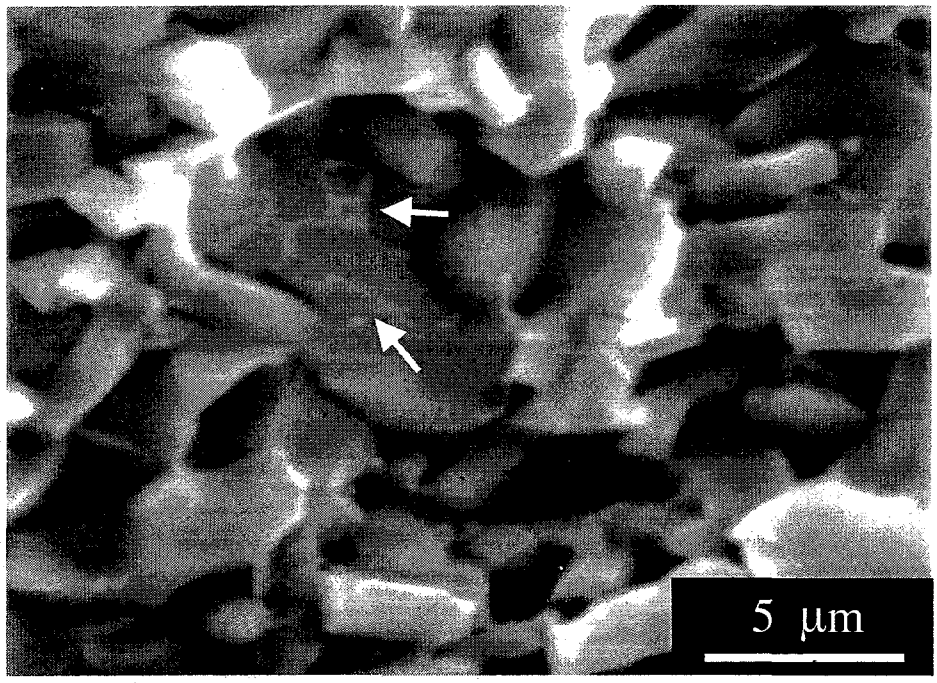

Figure 2-7: High magnification SEM micrograph of of fracture surface at 1200°C from the region denoted by the box in Figure 2-5. The presence of triple point material left on the surface of a SiC grain is shown by the arrows.

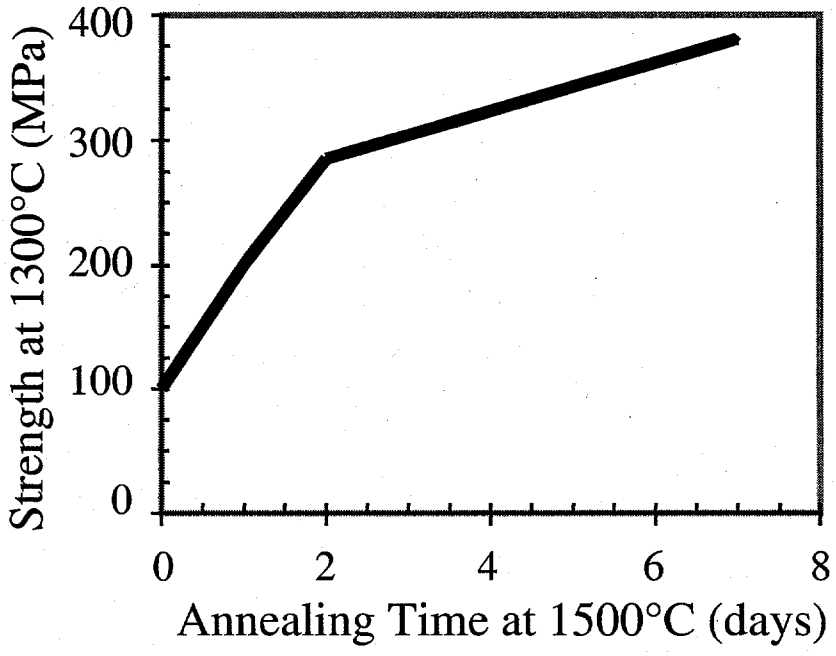

Figure 2-8: Bend strength at 1300°C as a function of annealing time at 1500°C.

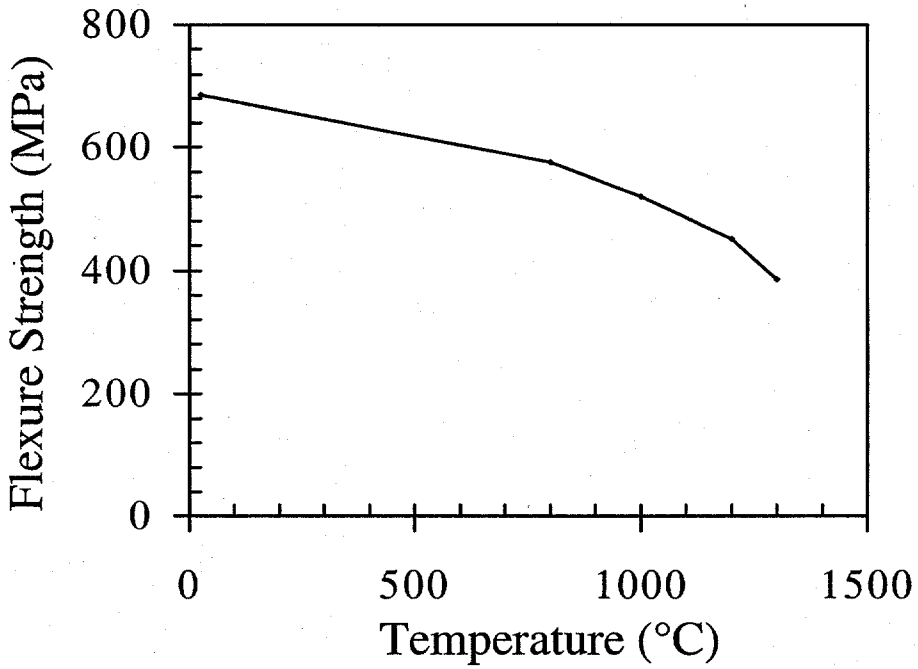

Figure 2-9: Bend strength as a function of temperature for ABC-SiC after annealing at 1500°C for 7 days.

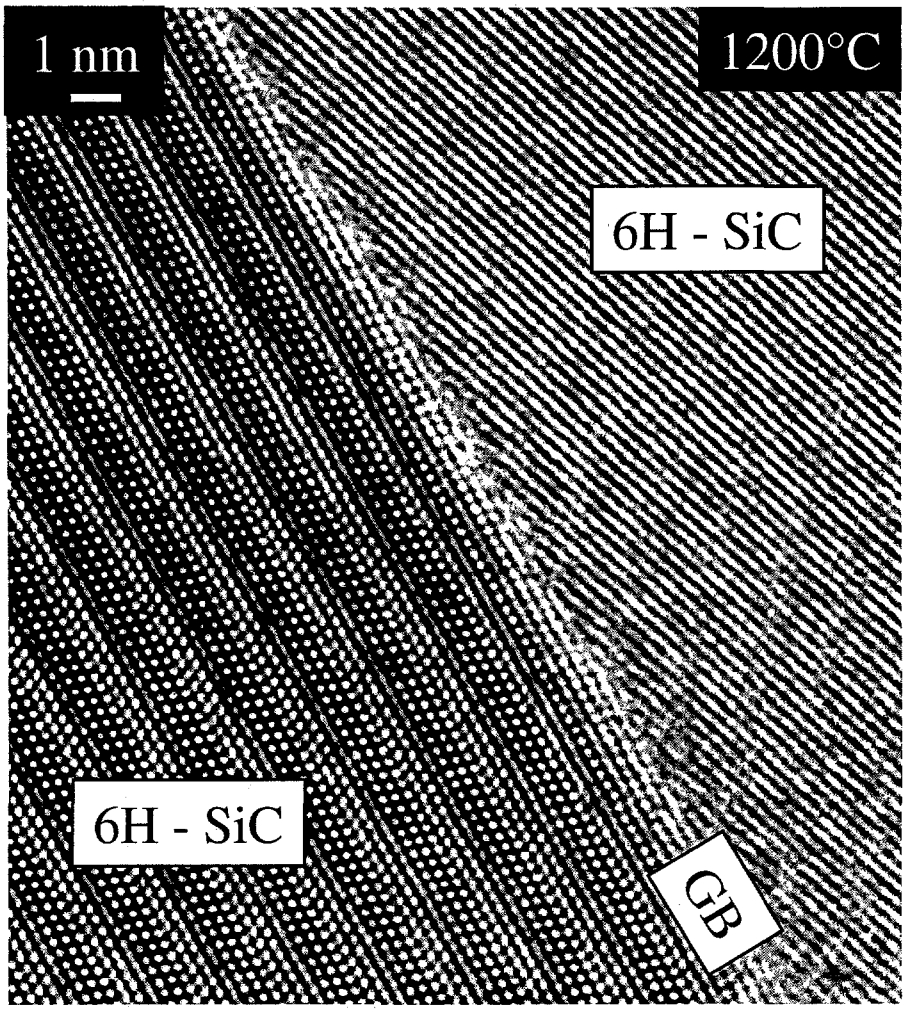

Figure 2-10: Atomic resolution TEM micrograph of the grain boundary after crystallization due to a heat treatment. No discernible amorphous layer is detected after annealing. Courtesy of Dr. X. F. Zhang.

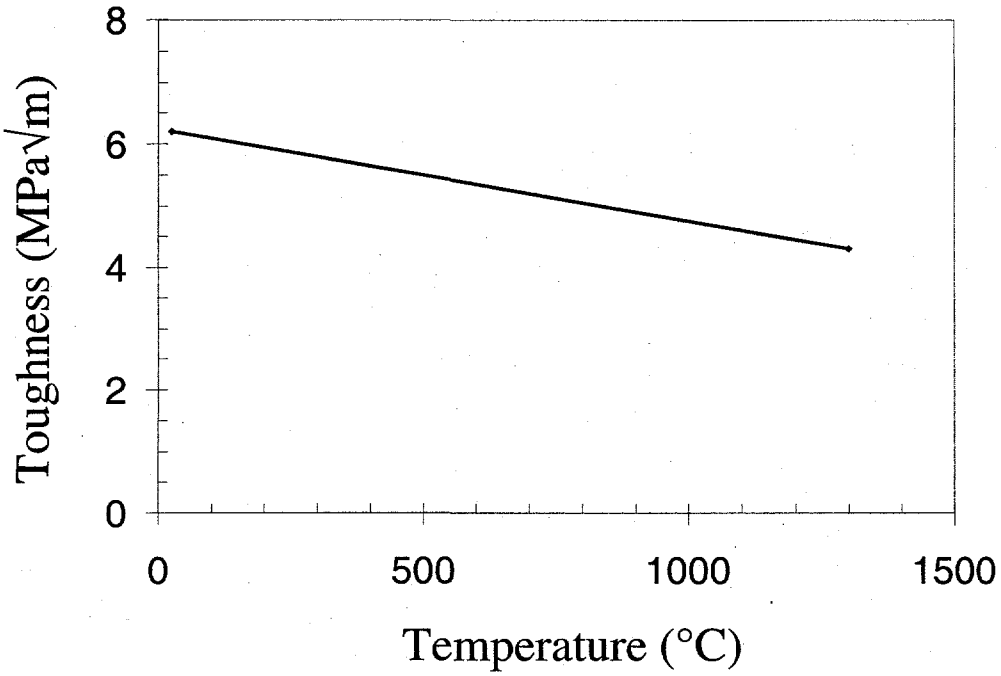

Figure 2-11: The variation in toughness at elevated temperature. This data is courtesy of Dr. Da Chen and Dr. R. O. Ritchie.

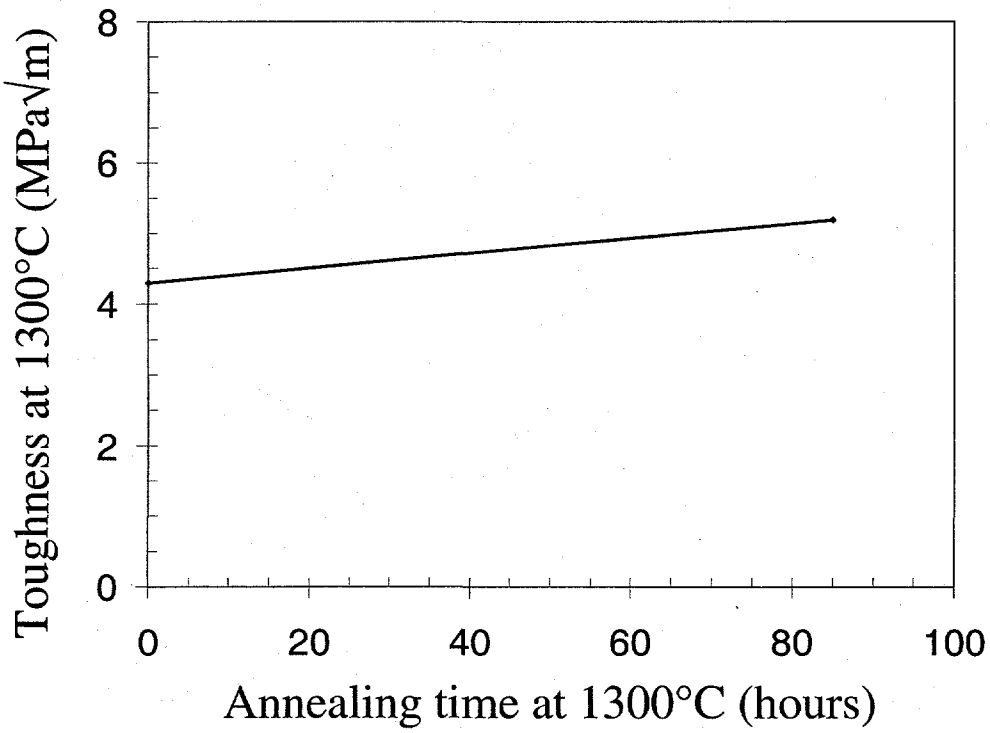

Figure 2-12: The toughness at 1300°C as a function of annealing time at 1300 °C. This data is courtesy of Dr. Da Chen and Dr. R. O. Ritchie.

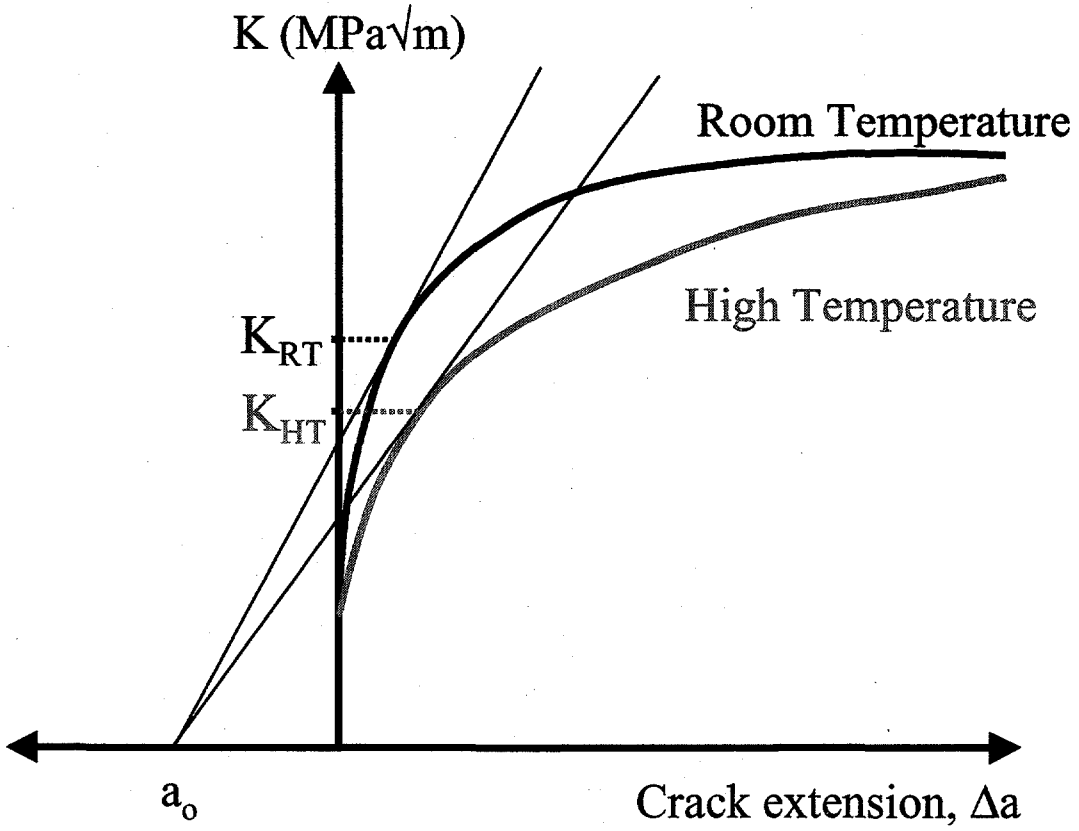

Figure 2-13: Schematic R-curve demonstrating how the toughness can change if the shape of the R-curve is altered. The case demonstrated is for a decrease in toughness at high temperature. For an initial crack size, a_o, the tangency condition shows that the toughness is higher at room temperature than high temperature, $K_{RT} > K_{HT}$. Conversely, if the a steeper R-curve is generated at high temperature then an increase in toughness would be expected.

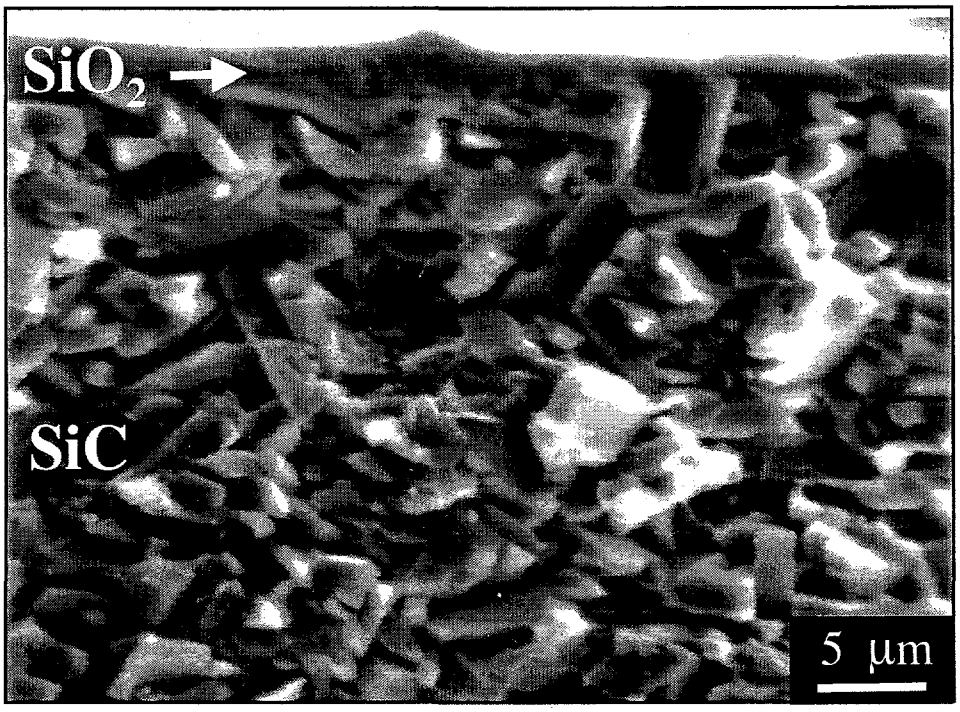

Figure 2-14: SEM micrograph of oxidized ABC-SiC. The oxide is shown in cross-section and is~ 2.3 μm thick.

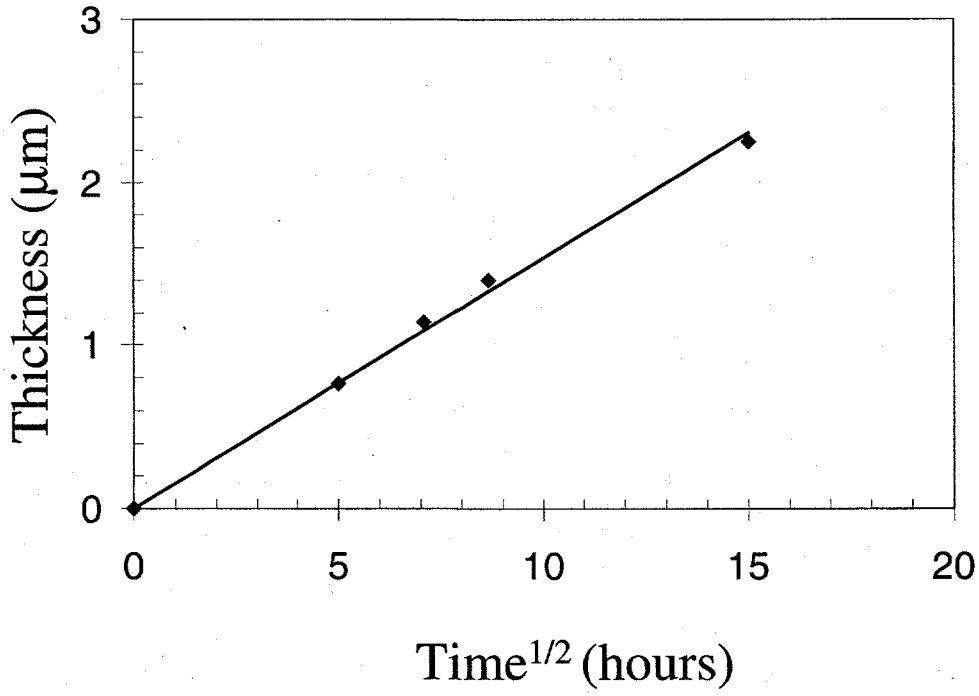

Figure 2-15: The oxidation of ABC-SiC follows parabolic kinetics, as demonstrated by the straight line in the thickness vs time$^{1/2}$ plot. This verifies the passivating nature of the oxide scale. As the oxide becomes thicker the oxidation rate decreases.

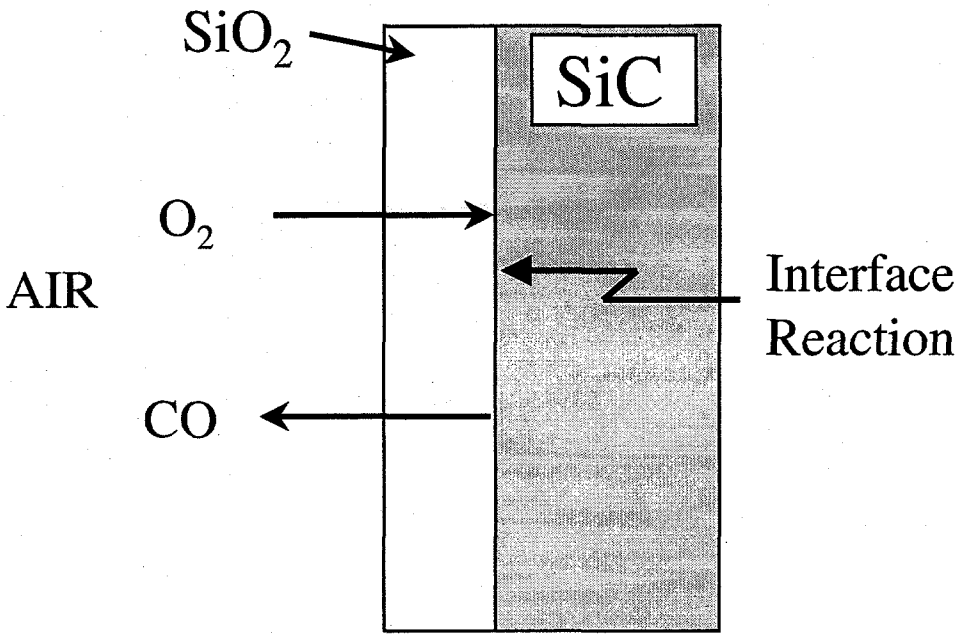

Figure 2-16: Schematic diagram of oxidation of SiC.

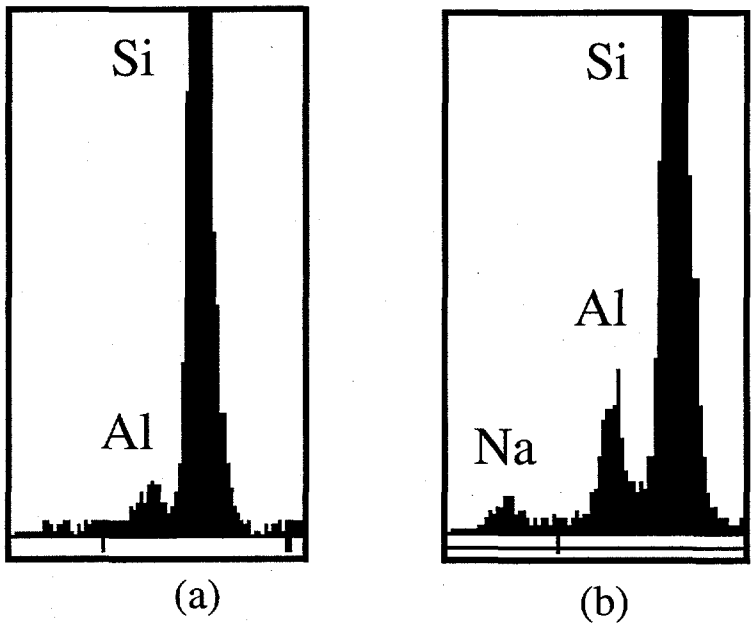

Figure 2-17: Energy dispersive spectrometry (EDS) of a polished ABC-SiC surface, (a), and EDS spectrum obtained from a plan view of the oxide. Both spectra were obtained at 500x using the entire screen area to collect the signal.

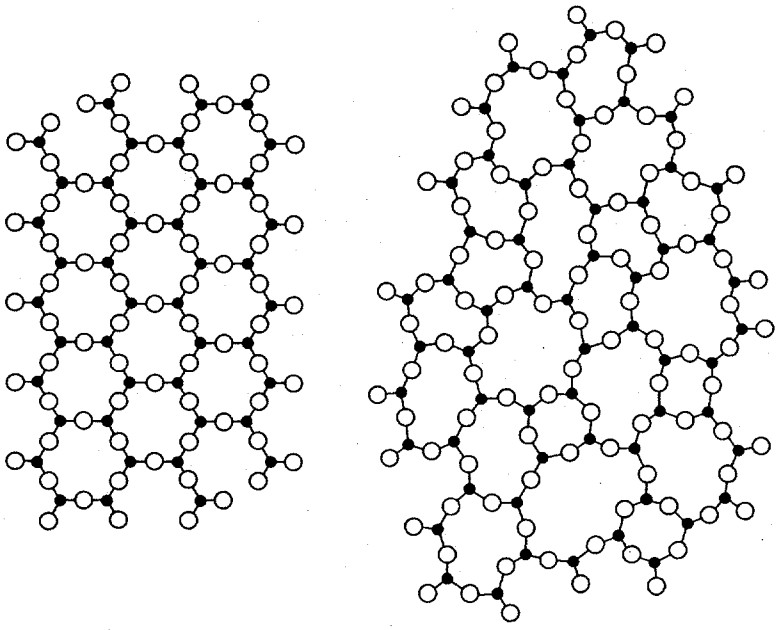

Figure 2-18: Schematic diagram of (a) ordered crystalline structure and (b) random glass network. From *Introduction to Ceramics*, 1976.

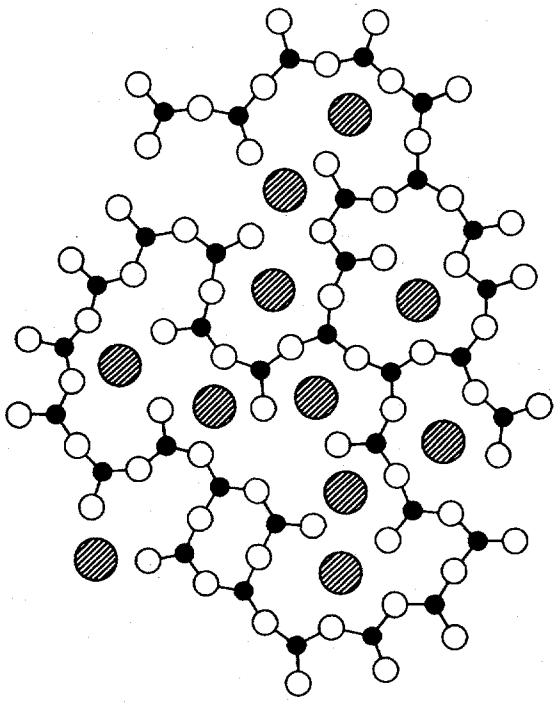

Figure 2-19: Schematic diagram of glass with impurities. The large shaded atoms represent impurities such as Na^+. From *Introduction to Ceramics*, 1976.

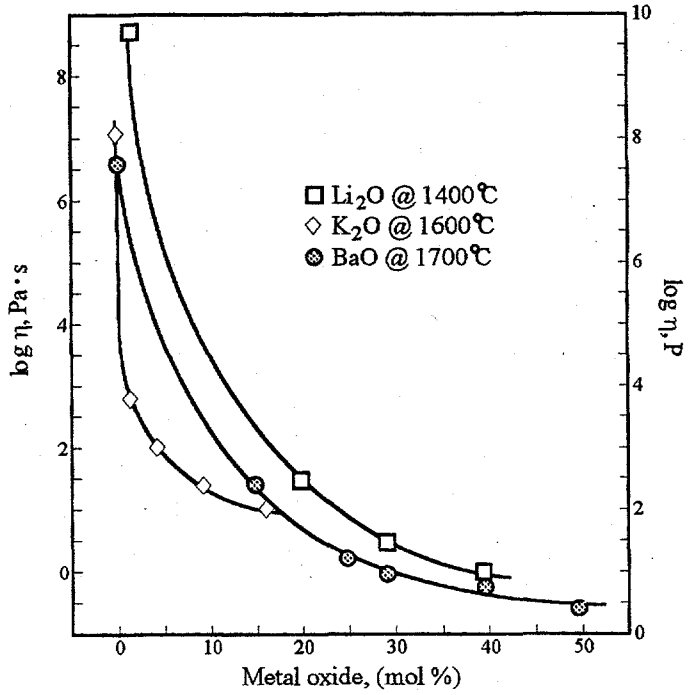

Figure 2-20: Effects of impurity concentration on the viscosity of silica at several temperatures. Adding ~10% impurities decreases the viscosity by 5 orders of magnitude. From *Introduction to Ceramics*, 1976.

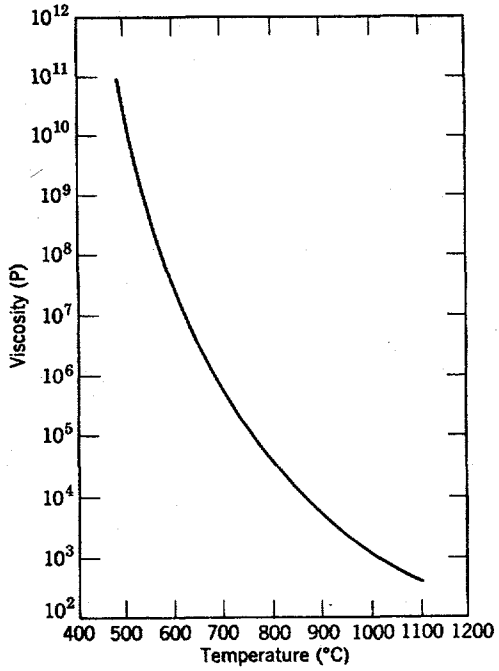

Figure 2-21: Dependence of viscosity on temperature for sodium disilicate. From *Introduction to Ceramics*, 1976.

CHAPTER 3: Transient Creep of ABC-SiC

3.1 Introduction

Many applications, such as heat exchangers, gas turbines, etc.,[1] require the use of materials under load at high temperatures. Under these conditions, a material will undergo initial elastic deformation, while slow plastic deformation will also be observed at sufficiently high temperatures. This time-dependent deformation is referred to as a creep deformation process. Creep is frequently the limiting materials parameter for high temperature applications. Although creep occurs at all temperatures, excessive distortion by creep is not experienced until high temperatures where strain rates are appreciable. In general, creep rates below ~0.4 T_m are exceedingly low.

Components at high temperature must meet two vital criteria to be useful. First, the creep rupture strength of the material must remain sufficiently high throughout the course of a components expected lifetime; catastrophic failure from overloading due to strength degradation by creep processes cannot be tolerated. Second, design dictates that certain dimensional tolerances must be maintained. Since design lives on the order of 10,000 hours are required for turbine blades and other aeroengine components,[2] a determination and an understanding of the creep response is essential for high temperature materials.

Creep response is typically characterized by three distinct regions in strain versus time plots. A schematic diagram of a creep curve is provide in Figure 3-1. As denoted on Figure 3-1, the regions A-C correspond to transient, steady-state, and tertiary creep, respectively. The first step in a creep curve is the instantaneous elastic deformation, ε_o. During transient, or primary creep, the strain rate, which is the slope of the strain versus

time curve at a given time, is characterized by a continuously decreasing creep rate. After this initial region, steady-state creep is observed where the strain rate, or creep rate, is nearly constant. For long tests, or high stress conditions, a third region is observed in the creep curve, called tertiary creep. Metals exhibit tertiary creep more often than ceramics, but this may be a result of ceramics typically being tested at low creep rates, and sufficient strain is not accumulated to move into this region. In fact, many ceramics show tertiary creep when subjected to higher loads.[3]

During primary creep the strain rate decreases until it reaches a near constant value, which marks the beginning of quasi-steady-state creep. In metals, the strain rate is decreased by work hardening, typically by dislocation-dislocation interactions. In SiC ceramic materials the origin of the transient regime is not so obvious since plastic deformation via dislocations is not readily available, even at temperatures of 1500°C. One of several mechanisms may be occurring independently or simultaneously, and this leads to transient creep in ceramics: (1) viscoelastic behavior,[4] (2) viscous flow of the grain boundary phase,[5,6,7] (3) crystallization of the interlayer,[8] and (4) chemical changes affecting the viscosity.[9]

3.1.1 Viscoelastic Behavior

Viscoelastic behavior in ceramics with a grain boundary phase is most likely manifested by grain boundary sliding. However, for materials with thick amorphous grain boundary phases, the viscoelastic behavior may simply reside in the glass itself.[10] When grain boundary sliding is present it must be accompanied by an accommodation mechanism, such as cavity formation, diffusion, and/or dislocations. Consequently, as

grain boundary sliding occurs the most likely scenario is elastic accommodation in the Si_3N_4 and second phase regions. Since the secondary phases have a lower elastic modulus the load is gradually transferred to the grain pockets. After a creep experiment, the residual internal stresses in the pockets, as a result of accommodating the grain boundary sliding, can subsequently be relieved by sliding after unloading the sample. Hence, some of the primary strain can be recovered by such a mechanism.

3.1.2 Viscous Flow

During a creep test some boundaries will be in tension and other in compression, independent of the type of test being performed. A viscous flow mechanism for transient creep has been developed for ceramics containing a grain boundary phase. The premise of this mechanism is that the grain boundary phase flows from regions of local compression to boundaries in tension. As strain develops in these materials, the separation between the respective boundaries changes. For a tensile test, the boundaries that lie normal to the stress axis increase in thickness, while the boundaries that lie parallel to the stress axis decrease in thickness. Obviously, the converse of this situation holds for compression creep tests. The rate of fluid flow, as the grain boundaries are modeled as behaving like a viscous liquid, is reduced in regions where the boundary separation is decreased. Consequently, the creep rate also decreases as the separation between grain is reduced, leading to transient creep behavior. Another feature of viscous flow creep is that transient creep in compression and tension differ. There are twice as many boundaries in tension than compression for tensile creep; hence the total strain possible from viscous flow is twice as high in tension. Ultimately, the creep process

permits grain-to-grain contact and this reduces the amount of deformation that can occur. Any additional creep must now invoke a different mechanism, such as diffusion, to enable further grain boundary sliding.

3.1.3 Crystallization

Devitrification of the grain boundary phase can also lead to transient creep behavior in ceramics. As detailed in Chapter 2, crystallization of the grain boundary film will necessarily be accompanied by a change in composition. Since the properties of the interlayer glass is strongly dependent on the composition, the creep rate changes with crystallization. Cyrstallization will likely increase the viscosity of the grain boundary phase and this inhibits grain boundary sliding, which is directly related to the viscosity of the interlayer. As crystallization proceeds, the gradually increasing viscosity is reflected in a similarly decreasing strain rate. Once the microstructure stabilizes, the creep process enters the steady-state regime.

3.1.4 Chemistry Effects on Transient Creep

A final mechanism that can cause primary creep is changing the viscosity by altering the chemistry of the interfacial glass at the creep temperature. Transient behavior for this mechanism is akin to crystallization, whereby the viscosity is slowly changing during the early stages of creep. However, it must be distinguished from the crystallization mechanism since the chemistry changes without necessarily altering the amorphous structure of the glass. This mechanism is more prevalent in oxidizing environments where there is a net flux of impurities, such as Al, from the relatively

impure grain boundary phase to the initially pure SiO_2 passivating scale.[11] The driving force for this process is the concentration gradient between the oxide and interfacial glass. The viscosity slowly increases as the chemistry changes, as with crystallization, and hence creep rates are reduced.

3.1.5 Steady-State Creep

Steady-state creep corresponds to the stage of creep where the strain rate is invariant, region B of Figure 3-1. For metals the steady-state regime is characteristic of the rate of strain hardening and recovery being equal. Both processes are related to dislocation mechanisms. In the context of ceramics, the rate of accommodation is equal to the rate of grain boundary sliding. The accommodation mechanisms typically include a diffusional mechanism, both bulk and grain boundary, and/or cavitation. A detailed description of the various steady-state creep mechanisms is provided in Chapter 4.

3.1.6 Tertiary Creep

The final region of the creep curve, C in Figure 3-1, is tertiary creep. The creep rates continuously increase during tertiary creep. The acceleration in the creep rate can be caused by and increase in the stress during constant load tests since the gauge cross-section is reduced in tensile tests. However, since constant-stress tests still show the existence of tertiary regimes, the effect of decreasing cross-section can be ignored. In metals, tertiary creep can be caused by necking, microstructural instabilities such as grain growth, recrystallization, or overaging of precipitates, or nucleation and growth of cracks.[2] For ceramics, the latter mechanism is most frequently encountered, and cavity

nucleation, growth, and coalescence leads to accelerated strain rates during tertiary creep. Details of the creep crack growth in ceramics was discussed in Chapter 2.

The transient creep behavior of ABC-SiC was investigated by performing several step tests, both by increasing the stress at a fixed temperature and increasing the stress for a given temperature. Additionally, a relaxation experiment was conducted to understand the mechanisms of primary creep in ABC-SiC. The steady-state creep response is presented in Chapter 4. Tertiary creep was not observed in the current studies; thus, these mechanisms were not investigated in the current work.

3.2 Experimental Procedures

3.2.1 ABC-SiC Processing

Processing of ABC-SiC was performed with submicron β-SiC powder (H. C. Starck, Germany). The SiC powder was mixed with 3 wt% Al, 0.6 wt% B, and 2 wt%C. The Al metal source (H-3 and H-10, Valimet, Stockton, CA) was in a powder form with a nominal diameter of ~ 5 μm. B was also introduced in a powder form (Callery Chemical Co, Callery, PA). In contrast, the C source was Apiezon wax (AVO Biddle Instruments, Blue Bell, PA). The calculated value of 2% C was doubled since the C yield upon pyrolysis was determined to be ~ 50%.[12] This C source also served as a binder in the system. The Apiezon wax was dissolved in toluene and the other powders were added to this solution and agitated with an ultrasonic probe for 5-10 minutes to minimize agglomerate formation. The ultrasonicated mixtures contained ~ 25 g of powder and a total of 4 steps were conducted to yield the 100 g batches typically produced. The

solution was stir dried, and the material was ground in a mortar and pestle prior to sieving through a 200 mesh screen.

Hot-pressing was conducted on the green compacts that were formed by uniaxial compression at 35 MPa in a metal die. Three samples were inserted into a graphite die lined with graphite foil. Graphite spaces were placed between each of the three samples. The foil and dies were not sprayed with BN. The furnace was heated under vacuum at ~ 350-400°C overnight, and then an automated temperature controller, using a ramp rate of 10°C/minute, was utilized. The temperature for hot-pressing was 1900°C, and the samples were loaded at 50 MPa. The temperature in the hot-press was monitored with a W-Rh themorcouple below ~ 1200°C. Above this temperature a dual wavelength pyrometer was used. The atmosphere was flowing Ar. The load was increased at a rate of 250 lb./minute, starting at 1000°C, and the load was removed at rate of 150 lb./minute, starting with 5 minutes left in the 1 hour soak at 1900°C. The samples were polished and sectioned, as detailed in Chapter 2. A flow chart of processing is provided in Figure 3-2.

3.2.2 Transient Creep Tests

The primary creep regime was evaluated by a couple of different step tests. The first test was to fix the temperature and increase the stress. The magnitude of transient creep was compared for the various stress levels. Tests were performed at 1200-1500°C, with the stress being varied by a factor of 1.5-3 at each temperature. Second, the stress was fixed at 100 MPa and a sample was crept at 1200°C, followed by creeping the same sample at 1300°C. Also, a relaxation experiment was conducted to determine the amount of recoverable strain.

3.2.3 Calculating Strain From Four-Point Bending Creep Studies

All creep experiments were conducted in four-point bending in the same graphite jig used for the high temperature strength measurements. The inner span and outer span were 0.375 inch and 1 inch, respectively. The initial stress for all creep tests is the initial outer-fiber stress, as provided by Equation 2.1. A swing arm was utilized to monitor the load point displacement.

Therefore, it is necessary to convert the load point displacement to creep strain. This was calculated by Hollenberg *et al.*,[13] and the primary assumption made for determining the stress exponent, n, and maximum strain during four-point bending creep is that the neutral axis does not shift. This assumes the creep rates in tension and compression are identical. Additionally, it is assumed that the geometry of the beam follows a perfect circle between the inner load points, and the beam is a straight line elsewhere, as depicted by segment s in Figure 3-3. A constitutive relation of the following form was assumed for the calculations:

$$\varepsilon(t,\sigma) = \sigma^n J(t) \tag{3.1}$$

where J(t) is the creep compliance and contains the time dependence of the strain. By substituting Equation 3.1 into Equation 3.2,

$$\varepsilon = \frac{z}{\rho} \tag{3.2}$$

where z is the distance from the neutral axis, and ρ is the radius of curvature, the stress can be solved for and substituted into the relationship for the bending moment. After integration and substitution the maximum stress is arrived at, Equation 3.3.

$$\sigma_{max} = \frac{3(L-a)P}{bh^2}\frac{(2n+1)}{3n} \tag{3.3}$$

This equation is the same as Equation 2.1 for cases of n = 1 (viscous creep). Strain is derived using the assumption of small deflections. For small deflections it is common to employ the following assumption.

$$\frac{1}{\rho} = \frac{d^2y}{dx^2} \tag{3.4}$$

By substituting into the integrated moment expression, a mixed boundary-value problem is obtained, Equation 3.5.

$$\frac{d^2y}{dx^2} = J(t)\left(\frac{M}{I_n}\right)^n \tag{3.5}$$

I_n is the complex moment of interia. To get y as a function of the measurable parameter of load, P, the following boundary conditions were used to solve this differential equation.

$$M = \frac{P(L-a)}{2} \text{ for } \frac{L-a}{2} < x < \frac{L+a}{2} \tag{3.6}$$

$$M = Px \text{ for } 0 < x < \frac{L-a}{2} \text{ and } \frac{L+a}{2} < x < L \tag{3.7}$$

$$\frac{dy}{dx} = 0 \text{ at } x = \frac{L}{2} \tag{3.8}$$

$$y = 0 \text{ at } x = 0 \tag{3.9}$$

Solving Equation 3.5 for y and then differentiating gives the relationship between the load-point displacement rate, $\dot{y}$, stress exponent, n, and load, P, Equation 3.10.

$$\log \dot{y} = n \log P + C \tag{3.10}$$

Plotting the measured load-point displacements, and plotting as a function of P on a log-log plot give the stress exponent for stead-state creep. To convert the load-point displacement into strain the maximum stress, Equation 3.3, is substituted into the constitutive relationship.

$$\varepsilon_{max} = \frac{2h(n+2)}{(L-a)[L+a(n+1)]} y \tag{3.11}$$

Equation 3.11 was used to calculate all strains, both for primary and secondary creep. The above equation is appropriate for small strains (~ 1-2%). For larger strains the loading is not entirely vertical and neglecting the shear contributions to the beam deflections would no longer be valid.

The assumption of no shift in the neutral axis is not valid for ceramics in bending creep. For Si_3N_4, the strain rates in tension have been measured to be more than 20 times greater than creep rates in compression.[14,15,16] However, it was shown by Chuang[17] that applying the method developed by Hollenberg *et al.*[13] provides an average value of the respective tensile and compressive creep response. This holds for the stress exponents, activation energy, and strain rates. Chuang[17] developed a method for calculating the tensile and compressive values from a single bend test, but this method requires testing stresses that vary by 2 orders of magnitude. Since a curve fitting routine is utilized in this method, the recommended stresses employed for the creep experiments would be 5 and 500 MPa. At the lower bound, the 5 MPa would not produce measurable creep in ABC-SiC. In contrast, a stress of 500 MPa would cause catastrophic failure upon loading. Since the curve fitting routine would introduce large errors when employing stresses that are quite similar, *ie.* only a factor of 3 different, this method was not applied to ABC-SiC for the current study.

The MTS system used for the current studies, detailed in section 3.2.3, did not permit tensile tests. Additionally, only bend test were performed since tensile creep specimens are extremely expensive.

3.2.4 Creep Aparatus

An MTS load frame and Centorr furnace were utilized for the creep experiments. The tungsten mesh filaments limited tests to inert atmospheres. The creep tests were performed in flowing Ar. A picture of this equipment is shown in Figure 3-4. ABC-SiC beams, both before and after annealing, were loaded into the furnace and the temperature was increased at a rate of 10°C/minute after manually increasing the temperature to 400°C. The samples were heated with a minimal load, ~ 5 N, and a soak of ~ 2 hours was conducted to allow the system to equilibrate prior to collecting creep data. A Honeywell controller was used to run the temperature program, and the temperature control was ± 1°C. The absolute temperature was determined by calibrating a B-type thermocouple against a K-type thermocouple; the calibration was verified by melting pure Cu and Ni. After the creep experiments were concluded, the samples were cooled at 10°C/minute with the final creep stress still applied. This eliminated stress relaxation during cooling and ensured the observed features were representative of the high temperature microstructure.

A swing arm, with a resolution of better than 1 μm, was used to monitor the load-point displacement. The swing arm was placed on the actuator of the MTS load frame. A computer was utilized for several features of data collection and control. A load control routine, utilizing HP VEE, was implemented to ensure that the load did not drift

during the experiments. The same HP VEE program collected the load, load-point displacement, and time data. Additional channels were utilized to collect temperature values for the room and cooling water, see section 3.2.4 for details on the temperature fluctuation corrections. A temperature fluctuation calibration routine was applied in real-time to correct the load-point displacement data for temperature changes.

3.2.5 Temperature Fluctuation Compensation

It was immediately obvious after the first creep test was started that temperature fluctuations in the system were causing erroneous results. The displacements were observed to decrease, which has no physical meaning. Consequently, the room temperature, cooling water temperature, and cooling water pressure were monitor to determine what effects changes in each property had on the creep data. It was determined that the cooling water and room temperature fluctuations were resulting in displacements that were overwelming the creep data. Examination of the load frame in Figure 3-4 reveals the origin of the perturbations in the data resulting from changes in temperature. The load frame consists of several feet of steel and just a degree change in the room temperature can cause dramatic changes in the displacements measured by the swing arm. Similarly, the grips expand and contract with changes in the cooling water and this alters the displacement readings.

To circumvent this problem sensors were placed on the load frame, to reflect changes in room temperature, and also on the cooling water inlet. The RTD sensors were glued into place with silicone. A liberal amount was placed on and around each sensor. This ensured the predominant signal read by the RTD was from the metal parts on which

they were attached. The signal from the RTD's was sent through a signal conditioner, and the computer read the voltage. Calibration was performed by loading a beam at room temperature, where no creep can occur, and monitoring the voltage and displacement fluctuations.

The fluctuations in the room temperature and cooling water temperature are shown in Figures 3-5 & 3-6. The displacement obtained for the same time is provided in Figure 3-7. By comparing Figures 3-5 and 3-6 with Figure 3-7 it is evident that for every perturbation in the cooling water temperature the displacement exhibited a similar fluctuation. By comparison, the room temperature varied slowly between morning and night, and this slow change was superimposed on the more rapid changes observed with the cooling water temperature.

Assuming that the thermal expansion coefficients are linear over the temperature range of interest, calibration factors were established for the fluctuations. This assumption introduced negligible error in the current experiments since the maximum temperature fluctuations are only ~ 5°C. To calculate the calibration factors, a routine was used to minimize the sum of the residual squared. Application of these calibration factors reduced 25 μm perturbations to ± 1-2 μm fluctuations. Since the slope of the strain versus time in the steady-state regime is the most important feature, the compensation for temperature fluctuations should introduce little error in the strain rates measured for ABC-SiC. The calibration factors applied to the perturbations in Figure 3-7 are shown in Figure 3-8.

3.3 Results and Discussion

3.3.1 Creep Step Tests

The creep curves of ABC-SiC at 1400°C for stresses of 50, 100, 150, and 200 MPa are all shown on the same plot to illustrate the effect of increasing load on primary creep, Figure 3-9. The largest transient creep strain was associated with the lowest stress. Similar features were observed in the step tests conducted at 1500°C for 50 and 100 MPa. The results are shown in Figure 3-10. These results are consistent with a transient creep mechanism whereby an exhaustive mechanism is operative. This could include viscous flow of the grain boundary phase or grain boundary sliding. As previously detailed, section 3.1.2, viscous flow becomes more difficult as the grain boundary layer decreases in thickness.[5] Likewise, when grain boundary sliding occurs the grains ultimately make contact and this inhibits further deformation.[8,18,19] Increasing contact points can reduce the load at any given point, thus reducing the driving force for continued sliding. Alternatively, interlocking can occur that inhibits further deformation for the applied stress.

The increased primary strain as the stress increased likely resulted from the enhanced driving force for sliding and/or viscous flow. The subsequent primary creep strain was small, and this suggests that a majority of the microstrucutural changes occurring during primary creep occur fast, even at low stresses. As grain rearrangement occurs the grains impinge upon each other. However, as the stress is increased additional rearrangement is possible, but the extent of this deformation is small. The final primary region in ABC-SiC at 1400°C, 200 MPa in Figure 3-9, shows that very little additional transient creep occurs once the grains become interlocked. At this point a new

mechanism, such as diffusion or cavitation, must become active for additional deformation to occur.

A step test was also conducted by increasing the temperature from 1200°C to 1300°C, while maintaining a stress of 100 MPa, Figure 3-11. Again, the primary creep exhibited for the second step was less than the initial deformation step. The mechanisms responsible for this behavior are believed to be the same as those for the step tests involving an increase in stress. At higher temperatures an additional driving force is provided. This is likely manifested through an alteration of the viscosity. Viscosity scales as the inverse of temperature; thus, grain boundary sliding, which is dependent on the viscosity of the glass, is promoted with the additional temperature. However, a significant portion of sliding occurred at the lower temperature during the first step, hence primary creep strain is reduced for the second test.

3.3.2 Origin of Viscoelastic Effects

The roles of viscoelastic effects and viscosity changes, either by crystallization or chemically introduced, must be discussed to ascertain the transient creep mechanism in ABC-SiC. Viscoelastic effects, which account for recoverable strain, can occur through viscoelastic deformation of the amorphous grain boundary phase[10] or by loading of triple-junction materials during grain boundary sliding.[8] Since the viscoelastic effect of the grain boundary layer was observed for a material with thick interlayers, and the grain boundary phase in ABC-SiC is typically only on the order of 1 nm, see Chapter 5, it does not appear that this mechanism is operative.

Since the secondary phase in Si-based ceramics possess a lower elastic modulus, there is a partial transfer of stress from the grains to these phases. Transient creep has been attributed to viscoelastic behavior resulting from this type of loading of the secondary phase(s). After the load is relieved, the residual stress in these pockets can be relieved by grain boundary sliding. This is the origin of the recoverable strain. However, the strain recovered for ABC-SiC was only ~10%. Therefore, it does not appear that viscoelastic effects are dominant in the transient creep of ABC-SiC.

3.3.3 Viscosity Changes

As described in Chapter 2, changing the viscosity will alter the rate of grain boundary sliding. Increasing the viscosity with increase the resistance to grain boundary shear. For ABC-SiC without a pre-anneal, the transient period can be attributed, at least in part, to crystallization of the grain boundary phase and the subsequent changes in viscosity. For samples that were not annealed, the primary region lasted approximately 3-4 days, independent of temperature. This suggests that crystallization lowers the amount of primary creep, but the extent of the transient creep strain can be attributed to other mechanisms. If crystallization alone was responsible for primary creep then the primary regime should be shorter at higher temperatures since crystallization kinetics would be enhanced.

Crystallization of the grain boundary interlayer is a well documented method for improving the creep resistance of Si_3N_4.[20,21,22] The degree that crystallization reduced the magnitude of the primary regime is difficult to assess since the strength of ABC-SiC drops to 100 MPa at 1300°C when it is not preannealed. Therefore, the stress range of

interest, ~ 100-200 MPa, was not assessable for ABC-SiC that was not annealed. However, crystallization of the grain boundaries in ABC-SiC can be expected to reduce the magnitude of the transient creep strain.

Chemical induced viscosity changes are unlikely to play a major role during primary creep of ABC-SiC. This is more prevalent in oxidizing environments, and thus precludes this mechanism in the current study. The long oxidation experiment, Chapter 2, revealed few composition changes. However, precipitates may induce a slowly changing chemistry and could impact transient creep.

3.3.5 Viscous Flow

Crystallization of the grain boundary interlayer likely minimized the amount of viscous flow of this phase during primary creep. Evaluation of boundaries parallel to and perpendicular to the stress axis revealed similar features. There was no direct evidence of redistribution of the grain boundary phase during creep, as has been observed in Si_3N_4.[6] Therefore, viscous flow was believed to play only a minimal role in transient creep of ABC-SiC

3.3.5 Transient Creep in ABC-SiC

Primary creep in ABC-SiC most likely proceeds by a grain boundary sliding mechanism. The grains rearrange in response to the applied stress, and the strain rates decrease as grain impinge (become interlocked). As additional contact points are generated, the load at any point, and thus the driving force for further deformation, is reduced. Consequently, the creep rates are also reduced. A minimal amount of transient

creep can be attributed to viscoelastic behavior as the secondary phases at multi-grain junctions is loaded due to a lower elastic modulus. Crystallization of the grain boundary phase reduces the amount of primary creep strain.

3.3.6 Comparison of Transient Creep in ABC-SiC and Hexoloy

Since the starting microstructure of ABC-SiC exhibits some grains with an interlocked morphology, see Chapter 5, it is hypothesized that the primary creep strain should be less than a microstructure relying on grain impingement to exhaust the transient regime. Figure 3-12 compares the creep of ABC-SiC and commercially available Hexoloy SiC (Carborundom, Mass., USA). Hexoloy is sintered with small amounts of B and C, and possesses an equiaxed microstructure with no amorphous grain boundary phase.[23] The primary creep strain for Hexoloy is ~3 times greater than ABC-SiC when tested under identical conditions. The interlocking nature of a small percentage of grains in ABC-SiC, and the plate-like morphology of these grains, effectively reduces the degrees of freedom. Grain sliding and rotation appears to be more difficult than with an equiaxed material, hence the primary creep strain was reduced. For a case where grain boundary sliding is the operative mechanism, it appears advantageous to engage as many grains as possible by interlocking. Provided triple-point cracking is not introduced upon loading, this microstructure should be the most conducive to low creep strains in the primary regime. However, it should be noted that it does not necessarily improve the steady-state creep resistance.

3.4 Conclusions

Primary creep of ABC-SiC proceeds by grain boundary sliding, and the strain rates are reduced as additional load bearing points are generated. Crystallization of the grain boundaries by pre-annealing the material reduces the total primary creep strain. The plate-like morphology of ABC-SiC grains, and the interlocking, appear to provide better resistance to creep in the transient regime.

3.5 References

[1] E. G. Butler and M. H. Lewis, "Prospects for Ceramics in Airborne Gas Turbine Engines," 4th International Symposium on Ceramics Materials and Components for Engines," Ed. R. Carlsson, T. Johansson, and L. Kahlman, Elsevier applied Science, pp. 32-49, (1992).

[2] R. W. Evans and B. Wilshire, *Introduction to Creep*, The Institute of Materials, London, (1993).

[3] S. M. Wiederhorn, B. A. Fields, B. J. Hockey, "Fracture of Silicon Nitride and Silicon Carbide at Elevated Temperatures," *Materials Science & Engineering A* (Structural Materials: Properties, Microstructure and Processing), **A176** [1-2] 51-60 (1994).

[4] C. J. Gasdaska, "Tensile Creep in an in Situ Reinforced Silicon Nitride," *J. Am. Ceram. Soc.*, **77** [9] 2408-18 (1994).

[5] M. M. Chadwick, D. S. Wilkinson, and J. R. Dryden, "Creep Due to a Non-Newtonian Grain Boundary Phase," *J. Am. Ceram. Soc.*, **75** [9] 2327-34 (1992).

[6] M. M. Chadwick, R. S. Jupp, and D. S. Wilkinson, "Creep Behavior of a Sintered Silicon Nitride," *J. Am. Ceram. Soc.*, **76** [2] 385-96 (1993).

[7] J. R. Dryden and D. S. Wilkinson, "Three-Dimensional Analysis of the Creep Due to a Viscous Grain Boundary Phase," *Acta Mater.*, **45** [3] 1259-73 (1997).

[8] S. M. Wiederhorn, B. J. Hockey, D. C. Cranmer, and R. Yeckley, "Transient Creep Behaviour of Hot Isostatically Pressed Silicon Nitride," *J. Mat. Sci.*, **28** [2] 445-53 (1993).

[9] Q. Jin, X. -G. Ning, D. S. Wilkinson, and G. C. Weatherly, "Redistribution of a Grain-Boundary Glass Phase during Creep of Silicon Nitride Cermaics," *J. Am. Ceram. Soc.*, **80** [3] 685-91 (1997).

[10] F. F. Lange, B. I. Davis, and D. R. Clarke, "Compressive Creep of Si_3N_4/MgO Alloys," *J. Mat. Sic.*, **15** [3] 601-18 (1980).

[11] D.R. Clarke and F.F. Lange, "Oxidation of Si_3N_4 Alloys: Relations to Phase Equilibria in the System Si_3N_4-SiO_2-MgO," *J. Am. Ceram. Soc.*,**63** [9-10] 586-93 (1980).

[12] J. Cao, "*In Situ* Toughened SiC Ceramics with Al-B-C Additions and Oxide-Coated SiC Platelet/SiC Composites," Ph.D. Thesis, University of California, Berkeley, pp. 22, (1996).

[13] G. W. Hollenberg, G. R. Terwilliger, and R. S. Gordon, "Calculation of Stresses and Strains in Four-Point Bending Creep Tests," *J. Am. Ceram. Soc.*, **54** [4] 196-99 (1971).

[14] M. K. Ferber, M. G. Jenkins, and V. J. Tennery, "Comparison of Tension, Compression, and Flexure Creep of Alumina and silicon Nitride Ceramics," *Ceram. Eng. Sci. Proc.*, **11** [7-8] 1028-37 (1990).

[15] S. M. Wiederhorn, D. E. Roberts, and T. -J. Chuang, and L. Chuck, 'Damage-Enhanced Creep in a Siliconized Silicon Carbide: Phenomenology," *J. Am. Ceram. Soc.*, **71** [7] 602-08 (1988).

[16] M. K. Ferber, M. G. Jenkins, "Evaluation of the strength and creep-fatigue behavior of hot isostaticallly pressed silicon nitride," *J. Am. Ceram. Soc.*, **75** [9] 2453-62 (1992).

[17] T. -J. Chuang, "Estimation of Power-Law Creep Parameters From Bend Test Data," *J. Mat. Sci.*, **21** 165-75 (1986).

[18] M. K. Ferber, M. G. Jenkins, T. A. Nolan, and R. Yeckley, "Comparison of the creep and Creep Rupture Performance of Two HIPed Silicon Nitride Ceramics," *J. Am. Ceram. Soc.*, **77** [3] 657-65 (1994).

[19] M. N. Menon, H. T. Fang, D. C. Wu, M. G. Jenkins, and M. K. Ferber, "Creep and Stress Rupture Behavior of an Advanced Silicon Nitride: Part II, Creep Rate Behavior," *J. Am. Ceram. Soc.*, **77** [5] 1228-34 (1994).

[20] J. -L. Ding, K. C. Liu, K. L. More, and C. R. Brinkman, "Creep and Creep Rupture of an Advanced Silicon Nitride Ceramic," *J. Am. Ceram. Soc.*, **77** [4] 867-74 (1994).

[21] J. A. Todd and Z. -Y. Xu, "The High Temperature Creep Deformation of Si_3N_4-$6Y_2O_3$-$2Al_2O_3$," *J. Mat. Sci.*, **24** 4443-52 (1989).

[22] D. C. Cranmer, B. J. Hockey, and S. M. Wiederhorn, "Creep and Creep-Rupture of HIP-ed Si_3N_4," *Ceram. Eng. Sci. Proc.*, **12** [9-10] 1862-72 (1991).

[23] J. E. Lane, C.H. Carter, and R. F. Davis, "Kinetics and Mechanisms of High Temperature Creep in Silicon Carbide: III, Sintered α-Silicon Carbide," *J. Am. Ceram. Soc.*, **71** [4] 281-95 (1988).

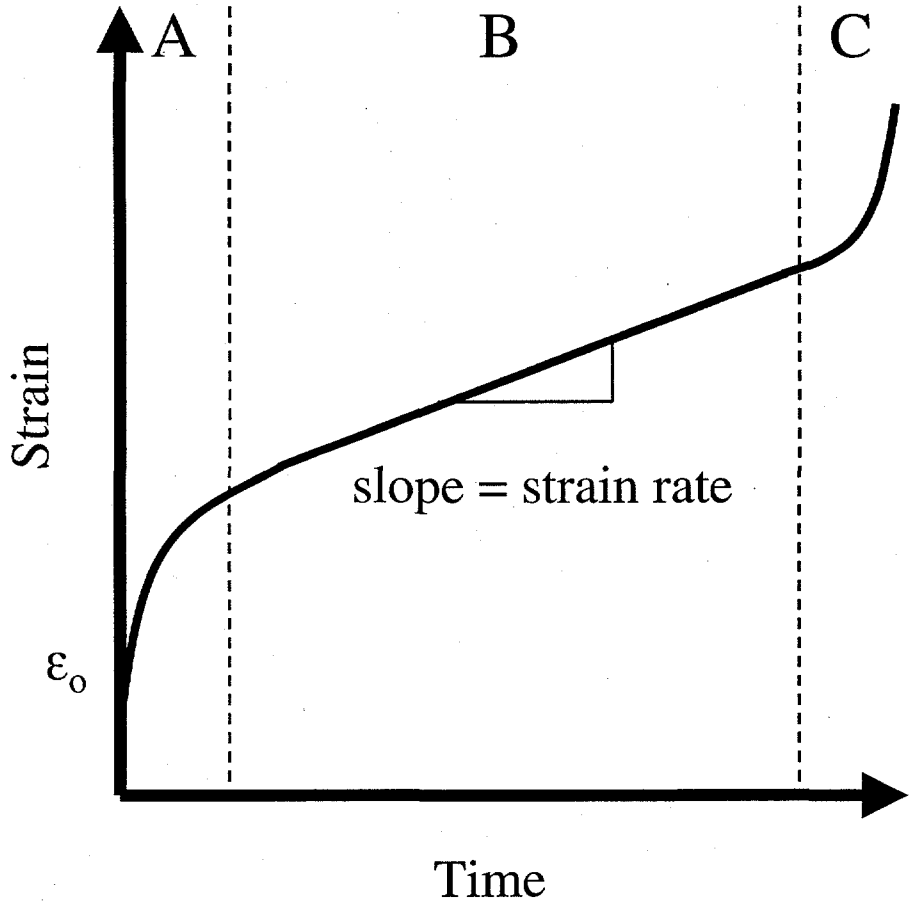

Figure 3-1: Schematic diagram of a creep curve. The first stage in creep is the transient regime, A, where the slope continuously decreases. B defines the steady-state creep, and C demonstrates tertiary creep, where the strain rate continually increases.

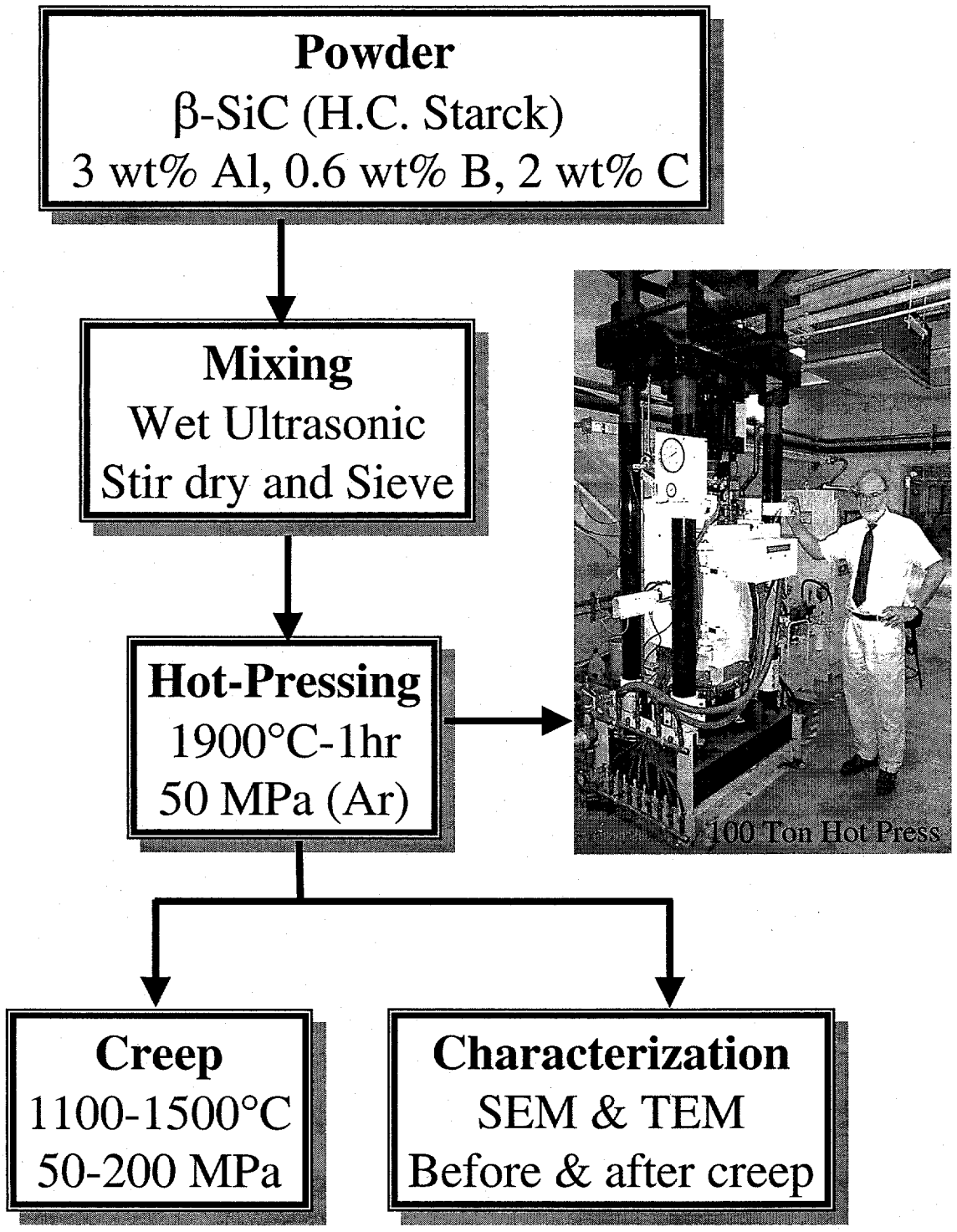

Figure 3-2: Processing and testing flowchart for ABC-SiC.

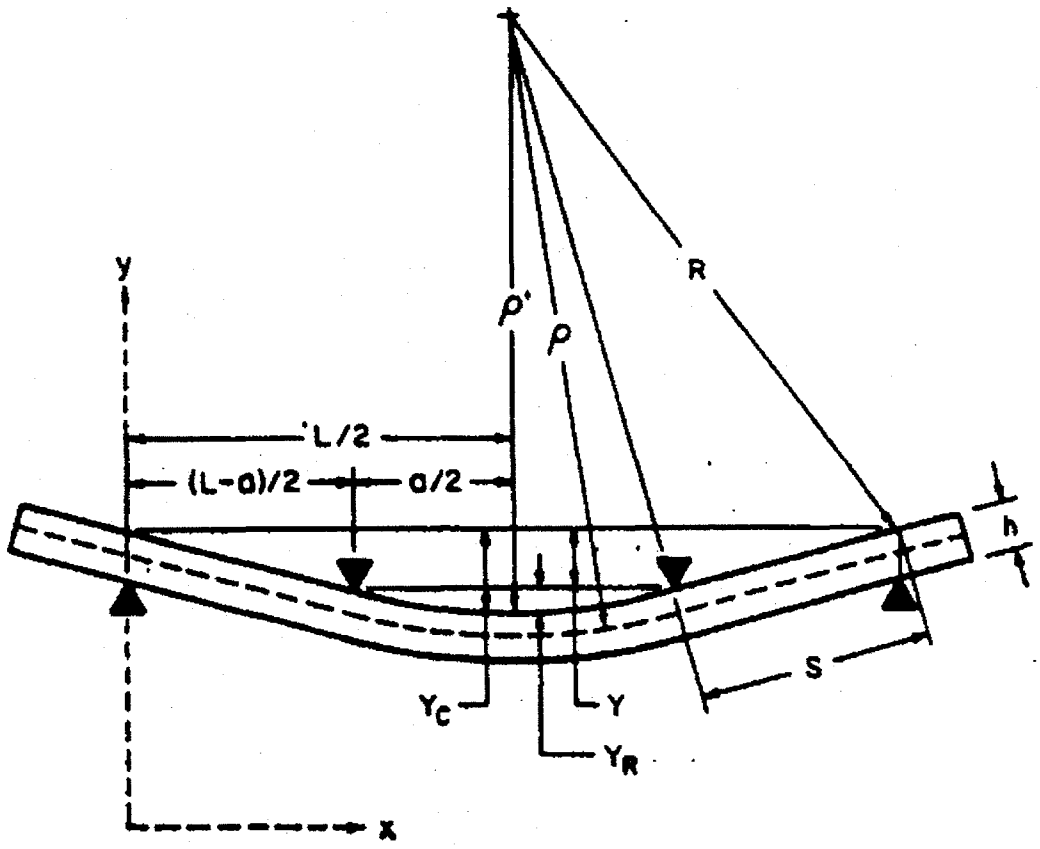

Figure 3-3: Diagram for the quantities used to calculate strain from load point displacement measurements.

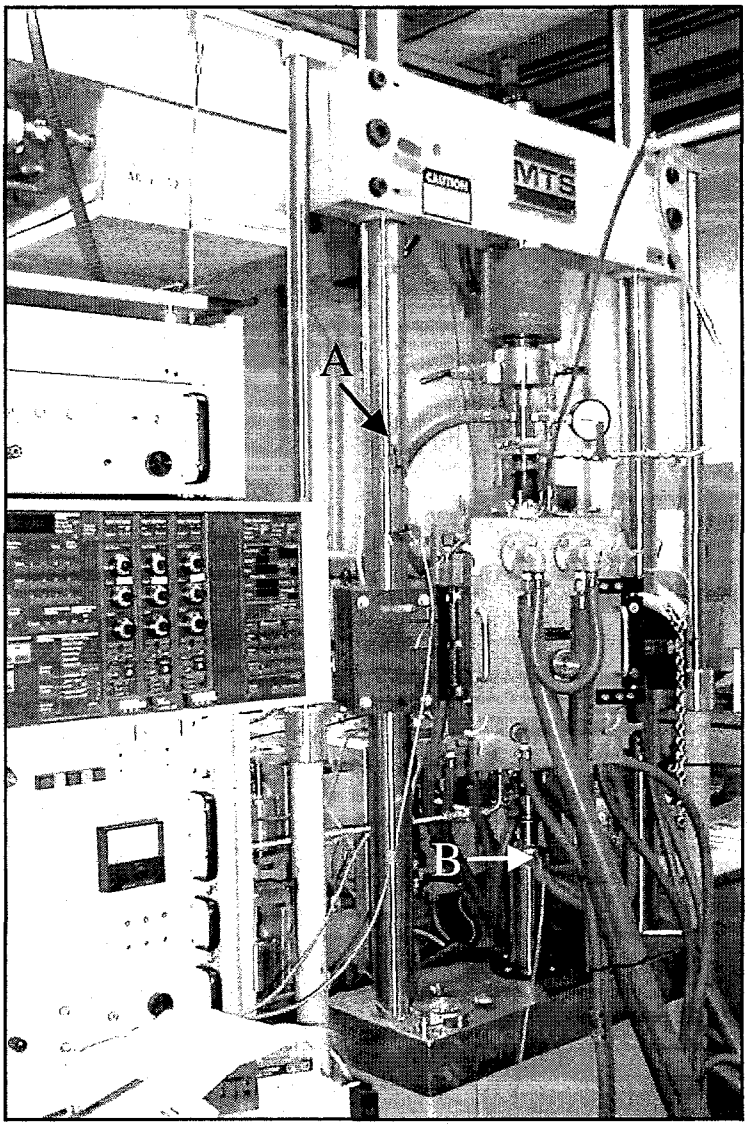

Figure 3-4: MTS load frame and Centorr furnace utilized for creep experiments. The RTD temperature sensors used to compensate for temperature fluctuations arelocated at the points A and B for the room and cooling water temperature, respectively.

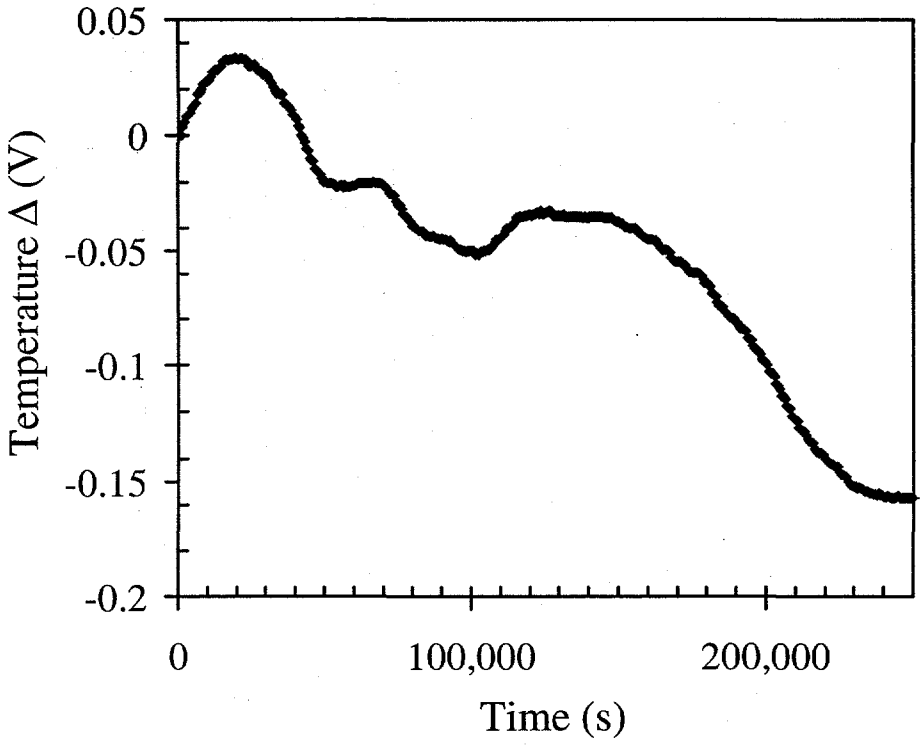

Figure 3-5: Fluctuations in the room temperature.

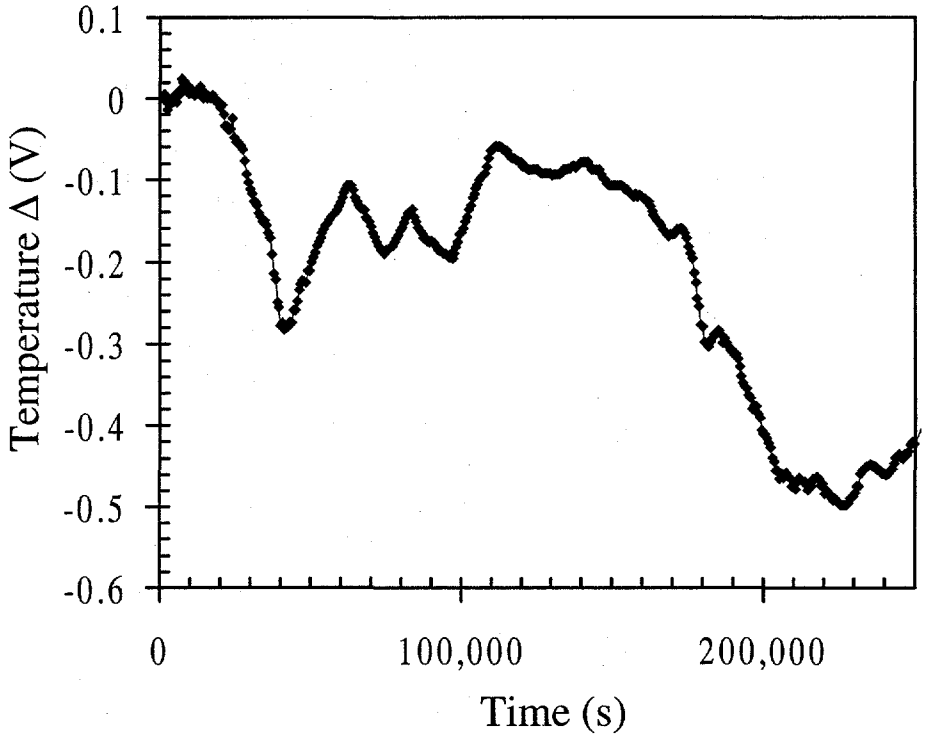

Figure 3-6: Cooling water fluctuations.

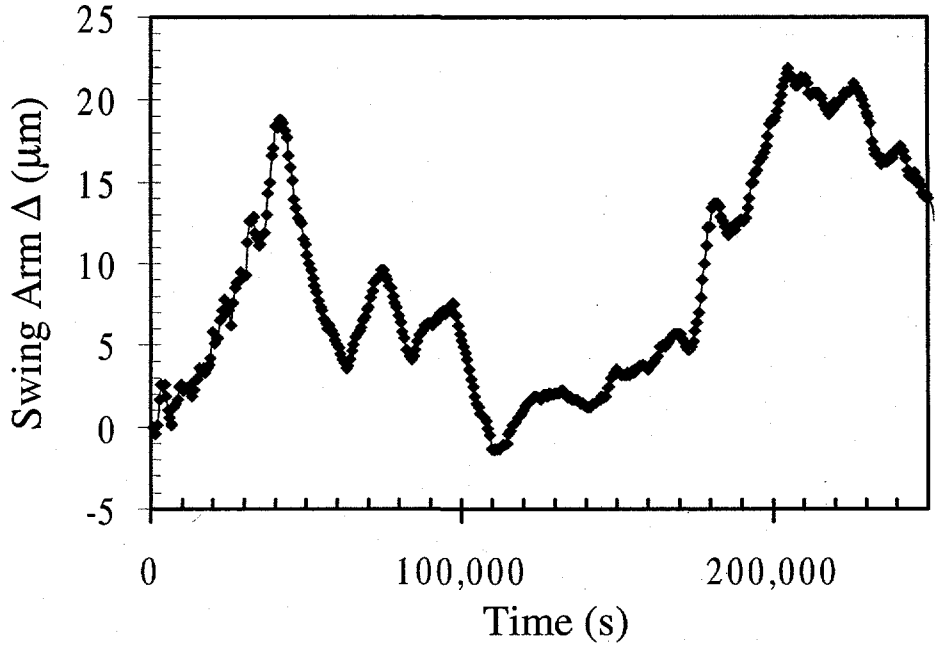

Figure 3-7: Load-point displacement fluctuations due to temperature changes. Since the beam was loaded at room temperature the swing arm should read zero.

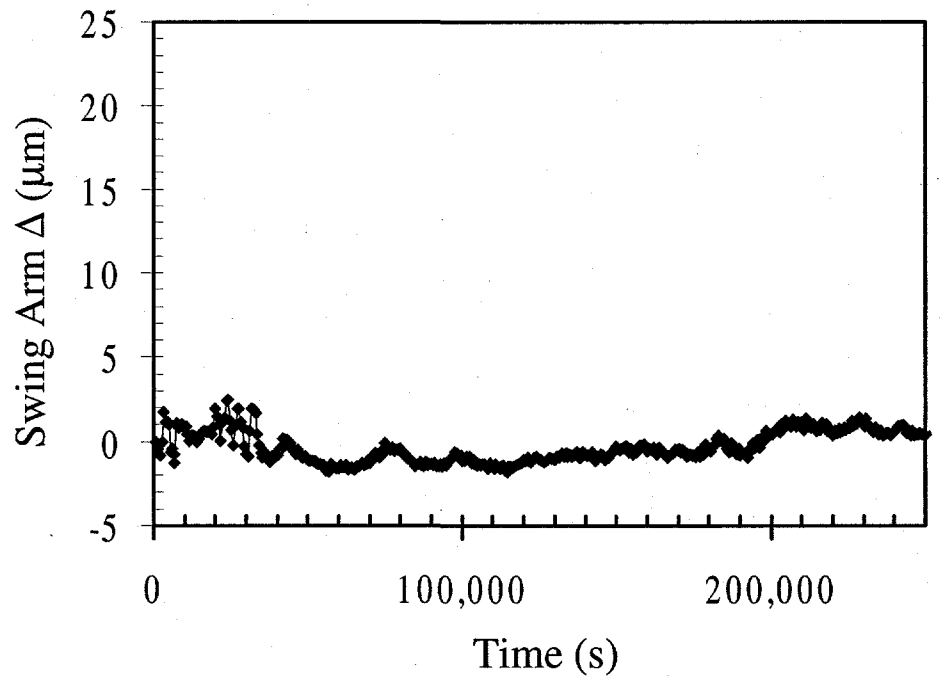

Figure 3-8: Temperature compensated curve from Figure 3-7. The perturbations are smoothed from greater than 25 μm to ~1-2 μm. While error may be introduced for any displacement measurement, the curve fit would result in a flat line as expected for no creep. Therefore, the temperature fluctuations should add only minimal error to the strain rate calculations.

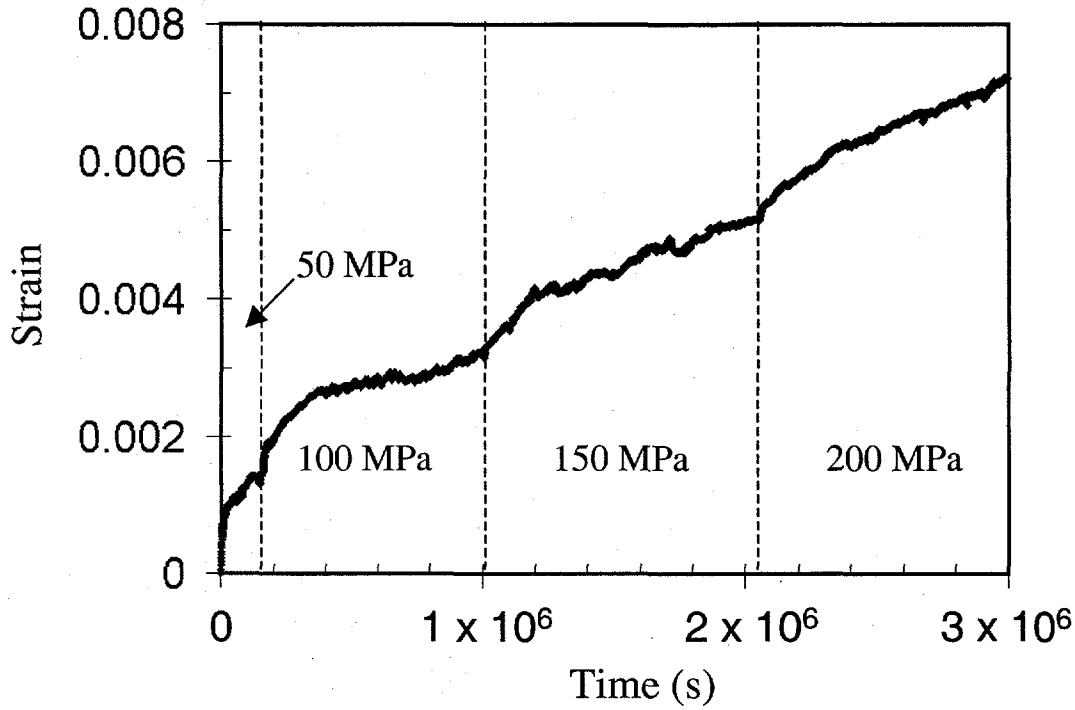

Figure 3-9: Creep curves for 1400°C 50, 100,150, and 200 MPa. Each successive curve, as the stress is increased, shows a small primary creep regime.

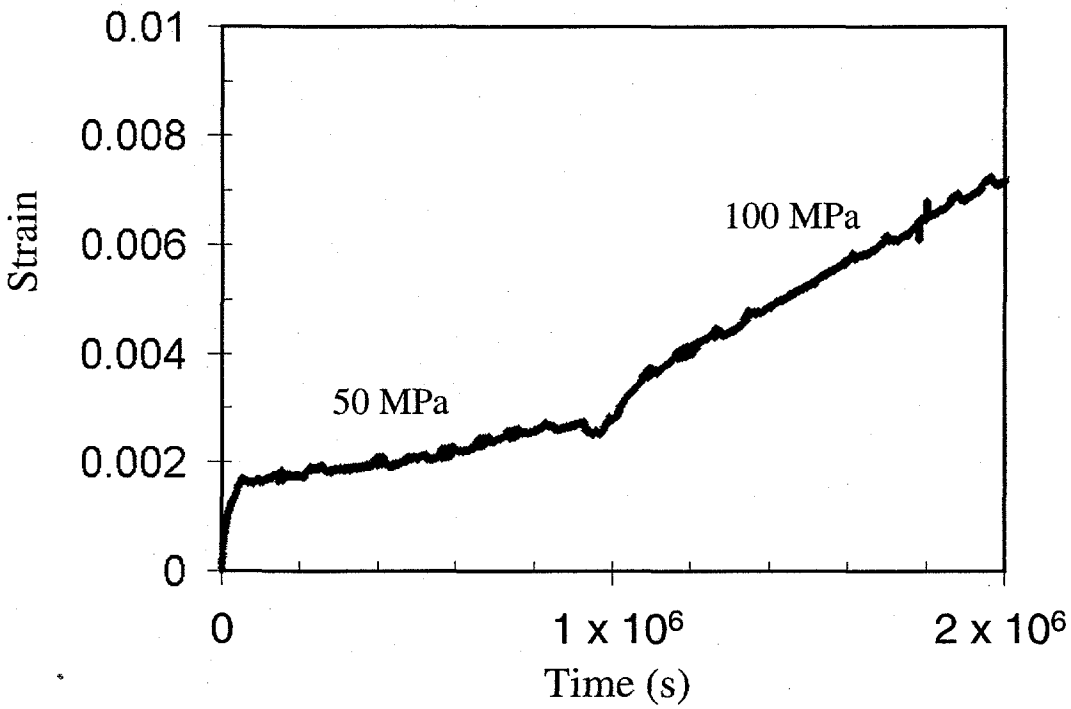

Figure 3-10: Creep curves for 1500°C, 50 and 100 MPa. Primary creep is diminished after initial deformation, even at a lower stress.

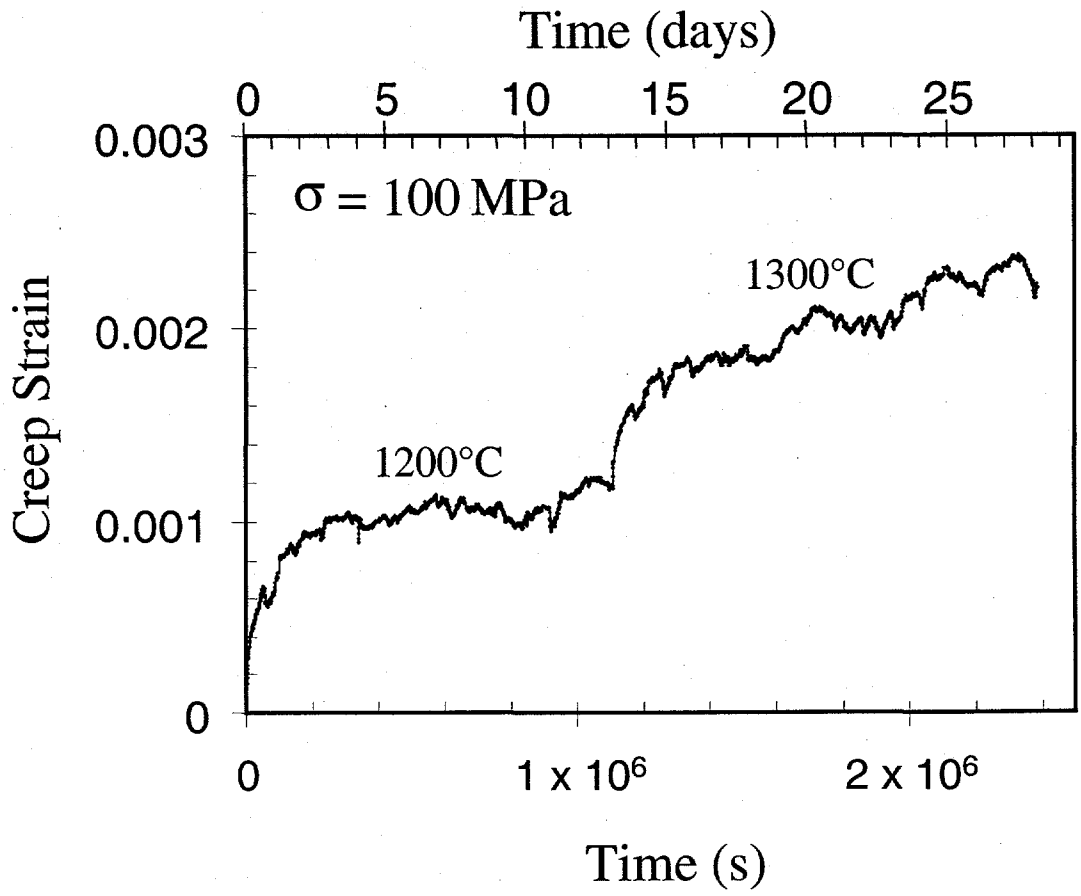

Figure 3-11: Creep curves at 1200 and 1300°C for 100 MPa. Primary creep dominates the strain for both materials.

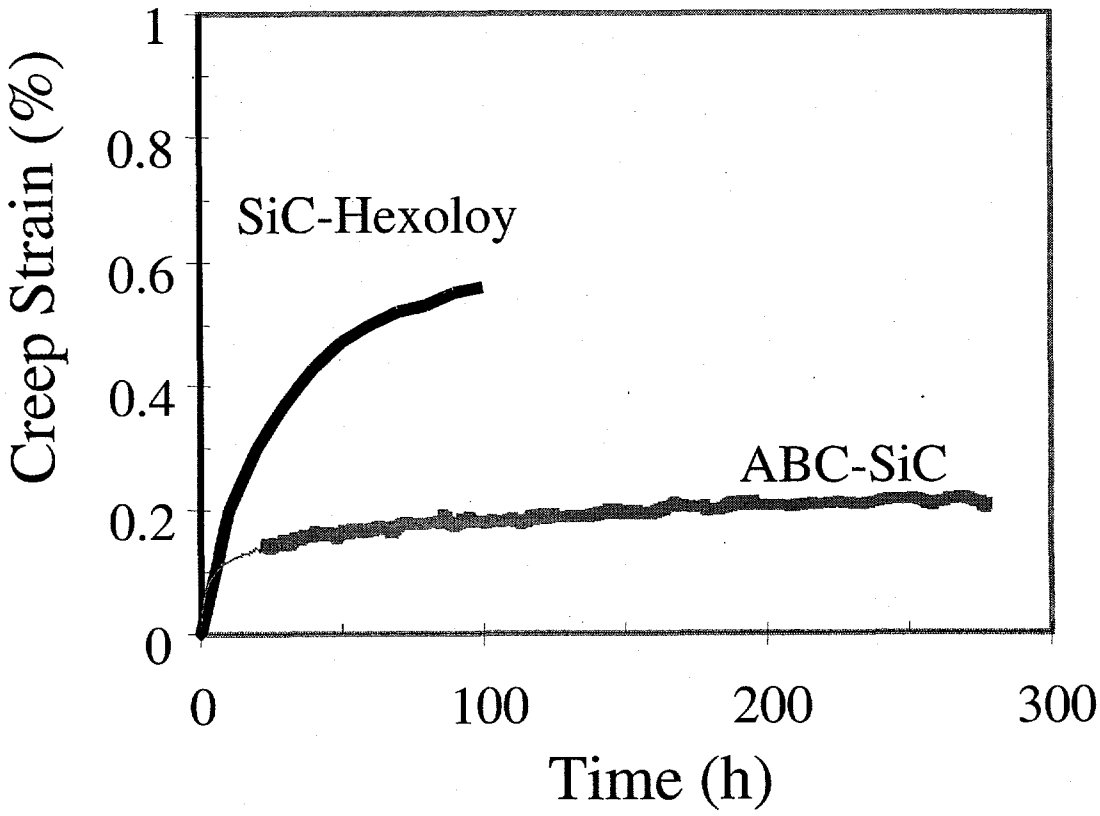

Figure 3-12: Comparison of creep curves for ABC-SiC and commercial SiC, Hexoloy.

CHAPTER 4: Steady-State Creep

4.1 Introduction

High temperature, time-dependent, deformation is characterized by three distinct regions, Figure 3-1. The first of the three regions in a creep curve is transient, or primary, creep and is characterized by a continuously decreasing strain rate. The mechanism for transient creep, as pertaining to ABC-SiC, is grain boundary sliding until the grains impinge, or become interlocked; this mechanism is similar to silicon nitrides that possess a grain boundary interlayer.[1] Various transient creep mechanisms are described in detail in Chapter 3.

After the grains impinge, a new mechanism must become operative to enable additional deformation. Mechanisms that now dominate the creep response are diffusion, dislocations, and/or cavitation. This results in a region of the creep curve where the strain rate is invariant, Figure 3.-1. This is the steady-state or minimum creep rate. Most materials exhibit a power law stress dependence, typically referred to as Norton "power law" behavior, Equation 4.1.[2]

$$\dot{\varepsilon} = \frac{AD_oGb}{kT}\left(\frac{b}{d}\right)^p\left(\frac{\sigma}{G}\right)^n \exp\left(\frac{-E_a}{RT}\right) \qquad (4.1)$$

In Equation 4.1, $\dot{\varepsilon}$ is the steady-state creep rate, A is a dimensionless constant, D_o is the diffusion frequency factor, G is the shear modulus, k is Boltzmann's constant, T is the absolute temperature, b is the Burger's vector, d is the grain size, σ is the stress, p is the exponent of the inverse grain size, n is the stress exponent, E_a is the activation energy for the diffusional process, R is the gas constant.

The activation energy E_a in the literature is generally reported from plots of log $\dot{\varepsilon}$ vs. 1/T, and the slope is equal to $-E_a/2.3R$. However, this actually represents the apparent activation energy. Calculating the activation energy in this fashion neglects the temperature dependence of the 1/kT term and the temperature dependence of the shear modulus. The true activation energy is obtained by plotting log $\dot{\varepsilon} G^{n-1} T$ vs. 1/T. The apparent activation energy is approximately the same for n = 1-2, but for large values of n the apparent activation energy is significantly higher than the true activation energy.[3]

The mechanisms of steady-state creep generally vary with the type of material, test temperature, and stress level. The various mechanisms of steady-state creep are described in the following sections, with special attention given to the dependence of stress, temperature, and grain size on the creep rates. These parameters, in conjunction with microstructural features, allow the controlling creep mechanism to be determined for a material. For materials with a grain boundary phase, such as ABC-SiC, creep is generally believed to occur by one or more of the following mechanisms: solution/precipitation,[4,5] cavitation,[6,7,8,9] and viscous flow of the glass phase.[10,1112,13,14,15,16] Additionally, diffusion mechanisms with a stress exponent of n =1 are common for creep of ceramics. This includes bulk diffusion,[17,18] grain boundary diffusion,[19] solution-precipitation,[20] and grain boundary sliding.[21] The high temperature creep of SiC (Hexoloy) (T > 1600°C) revealed that dislocation glide could be a creep mechanism.[22,23] Only the mechanisms most pertinent to the creep of ABC-SiC are presented.

4.1.1 Dislocation Creep

For metals and their alloys at intermediate to high stress, $T > \sim 0.5T_m$, creep deformation generally proceeds by a dislocation mechanism, glide or climb, controlled by either of these mechanisms.[24] For dislocation mechanisms, steady-state creep occurs when the rate of work hardening equals the rate of recovery. Dislocation multiplication and glide occur in the early stages of creep. Strain hardening is accomplished as dislocations become pinned at obstacles, such as precipitates, or are rendered sessile through dislocation-dislocation interactions. Simultaneously, recovery processes such as climb and cross-slip enable the dislocations to either be annihilated or form low energy configurations (sub-grain boundary structures). Therefore, steady-state creep occurs when the dislocation density is constant.

Numerous theoretical models have been developed for dislocation creep. Since dislocation creep involves intragranular motion of dislocation, and the grain boundaries are not involved like grain boundary sliding mechanisms, they are termed lattice mechanisms of creep. Therefore, the inverse grain size dependence, p, of Equation 4.1 is 0. The theoretical stress exponent, n, for most dislocation processes is 3-5. For the case of dislocation creep controlled by climb, the stress exponent is 4.5.[24] However, if the controlling step is glide, the stress exponent decreases to ~ 3.[25] The activation energy for such processes are lattice self-diffusion, chemical interdiffusion of solute atoms, and pipe diffusion, where mass transport occurs along the core of the dislocations. Table 4.1 compares the theoretical dependence of stress, grain size, and activation energy for the various creep mechanisms described in this section. It should be noted that it is unlikely to get a definative answer about the controlling creep mechanism (Chapter 6) from the

mechanical tests alone. Most mechanisms share one value of stress exponent, activation energy, or grain size dependence. Thus, characterization (Chapter 5) is essential to ascertain the creep mechanism(s).

4.1.2 Grain Boundary Mechanisms of Creep

In ceramics systems, the high Peierls stress, which is the inherent resistance to dislocation motion, often eliminates dislocation mechanisms except at extremely high temperatures and stresses. For $T > 0.5\ T_m$, and low stresses, creep deformation is generally controlled by bulk diffusion or grain boundary diffusion, with the latter mechanism being prevalent at lower temperatures and the former dominating creep at $\sim T > 0.7\ T_m$.[26] The non-dislocation mechanisms of creep all involve the boundaries, thus $p \neq 0$ for these deformation modes.

The various boundary mechanisms can be classified into two broad groups: Lifshitz sliding and Rachlinger sliding. In the former mechanism grain boundary sliding occurs with concomitant elongation of the grains in the tensile direction. This is illustrated schematically in Figure 4-1. In contrast, the latter mechanism grain boundary sliding is accommodated by mechanisms such as cavitation, but the grain size does not change, shown schematically in Figure 4-2. Both mechanisms involve adjacent grains becoming displaced with respect to each other.

Mechanism	Stress Exponent, n	Activation Energy, E_a	Grain Size, p
Dislocation glide and climb, controlled by climb	4.5	Lattice self diffusion	0
Dislocation glide and climb, controlled by glide	3	Chemical interdiffusion	0
Bulk diffusion	1	Lattice diffusion	2
Grain boundary diffusion	1	Grain boundary diffusion	3
Solution -precipitation	1	Heat of solution plus heat of migration	3
Grain boundary sliding with continuous glassy phase at boundary	1	grain boundary shearing	1
Sliding with grain boundary cavities	2	Lattice diffusion	2
Sliding with triple-point cavities	3.5	Lattice diffusion	2

Table 4.1: Theoretical dependence for various creep parameters of Equation 4.1.

4.1.3 Nabarro-Herring Creep (Bulk Diffusion)

At high temperatures and low stresses, grain boundary sliding is accommodated by a net flux of vacancies from regions of tensile stress to regions of compression. Therefore, an atomic flux from compressive to tensile boundaries occurs under theseconditions, Figure 4-3. When the flux of atoms is through the bulk of the grains it is termed Nabarro-Herring creep.[17,18] Materials exhibiting this type of deformation have a

stress exponent of 1. This model assumes that the grain boundaries are perfect sources and sinks of vacancies. The stress exponent may increase to 2 if this assumption does not hold.[27] The activation energy for bulk diffusion creep is simply the activation for self-diffusion. The constitutive equation for Nabarro-Herring creep is shown in Equation 4.2.

$$\dot{\varepsilon} = A\left(\frac{b}{d}\right)^{3}\left(\frac{\sigma}{G}\right)^{1}\exp\left(\frac{-E_{latt\ diff}}{RT}\right) \qquad (4.2)$$

4.1.4 Coble Creep (Grain boundary Diffusion)

A second accommodation mechanism, typically controlling creep at low stresses and $0.4\ T_m < T < 0.7\ T_m$, is grain boundary diffusion.[19] A vacancy flux from boundaries in tension to those in compression is accompanied by a flux of atoms to tensile boundaries to accommodate sliding. In contrast to Nabarro-Herring creep, the mass transport is through the grain boundaries, Figure 4-4. The activation energy is less for grain boundary diffusion than bulk diffusion due to the open structure of grain boundaries. Since the magnitude of the activation energy is related to the bond energies between the moving species and the neighboring atoms, and the open structure at grain boundaries results in fewer neighbors and fewer bonds, the activation energy for this process is lower than bulk diffusion.[28,29]

Figure 4-5 illustrates the variation in diffusion coefficient with temperature. At lower temperatures, the diffusion rate, which is the sum of both processes, is dominated by grain boundary diffusion since it has a lower activation energy. However, as the temperature increases and bulk diffusion becomes activated, this process dominates mass transport. Grain boundary diffusion still occurs in this regime, but the net flux is small since the volume of grain boundary paths is very small compared to the volume of the

bulk. Since the bulk diffusion process has a higher activation energy is drops rapidly with decreasing temperature, enabling grain boundary diffusion to become dominant at lower temperatures.

The constitutive equation for Coble creep is provided in Equation 4.3. While the equation exhibits the same stress dependency as Nabarro-Herrring creep, the activation energy and grain size dependence are different for the two mechanisms.

$$\dot{\varepsilon} = A\left(\frac{b}{d}\right)^{2}\left(\frac{\sigma}{G}\right)^{1}\exp\left(\frac{-E_{gb\,diff}}{RT}\right) \tag{4.3}$$

The parameters in the equation are the same as Equation 4.1.

4.1.5 Solution-Precipitation

A modification of Coble creep was presented by Raj[5] and by Pharr and Ashby.[4] Whereas Coble creep is defined by diffusion through the grain boundary, a solution-precipitation is defined by mass transport through the grain boundary phase. This mechanism is very common in ceramics with glassy phases at the grain boundaries. Specifically, this is very common in Si_3N_4 and is frequently verified by the presence of cavities.[30] This model assumes that grain-to-grain contact points are present in the material or develop during deformation. As grain boundary sliding occurs during the primary stage of creep, deformation proceeds until the grains make effectively hard contact and can no longer move. These high stress points result in stress enhanced dissolution; material is transported through the grain boundary interlayer to a region of low stress where it precipitates. This process is illustrated schematically in Figure 4-6.

The fundamental variation of strain rate, with appropriate parameters, is given in Equation 4.4

$$\dot{\varepsilon} = \frac{Aw\sigma\Omega^{2/3}}{d^3\eta} \tag{4.4}$$

In Equation 4.4 A is a dimensionless constant, w is the bonding phase thickness, Ω is the molar volume of the diffusing species, d is the grain size, and η is the effective viscosity. The viscosity is inversely related to the diffusivity through the Stokes-Einstein relationship, Equation 2.9. The viscosity, which is not present in the general Norton power law equation, 4.1, is introduced in the solution-precipitation model to account for the change in mass transport properties with variations in viscosity. This solution-precipitation mechanism is operative in the same temperature range as Coble creep, 0.4 $T_m < T < 0.7\ T_m$.

4.1.6 Viscous Flow

Creep by viscous flow of a grain boundary phase involves redistribution of the interlayer from boundaries in compression to those in tension, Figure 4-7. The functional dependence of strain rate, in its simplest form, is shown in Equation 4.5.[10]

$$\dot{\varepsilon} = \frac{A_1\sigma}{\eta}\left(\frac{w}{d}\right)^3 \tag{4.5}$$

The parameters are the same as for Equation 4.4. Recall, the temperature dependence of viscous flow and solution-precipitation, Equation 4.3, is incorporated into the viscosity term since viscosity is related to diffusivity. Since the thickness of the interlayer, w, is continuously decreasing, viscous flow is a transient process. For certain temperature

ranges this mechanism may account for the majority of the recorded creep curve. At temperatures below which diffusional creep processes may be activated, creep by viscous flow may be dominant.[13] However, at higher temperatures creep deformation is likely to be detected only as a large initial strain on loading.

4.1.7 Rachinger Sliding

Grain boundary sliding without simultaneous grain elongation is termed Rachinger sliding. The aforementioned creep mechanisms are all examples of Lifshitz sliding where the grain shape occurs during creep. Typically, Rachinger sliding results in cavitation at multi-grain junctions and/or two-grain junctions. Triple-point folds can also occur, but this is more specific to materials without a secondary phase, unlike ABC-SiC. Cavitation, while typically more prevalent during creep in tension than compression,[9] involves the dilation of the material to enable grain boundary sliding. In many high toughness silicon nitrides, silicate phases are present at multigrain junctions and these materials flow from cavitated regions to adjacent multigrain junctions to allow deformation, Figure 4-8. There are several cavitation mechanisms, all resulting in a stress exponent of $n \geq 2$.

4.2 Experimental Procedure

ABC-SiC samples were subjected to constant-load four-point bending at stresses ranging from 50-200 MPa, and the temperature was varied from 1100-1500°C. The stress reported is the maximum outer fiber stress at initial loading. Some stress relaxation occurs at the tensile surface as the neutral axis shifts towards the compressive side of the

beam. Likewise, the maximum stress on the compressive side increases.[31] This is caused by the inequality of the tensile and compressive response of ceramics, as detailed in Chapter 3. It should be emphasized that the redistribution results in obtaining an average value of the tensile and compressive creep properties.[32]

The temperature and stress dependence of ABC-SiC was calculated by fixing one parameter while varying the other. Tests were run until a steady-state region was apparent, and the stress dependence and thermal activation energy were calculated using these steady-state creep rates, Figure 4-9 & 4-10. The strains represented are all engineering strains, not true strains. Since the maximum strain measured was less than ~ 2%, the difference between the two values is very small. All samples were held at least 2 hours at the testing temperature prior to loading. This ensured that the system equilibrated prior to acquiring data. The beams were prepared as described in Chapter 2. Some specimens were annealed and some were tested without a heat treatment. The anneal ABC-SiC exhibited a shortened primary creep regime as the onset of steady-state can only occur once the material has a stable microstructure. The steady-state creep rates were not altered by annealing; hence, results from both types of samples are presented without distinction.

4.3 Results and Discussion

4.3.1 Creep Curves

Creep tests conducted at 1100°C, up to 150 MPa, exhibited a steady-state creep rate that is lower than can be measured with the current apparatus. Thus, the creep rate was less than 1 x 10^{-10}/sec. Similar results were obtained for tests run at 1200°C for the

same stress levels. The creep curves for 1200°C, 100 and 150 MPa, are shown in Figure 4-11. The feature that is immediately obvious from the curves is that transient creep dominates the strain. The total strain for 100 and 150 MPa was ~ 0.1 and 0.17%, respectively. The creep curves at 1100°C exhibited identical behavior to those shown for 1200°C in Figure 4-11. The noise in the data resulted from compensating for the aforementioned temperature fluctuations.

At 1300°C, the creep rates were high enough to measure with the swingarm employed in these experiments. The primary creep was again a prominent feature of the creep curve, lasting ~ 3-4 days. The creep curve measured at 85 MPa is shown in Figure 4-12. Since this was a step test, the primary regime is less than at 1200°C for the same stress. This results from the grains sliding during primary creep and thus less deformation is available after a material has been pre-stressed, as discussed in Chapter 3. The minimum creep rate, or steady-state creep rate, ranged from 3.5 x 10^{-10}/s for 1300°C, 85 MPa, up to 8 x 10^{-10}/s at 200 MPa.

Creep curves collected at 1400°C are shown in Figures 4-13 - 4-15 for 100, 150, and 200 MPa, respectively. The steady-state creep rates varied from 9 x 10^{-10}/s up to 1.7 x 10^{-10}/s for these tests. Figure 4-16 shows how the strain rate varies with strain. Similarly, representative creep curves for tests conducted at 1500°C, 50 and 100 MPa, are presented in Figures 4-17 & 4-18. The steady-state creep rates ranged from 2 x 10^{-10}/s to 4 x 10^{-10}/s for the respective stress states.

To compare the relative creep response at different temperatures the creep curves for 1200, 1300, 1400, and 1500°C, all for 100 MPa, are shown in Figure 4-19. This shows the range of creep rates experienced for ABC-SiC; the strain rates varied from

less than 1 x 10^{-10}/s at 1200°C to 5 x 10^{-9}/s at 1500°C. The creep rates measured for ABC-SiC are respectable even at 1500°C with a stress of 100 MPa.

In general, the primary creep regime lasted for ~ 3-4 days for each sample; these features were relatively independent of the test temperature and stress. Tertiary creep was not observed in any ABC-SiC creep experiment up to 1500°C and 100 MPa.

4.3.2 Stress Exponent, n

For the temperatures and stresses used in these creep experiments, the steady-state creep rate varied from less than 1 x 10^{-10}/s at 1200°C, 150 MPa, to 5 x 10^{-9}/s at 1500°C, 100 MPa. The stress dependence of creep rates for ABC-SiC was assessed by fixing the temperature and varying the stress. The results of the experiments are shown in Figure 4-20 for 1300-1500°C. Since the steady-state creep of most ceramic materials can be described by Norton power law behavior,[2] the data was fit to the following equation, 4.6,

$$\dot{\varepsilon} = A\left(\frac{\sigma}{\sigma_o}\right)^n \exp\left(\frac{-E_a}{RT}\right) \qquad (4.6)$$

where $\dot{\varepsilon}$ is the strain or creep rate, A is a constant, σ is the applied stress, σ_o is a normalizing parameter (σ_o = 1 MPa), n is the stress exponent, E_a is the apparent activation energy, R is the universal gas constant, and T is the absolute temperature. The lines on Figure 4-20 represent a least squares fit of the data, and thus the data appears to be well represented by Equation 4.6 for the range of stresses utilized in these experiments. For each temperature, the stress exponent, n, was calculated to be ~ 1. Since the tests were conducted in four-point bending, this represents an average value of the tensile, n_t, and compressive, n_c, stress exponents.[32] Likewise, the creep rates

extracted from strain vs. time plots, for example Figure 4-12, represent an average strain rate of the two components.

The creep resistance of ABC-SiC at 1400°C is comparable to or better than Si_3N_4 materials that have been published, Figure 4-21. The data is compared with Si_3N_4 and Si_3N_4/SiC nanocomposites. The creep rates at 1400°C for ABC-SiC and the Si_3N_4-8% Y_2O_3+15% SiC nanosize particles[33] are comparable at this test condition. However, they are both better than a commercial Si_3N_4 sintered with 4% Y_2O_3. It is instructive to compare creep rates of ABC-SiC with a Ni-based superalloy, Figure 4-22. The advantage of SiC in terms of creep resistance is obvious. The creep rate at 1200°C, a temperature that is relatively low for ABC-SiC, is 3 orders of magnitude lower than the single crystal superalloy. Another feature is that the superior creep resistance of ABC-SiC is enhanced as the temperature increases.

4.3.3 Apparent Activation Energy

The temperature dependence of creep for ABC-SiC was obtained by varying the temperature for a fixed outer-fiber stress. Figure 4-23 - 4-25 are plots of strain rate vs. 10^4/T. The apparent activation energy, E_a, was calculated to be ~ 225 kJ/mol for a stress of 100-200 MPa. For the range of stresses investigated, the activation energy appeared to be independent of the applied stress.

The creep data for ABC-SiC for 100 MPa, as a function of temperature, is shown in Figure 4-26 for a comparison with Si_3N_4 and Si_3N_4/SiC nanocomposites. The creep rates at 1400°C for ABC-SiC and the Si_3N_4-8% Y_2O_3+15% SiC nanocomposites are comparable. However, since creep of ABC-SiC is much less dependent on temperature, a

lower activation energy, ABC-SiC exhibits lower steady-state creep rates than Si_3N_4 as the temperature is increased to 1500°C. Another fascinating feature of ABC-SiC is that it is exhibiting comparable or better creep rates at stresses that are at a much higher percentage of its fracture strength than the silicon nitrides that it is compared against. For example, the Si_3N_4/SiC nanocomposite has a similar creep rate in bending at 1400°C, but the bend strength for this material is 895 MPa, compared to ~ 300 MPa for ABC-SiC.

4.4 Conclusions

The steady-state creep rates for ABC-SiC varied from less than 1 x 10^{-10}/s at 1200°C and 150 MPa to 5 x 10^{-9}/s at 1500°C, 100 MPa. These creep rates are comparable or better than other high strength, high toughness, silicon nitrides and even Si_3N_4/SiC nanocomposites.

The stress exponent for ABC-SiC is n =1. The stress exponent was invariant over the temperature range, 1200-1500°C, and for stresses up to 200 MPa. The apparent activation energy for creep in ABC-SiC is ~ 225 kJ/mol. The low stress exponent suggests that a diffusional mechanism is the controlling creep mechanism.

4.5 References

[1] S. M. Wiederhorn, B. J. Hockey, D. C. Cranmer, and R. Yeckley, "Transient Creep Behaviour of Hot Isostatically Pressed Silicon Nitride," *J. Mat. Sci.*, **28** [2] 445-53 (1993).

[2] F.H. Norton, *The Creep of Steel at High Temperatures.* McGraw-Hill, New York, 1929.

[3] W.R. Cannon and T.G. Langdon, "Review: Creep of Ceramics, Part 1, Mechanical Characteristics," *J. Mat. Sci.*, **18** 1-50 (1983).

[4] G.M. Pharr and M.F. Ashby, "On Creep Enhanced by a Liquid Phase," *Acta Metall.*,**31**, 129-38 (1983).

[5] R. Raj, "Creep in Polycrystalline Aggregates by Matter Transport Through a Liquid Phase," *J. Geophys. Res.*, **87**, 4731-39 (1982).

[6] J.-L. Ding, K. C. Liu, K. L. More, and C. R. Brinkman, "Creep and Creep Rupture of an Advanced Silicon Nitride Ceramic," *J. Am. Ceram. Soc.*, **77** [4] 867-74 (1994).

[7] M. N. Meno, H. T. Fang, D. C. Wu, M. G. Jenkins, M. K. Ferber, K. L. More, C. R. Hubbard, and T. A. Nolan, "Creep and Stress Rupture Behavior of an Advanced Silicon Nitride: Part I, Experimental Observations," *J. Am. Ceram. Soc.*, **77** [5] 1217-27 (1994).

[8] M. N. Meno, H. T. Fang, D. C. Wu, M. G. Jenkins, and M. K. Ferber, "Creep and Stress Rupture Behavior of an Advanced Silicon Nitride: Part II, Creep Rate Behavior," *J. Am. Ceram. Soc.*, **77** [5] 1228-34 (1994).

[9] W. E. Luecke, S. M. Wiederhorn, B. J. Hockey, R. F. Drause, Jr., and G.G. Long, "Cavitation Contributes Substantially to Tensile Creep in Silicon Nitride," *J. Am. Ceram. Soc.*, **78** [8] 1085-96 (1995).

[10] D.C. Drucker, "Engineering and Continuum Aspects of Hight-Strength Materials," pp. 795-833 in *High Strength Materials.* Edited by V.F. Zackay. Wiely, New York, 1965.

[11] J.R. Dryden, D. Kucerovshy, D.S. Wilkinson, and D.F. Watt, "Creep Deformation Due to a Viscous Grain Boundary Phase," *Acta Metall.*,**37**, 2007-15 (1989).

[12] M. M. Chadwick, D. S. Wilkinson, and J. R. Dryden, "Creep Due to a Non-Newtonian Grain Boundary Phase," *J. Am. Ceram. Soc.*, **75** [9] 2327-34 (1992).

[13] M. M. Chadwick, R. S. Jupp, and D. S. Wilkinson, "Creep Behavior of a Sintered Silicon Nitride," *J. Am. Ceram. Soc.*, **76** [2] 385-96 (1993).

[14] C. J. Gasdaska, "Tensile Creep in an in Situ Reinforced Silicon Nitride," *J. Am. Ceram. Soc.*, **77** [9] 2408-18 (1994).

[15] J. R. Dryden and D. S. Wilkinson, "Three-Dimensional Analysis of the Creep Due to a Viscous Grain Boundary Phase," *Acta Mater.*, **45** [3] 1259-73 (1997).

[16] Q. Jin, X. -G. Ning, D. S. Wilkinson, and G. C. Weatherly, "Redistribution of a Grain-Boundary Glass Phase during Creep of Silicon Nitride Cermaics," *J. Am. Ceram. Soc.*, **80** [3] 685-91 (1997).

[17] F.R.N. Nabarro, "Deformation of Crystals by the Motion of Single Ions," pp. 75-90 in *Report of a Conference on Strength of Solids* (H.H. Wills Physical Laboratory, University of Bristol, July 7-9, 1947). Physical Society, London, U.K., 1948.

[18] C. Herring, "Diffusional Viscosity of a Polycrystalline Solid," *J. Appl. Phys.*, **21**, 437-45 (1950).

[19] R.L. Coble, "A Model for Boundary Diffusion Controlled Creep in Polycrystalline Materials," *J. Appl. Phys.*, **34** [6], 1679-82 (1963).

[20] R. Raj and C. K. Chyung, "Solution-Precipitation Cree in Glass Ceramics," *Acta Metall.*,**29**, 159-66 (1981).

[21] W.R. Cannon and T.G. Langdon, "Review: Creep of Ceramics," *J. Mat. Sci.*, **18** 1-50 (1983).

[22] J. E. Lane, C.H. Carter, and R. F. Davis, "Kinetics and Mechanisms of High Temperature Creep in Silicon Carbide: III, Sintered α-Silicon Carbide," *J. Am. Ceram. Soc.*, **71** [4] 281-95 (1988).

[23] R. D. Nixon and R. F. Davis, "Diffusion-Accommodated Grain Boundary Sliding and Dislocation Glide in the Creep of Sintered Alpha Silicon Carbide," *J. Am. Ceram. Soc.*, **75** [7] 1786-95 (1992).

[24] J. Weertman, " Steady-State Creep Through Dislocation Climb," *J. Appl. Phys.*, **28** [3] 362-4 (1957).

[25] J. Weertman, *J. Appl. Phys..*, **28** 1185 (1957).

[26] R. W. Evans and B. Wilshire, *Introduction to Creep*, The Institute of Materials, London, (1993).

[27] B. Burton, *Mater. Sci. Eng.*,**10** [9] (1972).

[28] D. A. Porter and K. E. Easterling, *Phase Transformations in Metals and Alloys,* Chapman and Hall, London (1992).

[29] P. G. Shewmon, *Diffusion in Solids,* J. Williams Book Company, Jenks, OK. (1983).

[30] D. C. Cranmer, B. J. Hockey, and S. M. Wiederhorn, "Creep and Creep-Rupture of HIP-ed Si_3N_4," *Ceram. Eng. Sci. Proc.*, **12** [9-10] 1862-72 (1991).

[31] T. -J. Chuang and S. M. Wiederhorn, "Damage-Enhance Creep in a Siliconized Silicon Carbide: Mechanics of Deformation," *J. Am. Ceram. Soc.*, **71** [7] 595-601 (1988).

[32] T. -J. Chuang, "Estimation of Power-Law Creep Parameters From Bend Test Data," *J. Mat. Sci.*, **21** 165-75 (1986).

[33] A. Rendtel, H. Hubner, M. Herrmann, and C. Schubert, "Silicon Nitride/Silicon Carbide Nanocomposites Materials: II, Hot Strength, Creep, and Oxidation Resistance," *J. Am. Ceram. Soc.*, **81** [5] 1109-20 (1998).

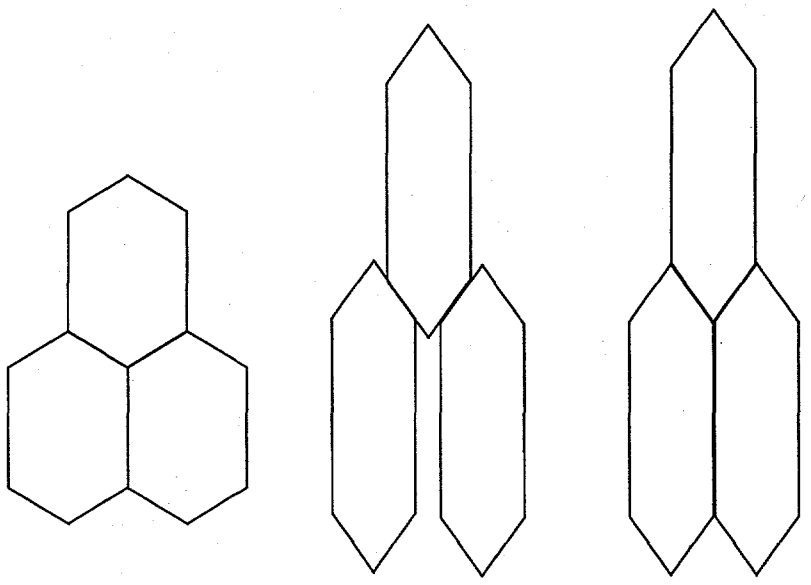

Figure 4-1: Schematic diagram illustrating the necessity of grain boundary sliding when diffusional creep mechanism are operative. Diffusional creep of the grains in (a) results in elongated grains, (b). To avoid large cavitation grain boundary sliding is necessary. The converse is also true. Creep can proceed by grain boundary sliding accommodated by diffusion.

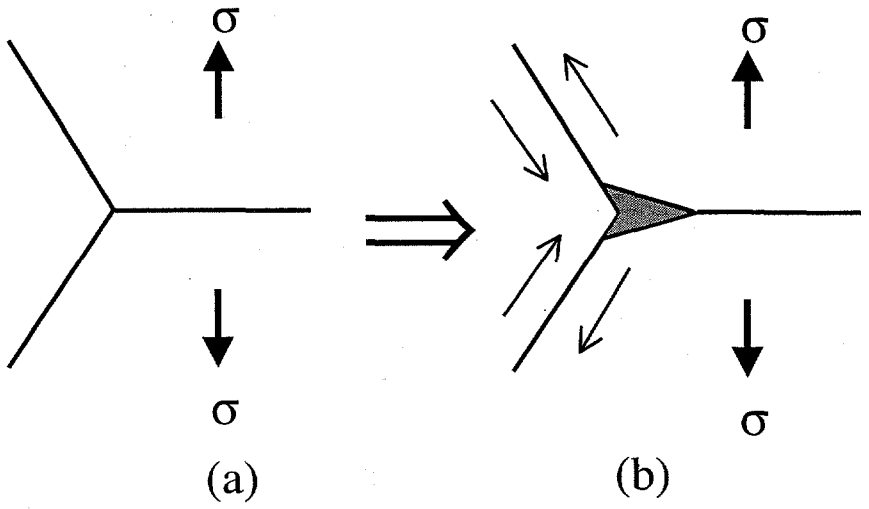

Figure 4-2: Schematic diagram demonstrating how cavities can form at triple-points when grain boundary sliding occurs. (a) shows a triple point subjected to a stress, and (b) shows a triple-point cavity that nucleated in response for the indicated sliding directions.

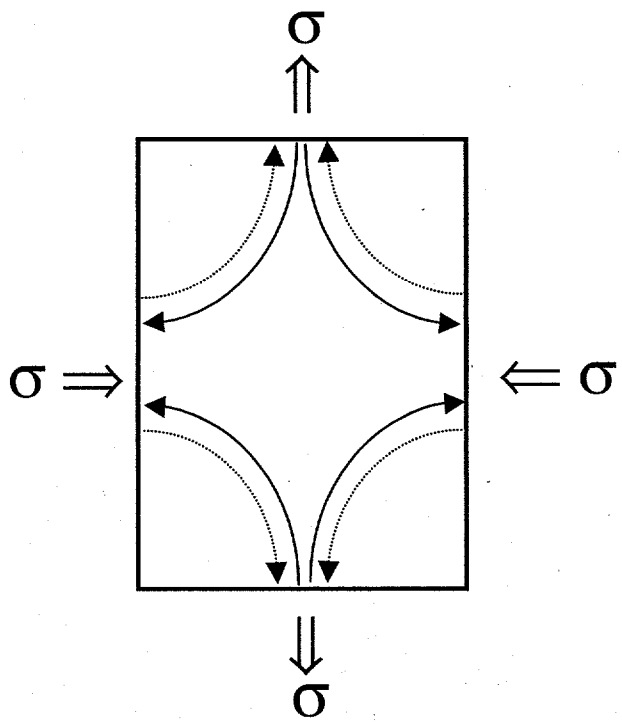

Figure 4-3: Schematic diagram illustrating Nabarro-Herring creep. The solid arrows represent the direction of vacancy flow and the dashed arrows show the direction of atom movement.

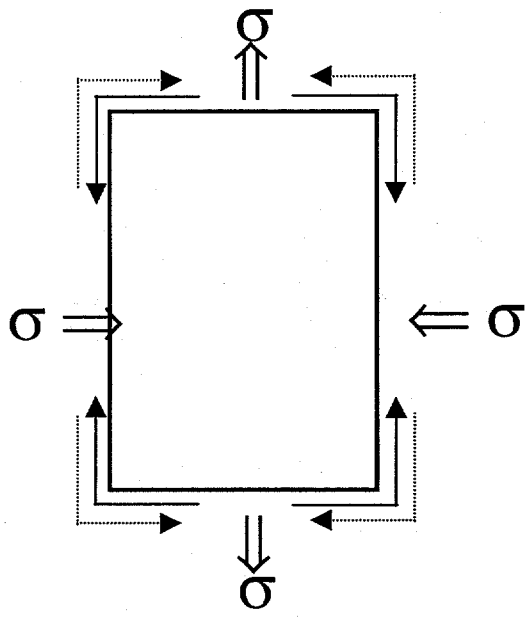

Figure 4-4: Schematic diagram illustrating Coble creep. The solid arrows represent the direction of vacancy flow and the dashed arrows show the direction of atom movement. In contrast to Nabarro-Herring creep, diffusion is along the grain boundaries.

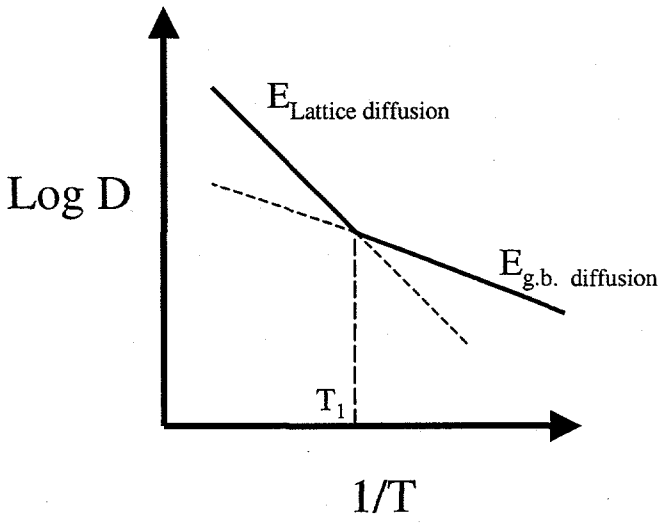

Figure 4-5: Schematic diagram illustrating how the diffusion coefficient, D, changes with temperature. At high temperatures bulk diffusion dominates since the volume of diffusion paths is much greater than the volume in the grain boundaries. However, bulk diffusion shows a stronger temperature dependence, higher E_a, and therefore grain boundary diffusion is the dominant mechanism at lower temperatures.

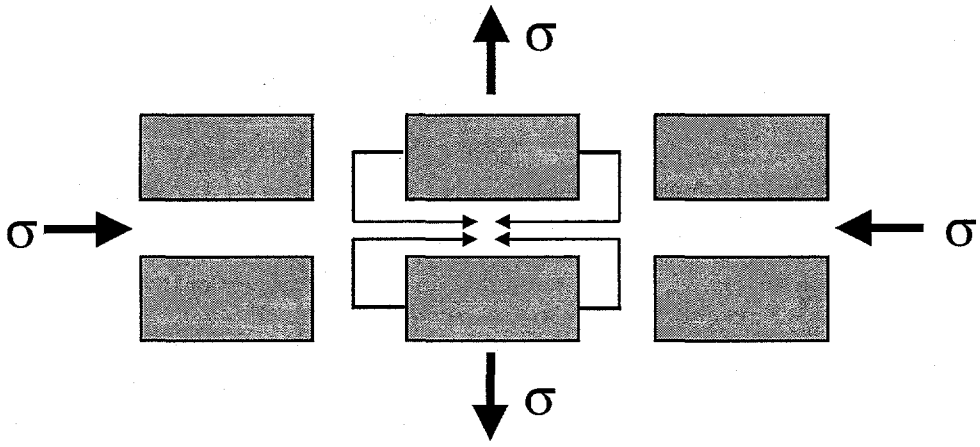

Figure 4-6: Schematic diagram showing a solution-precipitation process. Material is removed from boundaries in compression, diffuses through the grain boundary layer and precipitates at a boundary in tension.

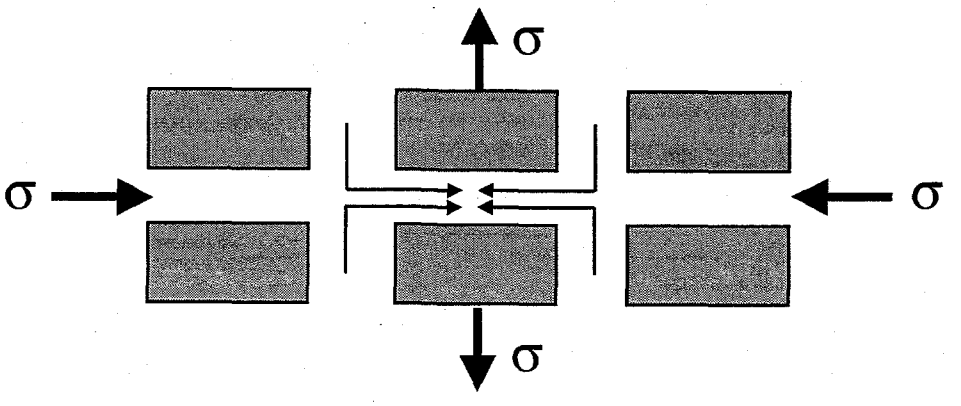

Figure 4-7: Schematic diagram illustrating a viscous flow creep mechanism. The glassy grain boundary phase is redistributed from boundaries in compression to those in tension.

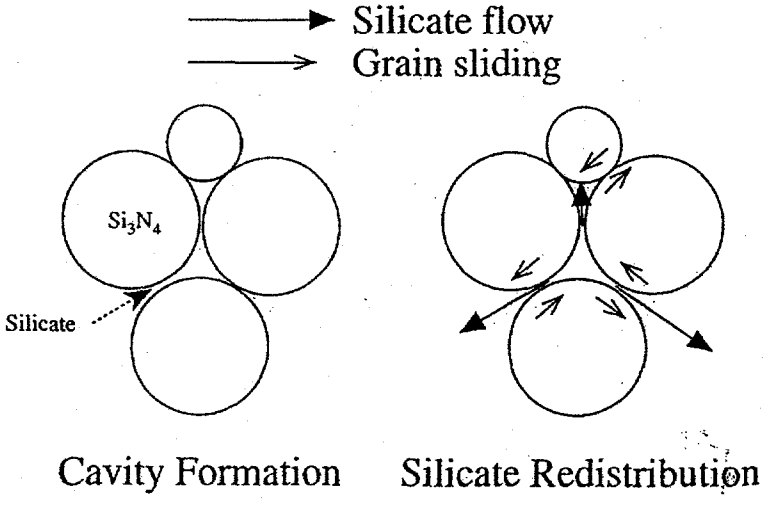

Figure 4-8: Schematic diagram showing the redistribution of a silicate phase at multi-grain junctions during cavitation.

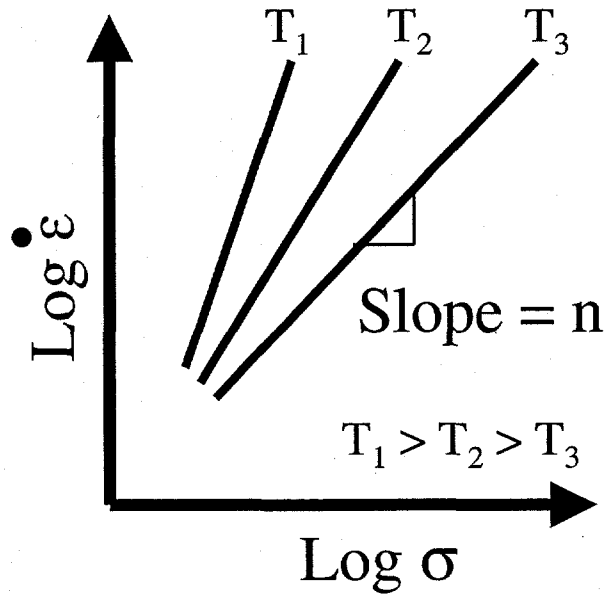

Figure 4-9: Schematic diagram demonstrating how the stress exponent, n, is calculated from the creep data. This case shows and example of n increasing with increasing temperature. For cases where n does not change, the higher temperature lines simply sit at higher strain rates and possess the same slope.

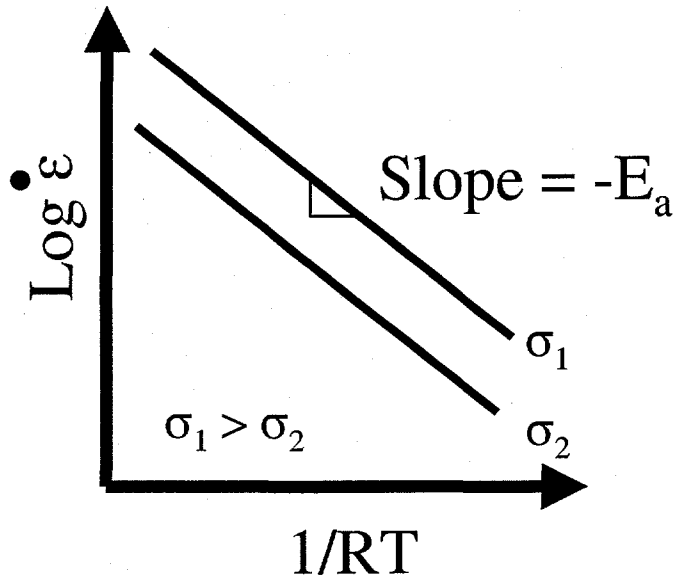

Figure 4-10: Schematic diagram showing how the activation energy, E_a, is calculated. The figures illustrates a constant activation energy over the temperature range.

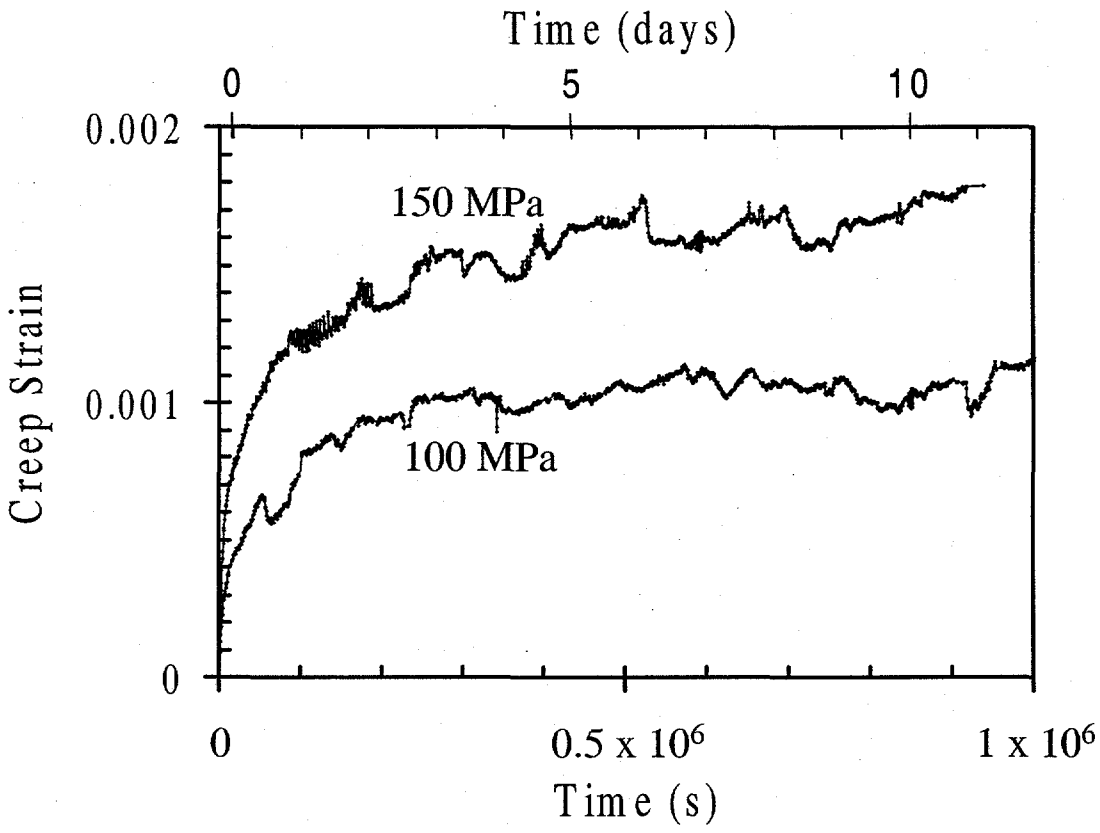

Figure 4-11: Creep curves for 1200°C, 100 and 150 MPa. Higher stresses result in larger primary creep strains.

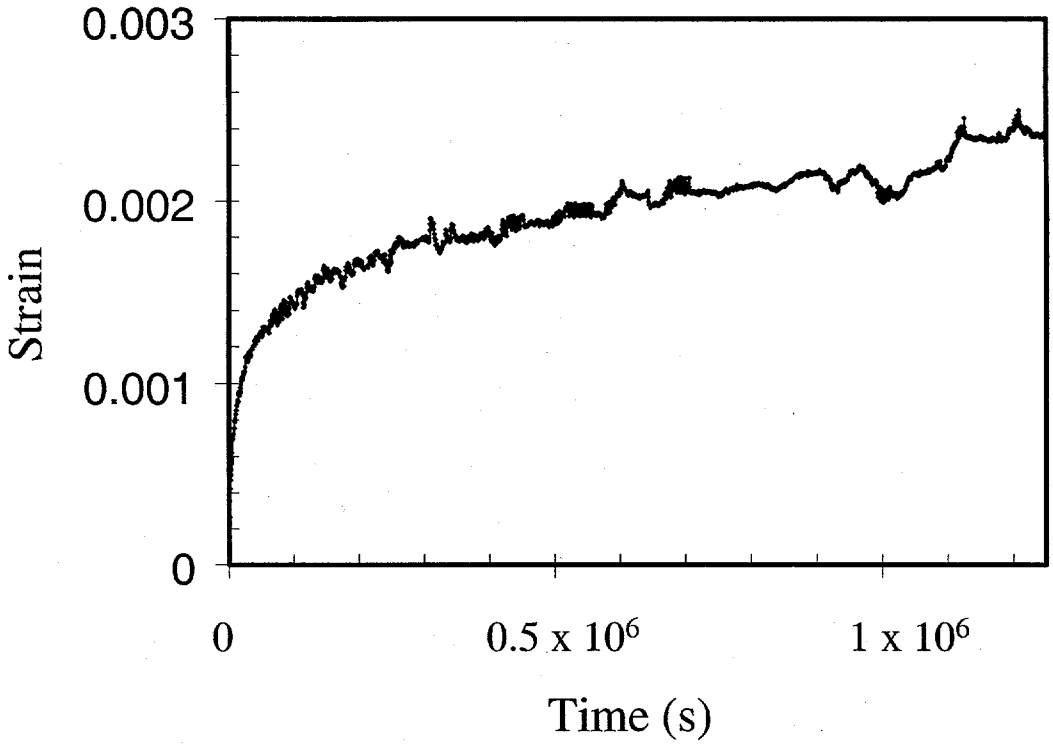

Figure 4-12: Creep curves for 1300°C, 85 MPa. The primary creep regime lasted approximately 3-4 days.

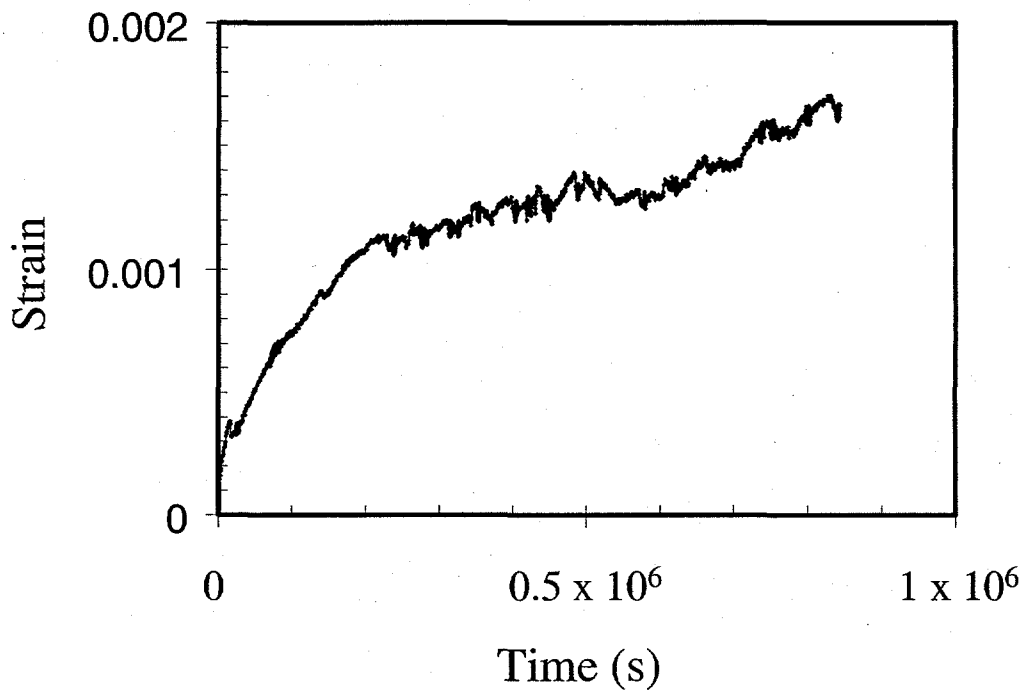

Figure 4-13: Creep curve for 1400°C, 100 MPa.

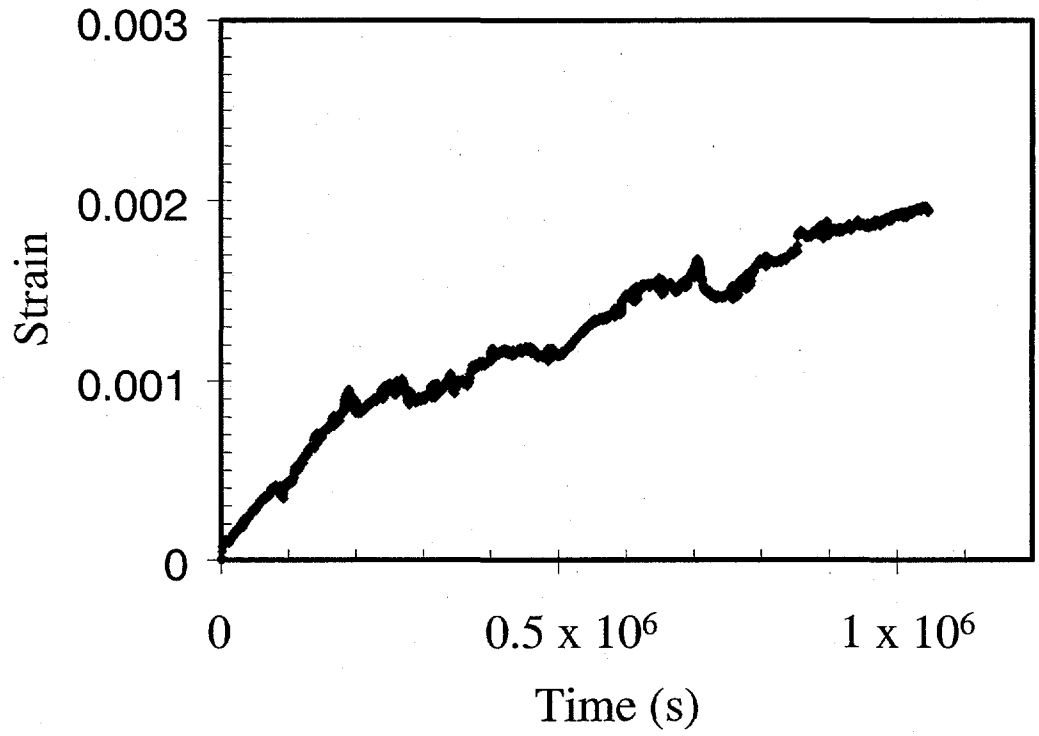

Figure 4-14: Creep curve for 1400°C, 150 MPa.

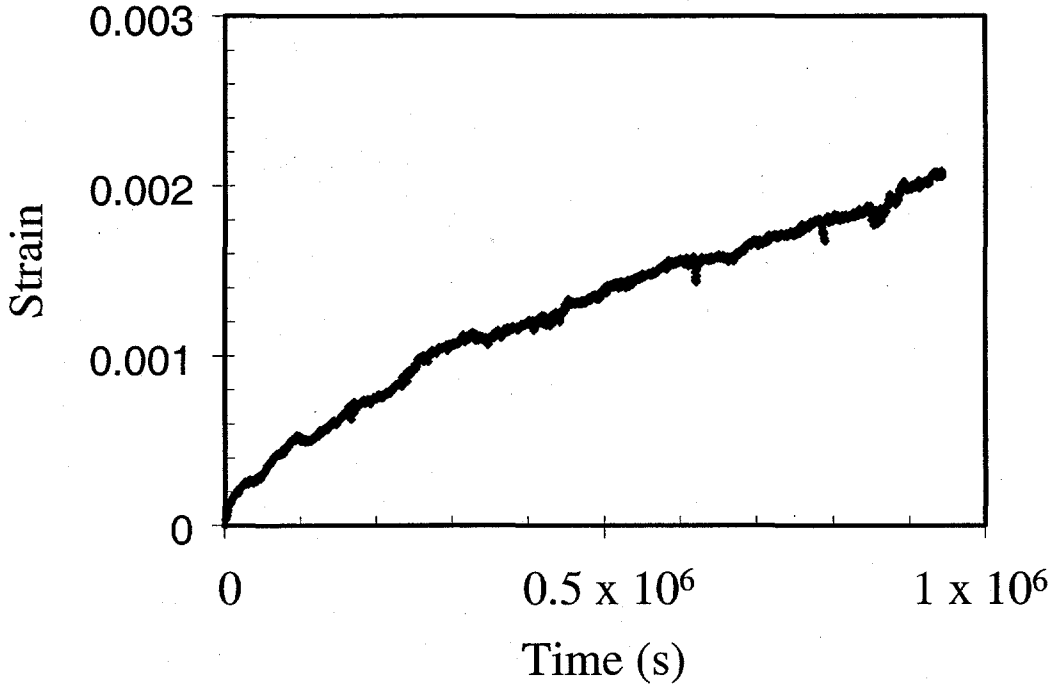

Figure 4-15: Creep curve for 1400°C, 200 MPa.

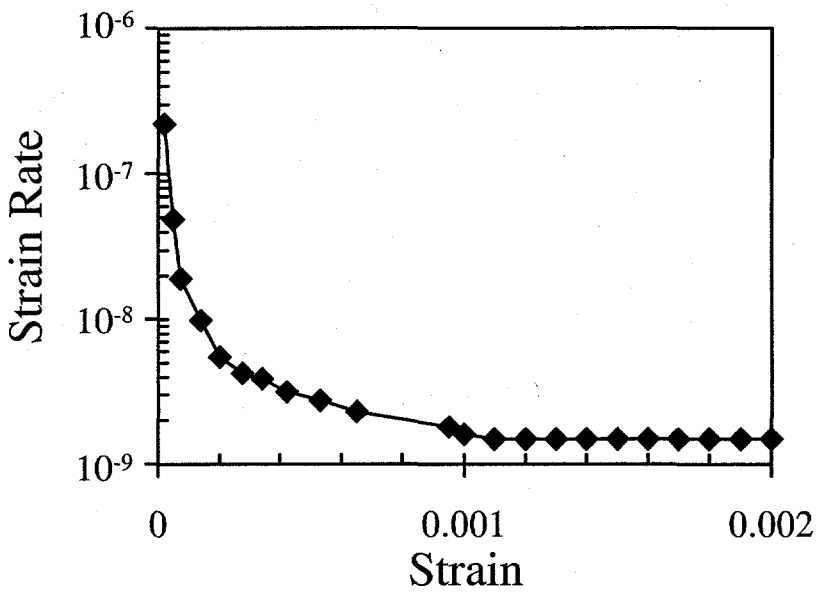

Figure 4-16: Strain rate as a function of strain for the creep curve in Figure 4-15. This curve is representative of all creep experiments. The strain rate decreased until a steady-state was observed.

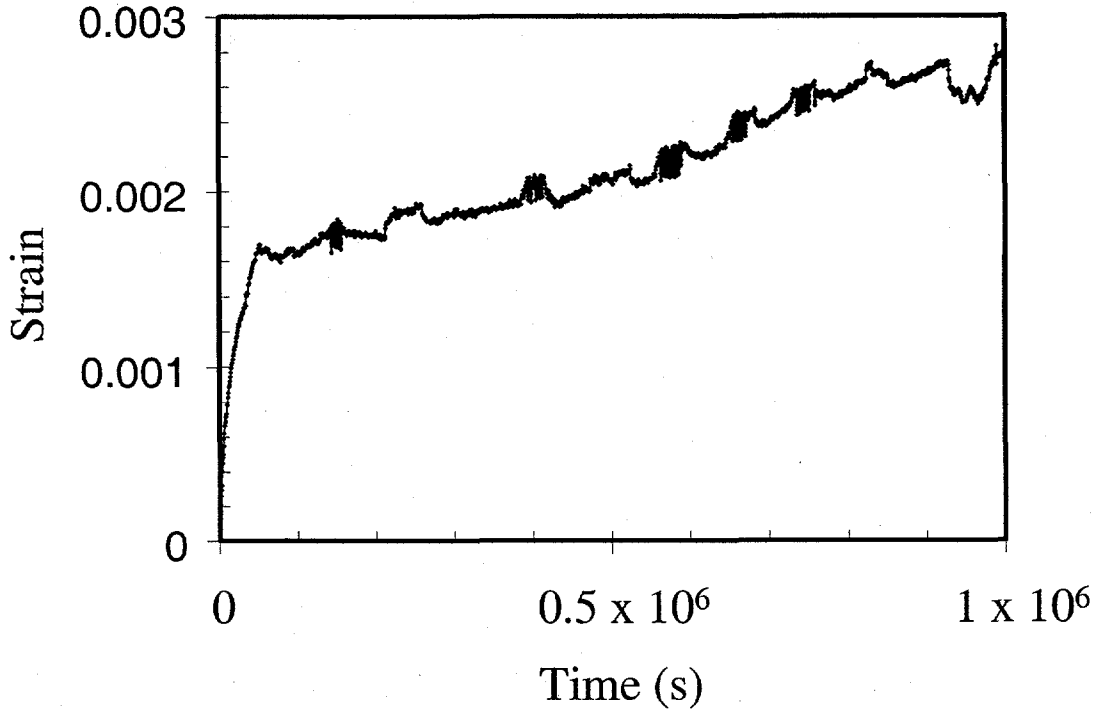

Figure 4-17: Creep curve for 1500°C, 50 MPa.

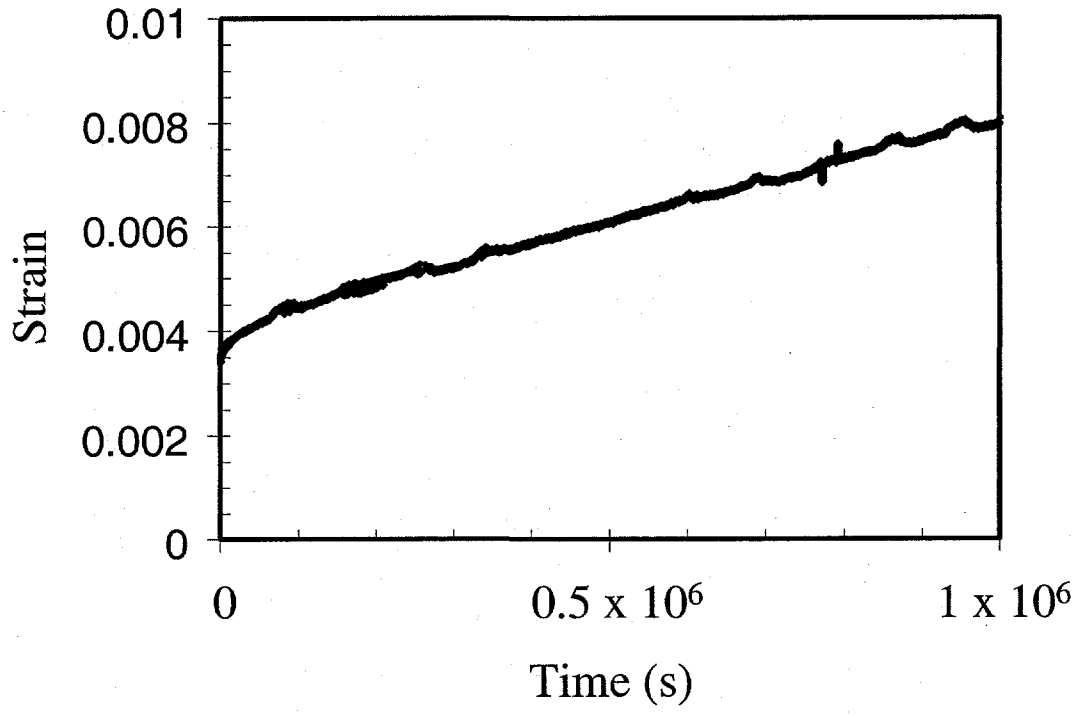

Figure 4-18: Creep curve for 1500°C, 100 MPa.

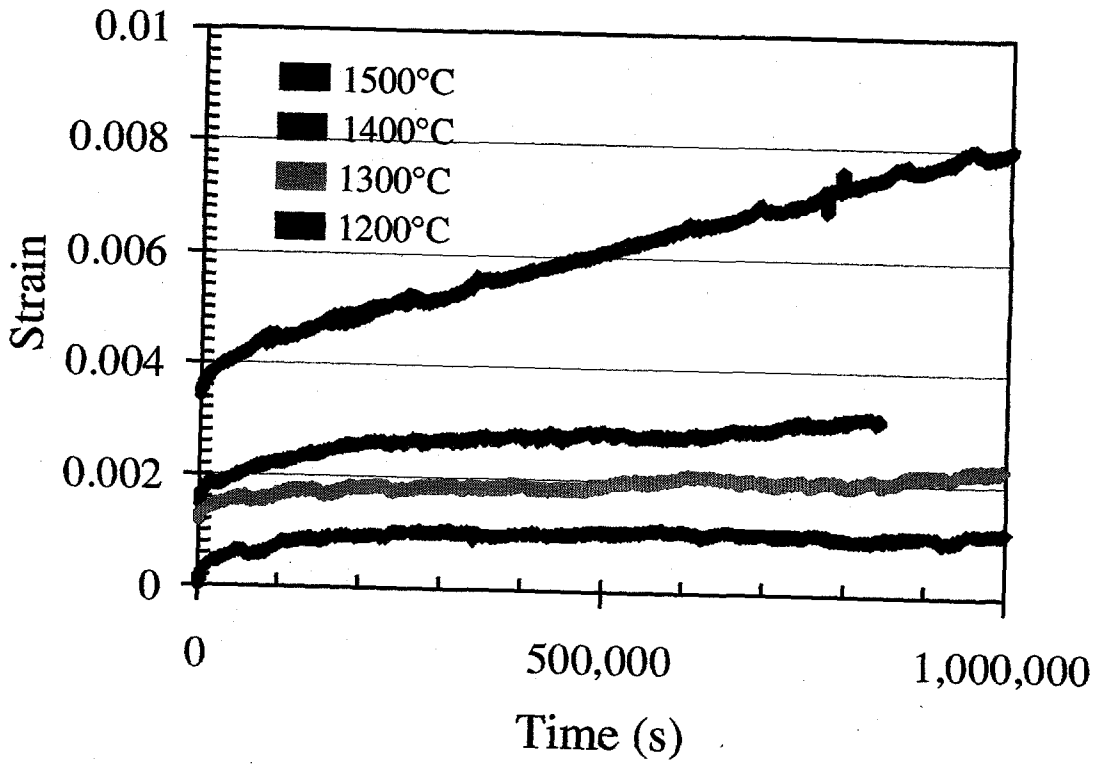

Figure 4-19: Creep curve for 1200-1500°C, 100 MPa.

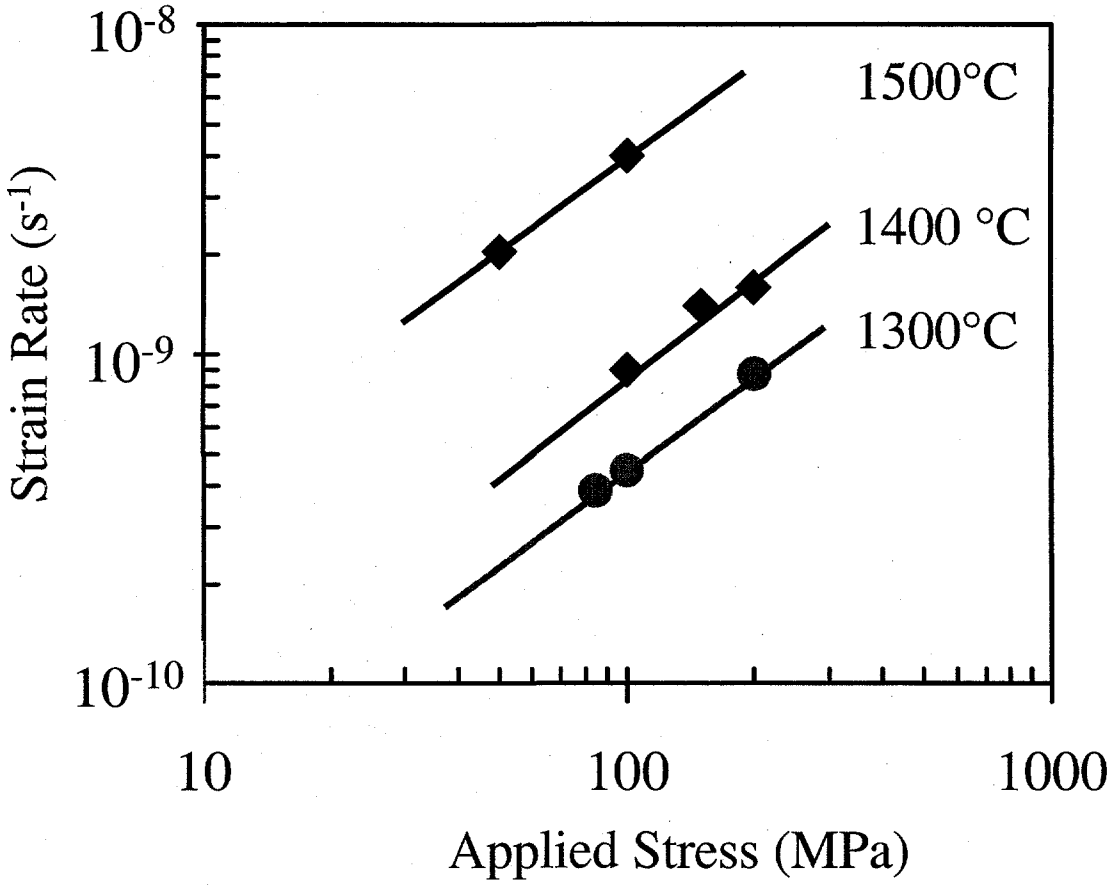

Figure 4-20: Stress exponent data for ABC-SiC. For 1300-1500°C, the stress exponent was ~ 1. This suggests that a diffusional creep mechanism is present.

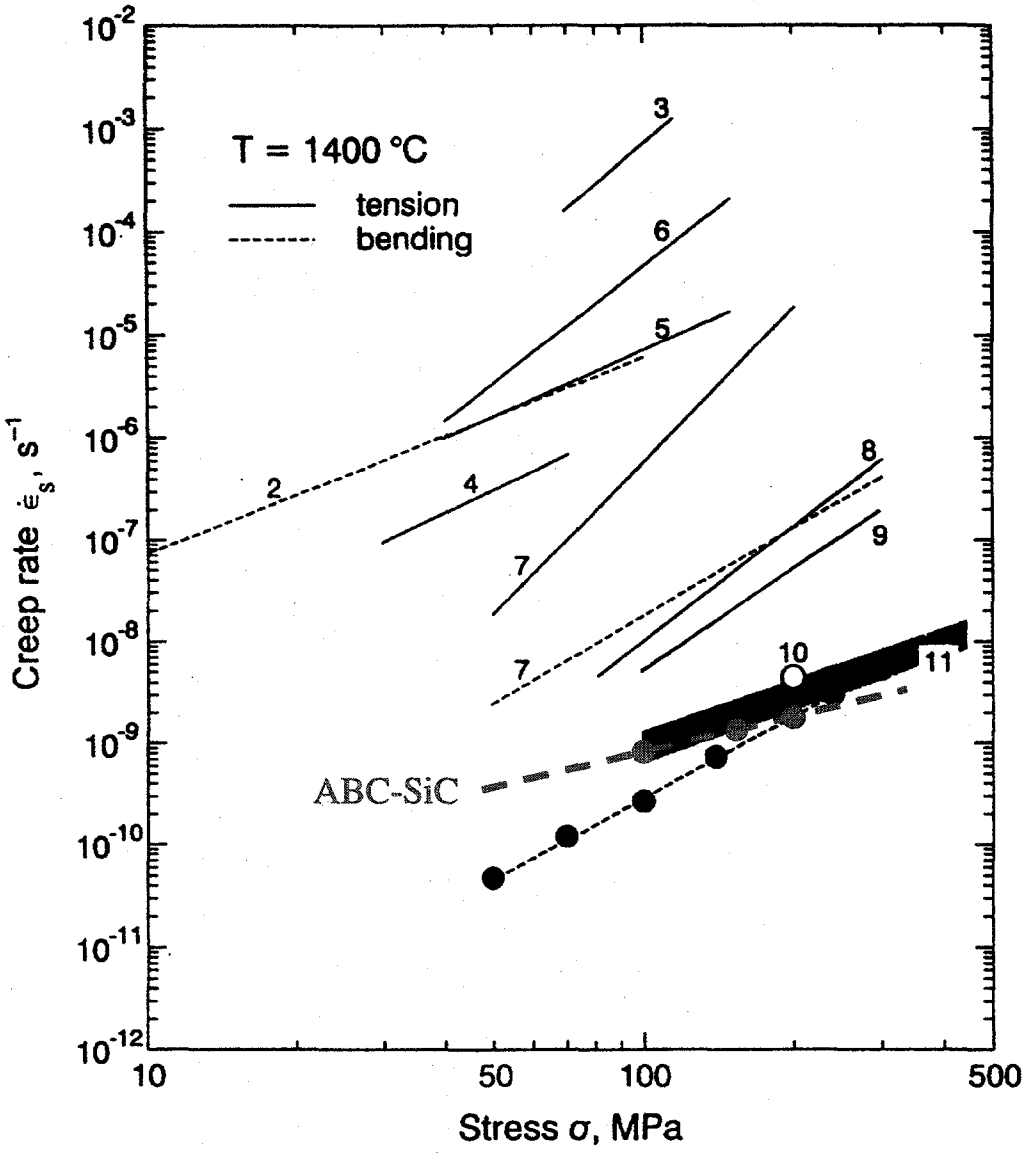

Figure 4-21: Comparison of ABC-SiC and various silicon nitrides and silicon nitride/silicon carbide nanocomposite creep rates. All creep tests conducted at 1400°C. Curves 1-11 are for various grades of silicon nitride. See ref. 33 for the specifics of these materials. ABC-SiC is in red.

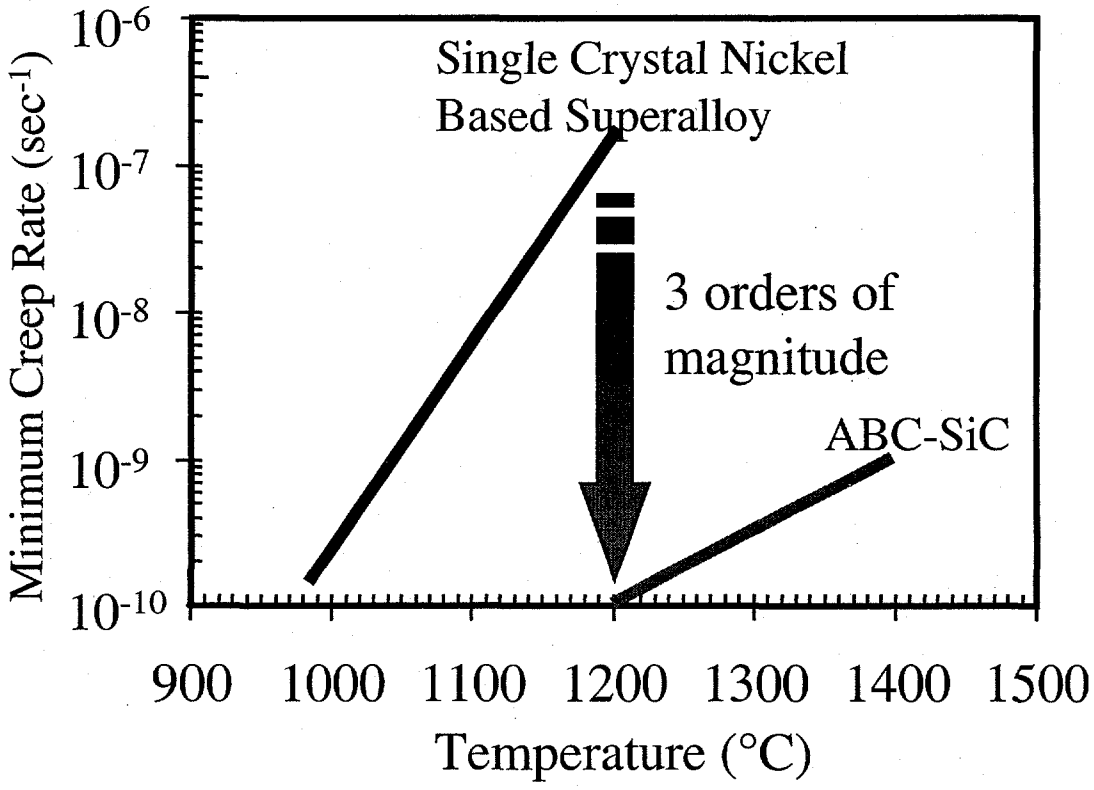

Figure 4-22: Comparison of ABC-SiC and a single-crystal Ni-based superalloy.

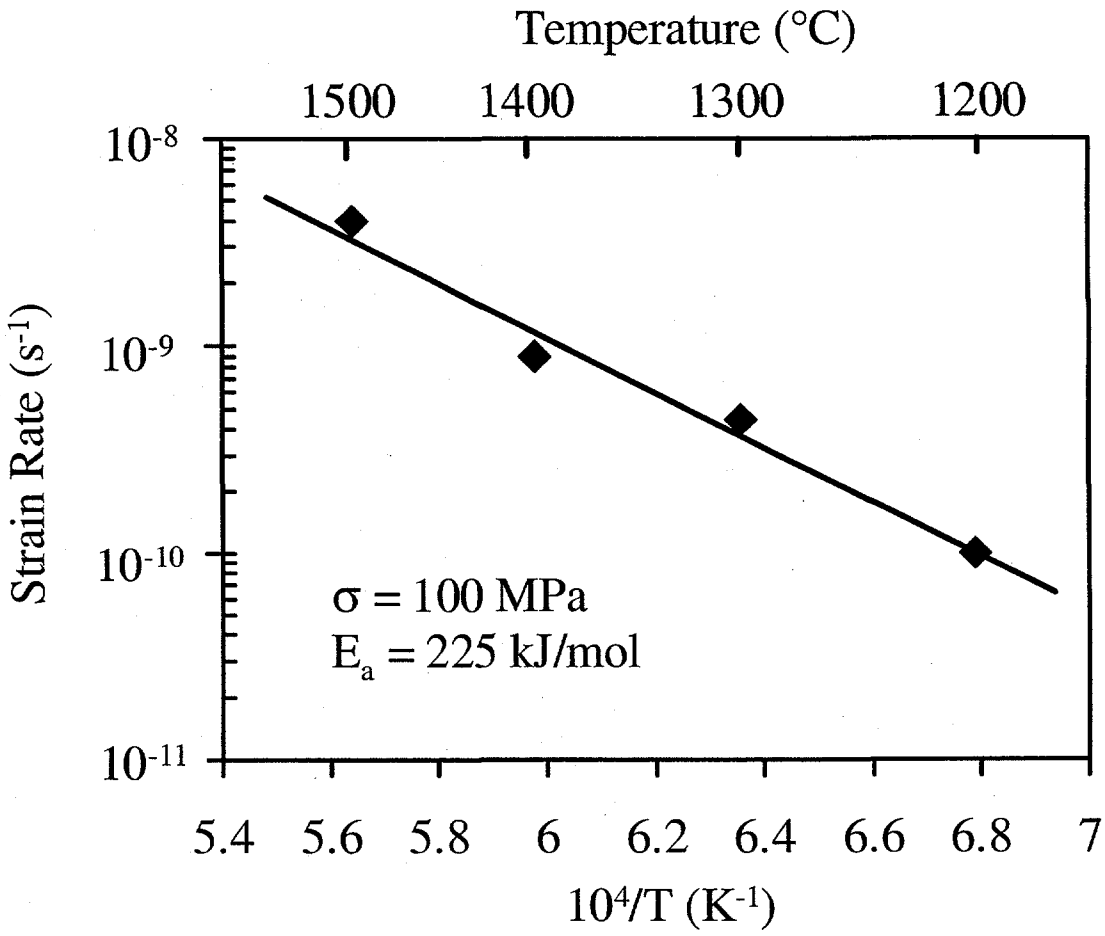

Figure 4-23: Activation energy for ABC-SiC for 100 MPa.

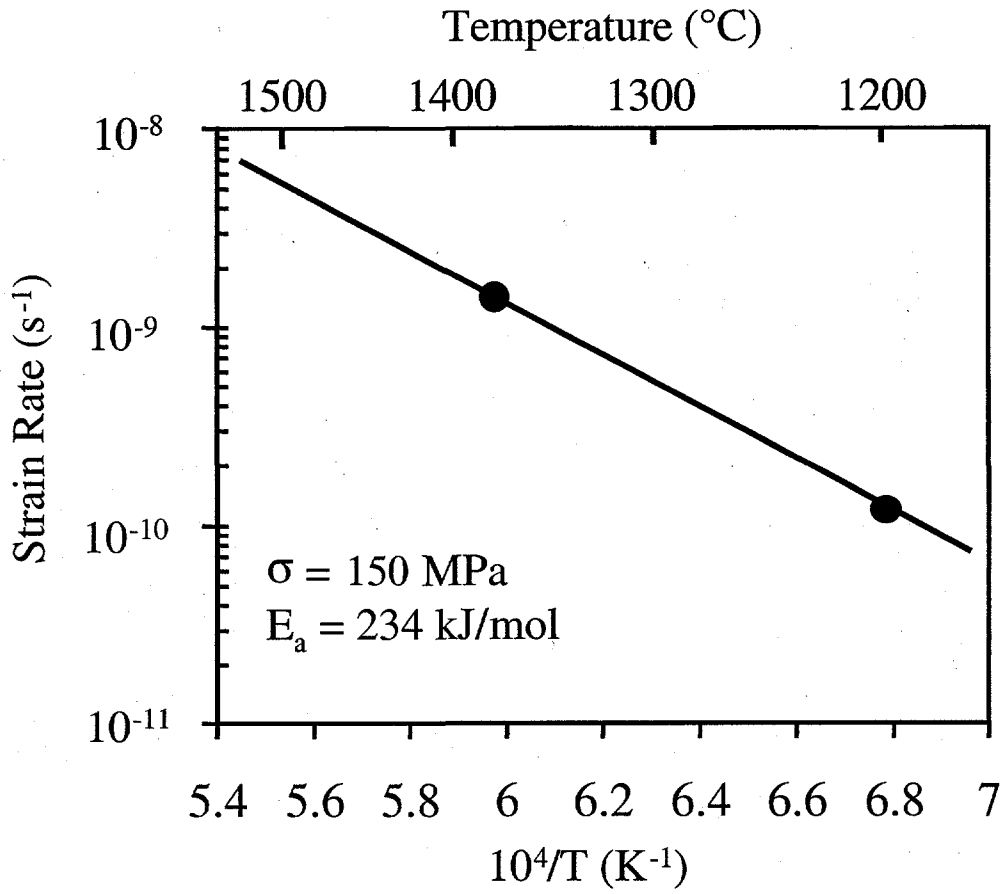

Figure 4-24: Activation energy for ABC-SiC for 150 MPa.

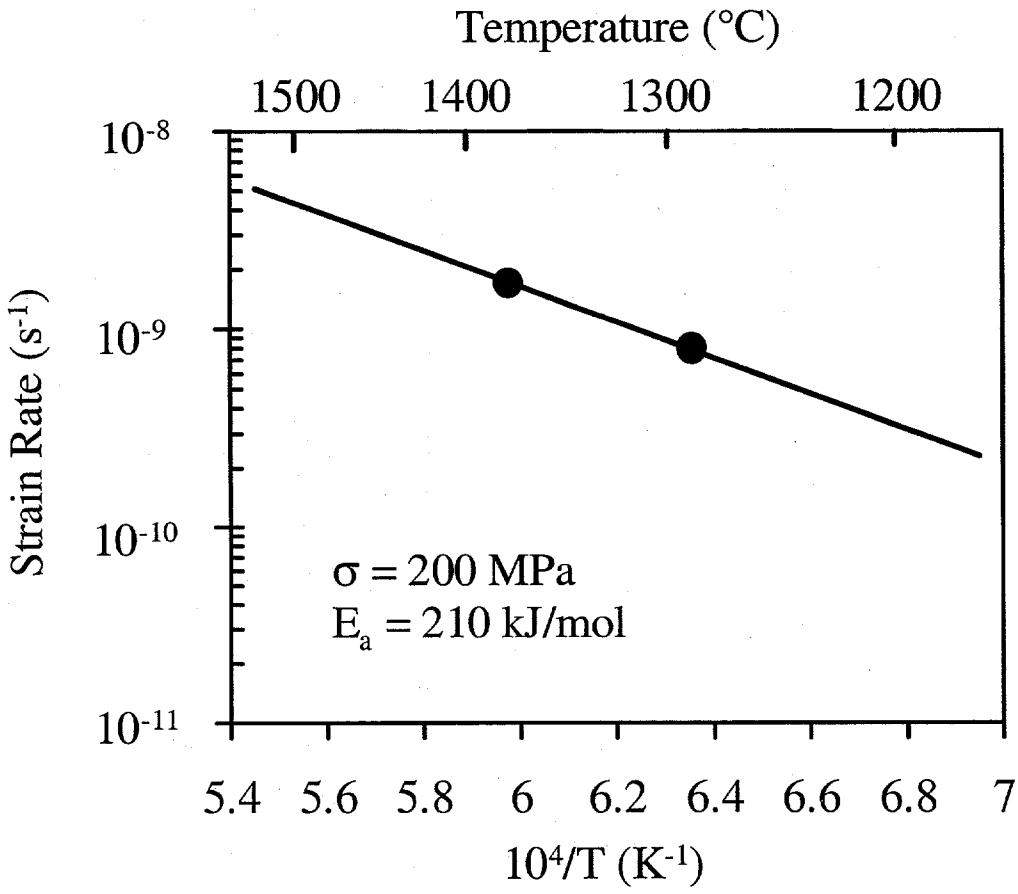

Figure 4-25: Activation energy for ABC-SiC for 200 MPa.

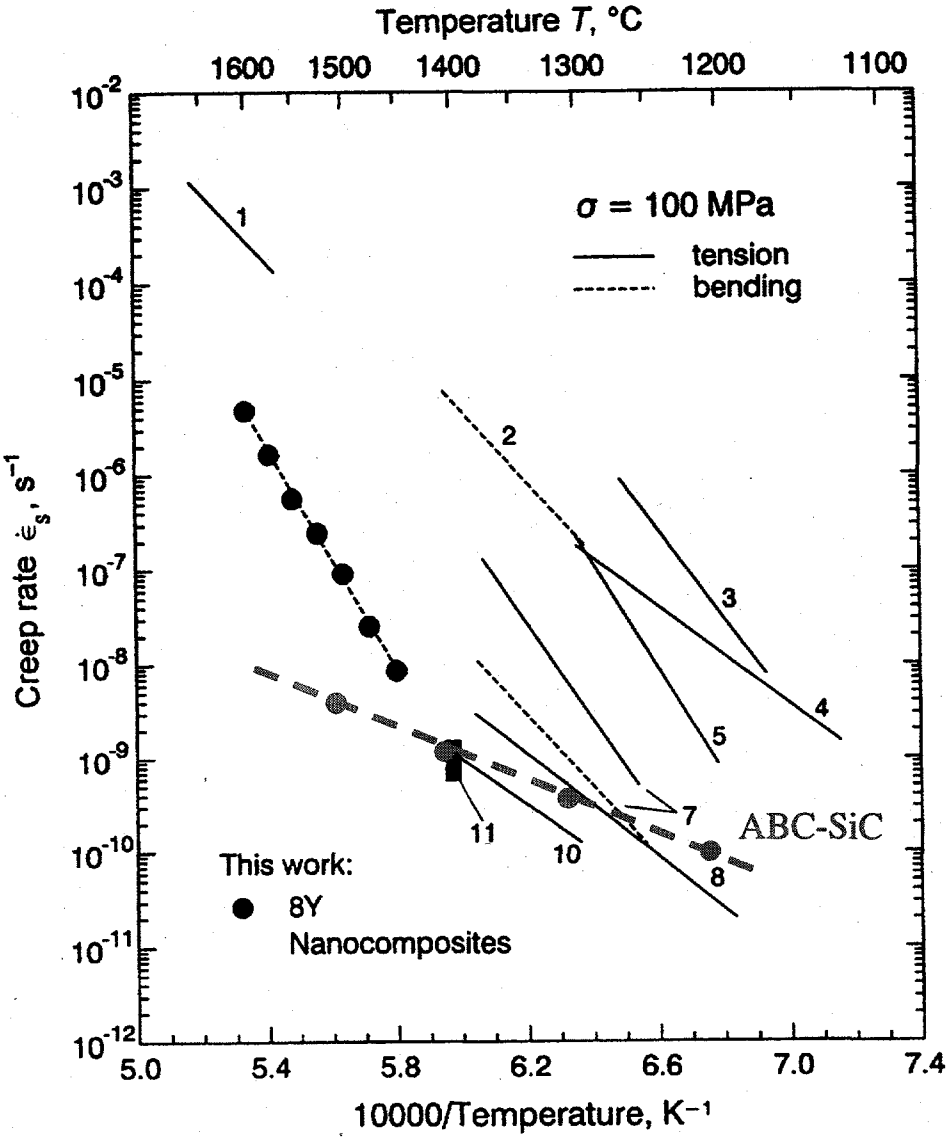

Figure 4-26: Comparison of ABC-SiC, silicon nitrides, and silicon nitride/silicon carbide nanocomposite creep rates and activation energies. All creep tests were performed at 100 MPa. Curves 1-11 are for various grades of silicon nitride. See ref. 33 for the specifics of these materials. ABC-SiC is in red.

CHAPTER 5: Microstructural Changes During Creep

5.1 Introduction

Evaluation of the creep response of a material generally involves determining the creep rates at steady-state and the operative creep mechanism(s), including the controlling creep mechanism. Also, the amount of primary creep and the creep rupture data, where the lifetime for various stress levels is established, are critical parameters in characterizing the high temperature response of a material. Primary creep of ABC-SiC was presented in Chapter 3 and creep rupture data was not collected due to the exceedingly long times to failure for the stress levels utilized in the current study. In silicon nitride, tests are sometimes conducted for several thousand hours to obtain creep rupture data.[1] Since we can only test one sample at a time, the creep rupture data of ABC-SiC was not collected.

The steady-state creep rates were evaluated for ABC-SiC, and these values were used to determine the functional dependence of these rates, Chapter 4. ABC-SiC followed a Norton power law behavior, and the stress exponent was calculated to be $n \sim 1$. Additionally, the temperature dependence was investigated and the apparent activation energy was $E_a \sim 225$ kJ/mol. These values are critical in evaluating the controlling creep mechanism, but it is not uncommon for several of the parameters from the power law behavior, such as stress exponent and activation energy, to be shared by more than one mechanism, as shown in Table 4.1. Therefore, determination of the controlling creep mechanism is only possible by correlating the mechanical data from the creep tests with microstructural features after creep.

Characterization of dislocations, stacking faults, cavities, and changes in the grain size, etc. facilitates determination of the creep mechanisms. Clearly, if a high stress exponent is observed for a material, which could be a dislocation mechanism[2] or cavitation mechanism,[3] characterization can clearly distinguish if one or both of these mechanisms is present. Additionally, the nature of the grain boundaries, both the structure and chemistry, was characterized since the properties of these interlayers typically dominates the high temperature properties of ceramics like ABC-SiC.

The following sections provide a characterization of ABC-SiC before and after creep. The microstrucutral features pertinent to ascertaining the creep mechanism(s) in ABC-SiC are presented.

5.2 Experimental Procedure

Characterization was performed in a scanning electron microscope (SEM) to evaluate surfaces and fracture surfaces before and after creep experiments. Energy dispersive spectrometry (EDS) was performed to evaluate the chemical content of features. The microstructure was also evaluated by transmission electron microscopy (TEM), both conventional and high resolution. Features before and after creep were compared and contrasted. Additionally, features from the compressive and tensile edges of the crept beams were compared.

The phase content of ABC-SiC was determined from X-ray diffraction (XRD). The method developed by Ruska *et al.*[4] was utilized to quantify the amounts of the phases after hot-pressing. The peak intensities substituted into the system of equations, Table 5.1, were determined by integrating the area of the respective peaks using DIFFRAC AT

software (SOCABIM SARL, Paris, France). All integration was performed after subtracting for the background. For cases where the solution to the equations provided a negative value for one of the polytypes, the intesity for that polytype was set to zero and the equations were resolved.

15R		6H		4H		3C	Peak	d(nm)
3.2a			+	9.9c			= A	0.266
11.2a	+	19.4b					= B	0.263
26.0a			+	38.9c			= C	0.257
31.1a	+	59.2b	+	25.1c	+	100.0d	= D	0.251
		18.1b	+	34.1c			= E	0.235
2.4a	+	6.5b			+	13.1d	= F	0.217

Table 5.1: Equations used to determine amounts of various phases in SiC from XRD.

ABC-SiC fracture paths before and after creep were examined in a SEM. The specific features evaluated were the mode of fracture and the morphology of triple point materials. Maintaining intergranular fracture is paramount for *in-situ* toughened ceramics, since toughening is derived from crack bridging.[5] Therefore, it is essential that any changes in the microstructure, either stress or temperature induced, do not result in transgranular fracture. Indications of viscous ligaments on the fracture surfaces were also monitored.

The TEM evaluation was conducted at 200 kV. Examination was performed on ABC-SiC after hot-pressing and after creep tests. Since the creep tests were conducted in bending, one edge was subjected to compressive loading and the opposite edge experienced a tensile load. Three samples were cut from the crept beams; the thin slices were cut with a low speed diamond saw and were approximately 300-500 μm thick.

Figure 5-1 shows the regions where samples were obtained. Between the inner load points in Figure 5-1 there is a constant moment, and thus caution was exercised to ensure the sections representing the stressed material were obtained from this region. An additional sample was sectioned from the end of the beam, outside of the outer load points, so features that were a function of the high temperature exposure could be distinguished from stress induced microstructural changes.

Following sectioning, the tensile and compressive samples were mounted on glass with the outer edge of the section up. Next, ~100 μm was removed to eliminate surface effects which were introduced due to thermal etching in the Ar environment, and the samples were polished to a 6 μm finish. The samples were then turned over and manually ground to ~100 μm and also polished to a 6 μm finish. 3 mm disks were cuts from the thin sections with an ultrasonic cutter using SiC grit. One side was polished to a 1 μm finish, and the samples were dimpled until the sample was translucent and polished to a 1 μm finish. Samples were then ion milled until the samples were perforated. ABC-SiC is conductive enough that charging is not a concern. Therefore, the samples were not coated.

ABC-SiC before and after creep was evaluated in the TEM. The grain size, dislocation density, cavity density, and stacking fault density were some of the features evaluated. The grain boundary structure and composition was determined by HR-TEM using a 200 kV field-emission-gun Phillips CM200 TEM. Chemical analysis of the grain boundaries was performed by using a spot size of ~ 8 nm and comparing signals from the boundary regions with signals from the SiC grains. This enabled the excess Al at the

boundaries to be determined. Similar characterization was performed on samples from both the tensile, compressive, and unstressed regions.

All creep samples were cooled from the test temperature to room temperature with the load applied. This eliminated possible relaxation effects that could alter the microstructure during cooling. The cooling rate was 10°C/minute to avoid damage resulting from thermal shock.

5.3 Results and Discussion

5.3.1 ABC-SiC after Hot-Pressing

The microstructure of as prepared ABC-SiC consists of plate-like grains that have a maximum aspect ratio of ~4-5, Figure 5-2. The morphology of these plate-like grains should be distinguished from the high toughness silicon nitrides that typically possess high aspect ratio grains but have an acicular, or needle-like shape.[6] The inset diffraction pattern exhibits streaking due to the high density of stacking faults. Recall, the energy difference between the various alpha polytypes is very low, Chapter 1, thus a high density of stacking faults is present. Another feature observed in some alpha grains was the presence of isolated dislocations, Figure 5-3. These dislocations, always in very low densities, are likely to be partial dislocations bounding stacking faults.

The XRD diffraction pattern from a hot-pressed ABC-SiC disk is shown in Figure 5-4. The phase content is ~ 46% 6H, 49% 4H, and 5% 3C, as determined by the method developed by Ruska et al.[4] This material exhibits a lower aspect ratio and less interlocking than previous ABC-SiC, which routinely exhibited aspect ratios of 7.[7] However, interlocking regions are observed in the current ABC-SiC, but at a low density.

The grain boundary amorphous phase, typically ~1 nm thick in the hot-pressed material, is rich in Al, Si, B, and C.[8] A grain boundary is shown in Figure 5-5, which reveals the amorphous nature of the interlayer after hot-pressing. Also, EDS spectra for the grain and grain boundary regions are shown in Figure 5-6. The presence of O is the boundaries likely originates from the native oxide, SiO_2, on the SiC starting powder. The S impurity found at the grain boundary is probably introduced from furnace contamination. The remaining sintering additives form bulk secondary phases, at triple-junctions and multigrain-junctions, and have been identified as $Al_4B_7C_8$ and Al_4O_4C.[7,9,10]

5.3.2 ABC-SiC Microstrucutre After Creep: $T \leq 1300°C$

Following creep, the microstructure was evaluated in the TEM. No significant changes in grain size and aspect ratio were discerned for samples after creep tests between 1100-1500°C, for a duration of up to 5 weeks. The general morphology of the grains did not appear to be altered during the tests. Similarly, the stacking fault density is similar before and after creep tests.

Creep rates were less than 1×10^{-10}/s for stresses up to 150 MPa at 1100 and 1200°C. The resultant microstructure exhibited few changes compared to hot-pressed ABC-SiC. In many of the residual β-SiC grains (FCC) dislocations were observed, Figure 5-7. This feature was evident in both the tensile and compressive edges of the beam. However, TEM evaluation of the region outside the four-point bend jig revealed no dislocations in the β phase. The α grains did not reveal dislocations structures different from the isolated partial dislocations of the as-prepared samples. As can be seen in Figure 5-8, the dislocations typically start and/or end at the grain boundaries. There

are no organized slip bands and no evidence of dislocations extending from one grain to the next. It should be emphasized that these dislocations were in isolated β-SiC grains, which comprise only ~ 5% of the microstructure. These dislocations were likely introduced as the grains rearrange upon loading and high stresses build up at contact points. Also, there was no evidence of cavitation, as is commonly observed with Si_3N_4.[1,3,11,12] The primary creep regime dominated strain for these samples, and caviation does not appear to be a dominant deformation mechanism for ABC-SiC at these temperatures. However, it should be noted that the overall strain in these samples was less than 0.4%, and cavitation may become more pronounced for larger strains. However, tests to evaluate this were precluded by the long duration to achieve large strains with the low strain rates.

In ABC-SiC, the grains rearranged through grain boundary sliding, and locally the stress increased at contact points where grains impinged, as described in Chapter 3. This stress can be relieved through mechanisms such as cavitiy formation and dislocations. Therefore, the dislocations are formed in the β grains in response the locally high stress during the transient period. As more grain-to-grain contact occurs, the load at any individual point decreases, thus leading to the transient behavior.

Dislocations were absent in the α grains in samples crept at less than 1400°C. This is not surprising given the limited number of slip planes in the hexagonal structure of the α phases. Slip has been shown to be very dependent upon orientation of the basal planes relative to stress axis, as evidenced by the high creep rates of single crystal α-SiC with the loading direction at 45° from [0001] toward $[11\bar{2}0]$, but creep rates are extremeley low when samples are loading perpendicular to [0001].[13] Since β-SiC has 12

slip systems, compared to the 3 in hexagonal α-SiC, the likelihood of achieving a stress high enough to introduce a dislocation in β-SiC is much higher.

5.3.3 ABC-SiC Microstrucutre After Creep: T ≥ 1400°C

After creep at temperatures above 1300°C, the grain size and morphology was unaltered, as with the lower temperatures. However, the dislocation density dramatically increased as temperature increased. In contrast to the lower temperatures, dislocations were observed in many grains, including the α grains. These features were similar in both the tensile and compressive specimens. Again, the non-stressed region did not exhibit these dislocation structures. Figure 5-9 shows a typical dislocation structure in an α grain after creep at 1400°C for a strain of ~ 0.8%. While dislocations were observed in many grains, there was little evidence of slip bands and polygonization due to dislocation climb. Many of the dislocations appeared to originate at two grain interfaces. On only one occasion was a slip band observed in ABC-SiC, Figure 5-10. This occurred in a residual β grain, but the low density suggests that dislocation glide is not a significant deformation mechanism in ABC-SiC.

Additionally, large precipitates within the grains, identified at Al_2O_3, resulted in high densities of dislocations that originated at the SiC/precipitate interface, Figure 5-11. As the temperature of the creep tests increased, dislocations were observed in the α-SiC grains since more slip systems were operative given the additional energy to overcome the high Peierls stress in SiC. Alumina particles were observed in a low percentage of the grains, and it is believed that the particles were entrapped during grain growth of the α grains.

The dislocations were similar to those observed by Lane *et al.*[14] for α-SiC, sintered with B and C, where graphite and C particles were present. However, these tests were conducted in compression at higher temperatures and stresses. Lane *et al.*[14] revealed the presence of slip bands and dislocation climb, both processes which were not observed in ABC-SiC at temperatures up to 1500°C. While numerous dislocations were present, dislocations moving orthogonal to the original slip direction, which is evidence of climb, were seldom observed. Since the dislocations do not appear to be a dominant mechanism of creep, the Burger's vectors were not analyzed. However, they are likely to be a/6⟨112⟩ partial dislocations, which move by glide on {111} planes, in the cubic β-SiC grains,[15] and a/3[01$\bar{1}$0] Schockley partial dislocations in the hexagonal α-SiC grains.[14]

In addition to increasing the dislocation density with increasing temperature, small precipitates were observed for samples crept at 1300°C and above. These precipitates were identified as being Al and C rich.[16] After creep at 1400°C, Figure 5-12, precipitates were observed with a density of ~ 1 x $10^{15}/m^2$. The origin of the precipitates is believed to be the presence of Al and C being in excess of their solubility in the SiC grains. The solubility of Al in SiC is ~ 0.5% at 2000°C, but drops to ~ 0.1% at room temperature.[17] As the material was cooled from the hot-pressing temperature, the kinetics of precipitation was too slow for the cooling rate employed. However, upon subsequent heat treatments these species, present above their solubility limit, precipitated out. These precipitates were similar to those observed by Lane *et al.*[14,18] for sintered α-SiC where B_4C precipitates, containing a small amount of Si, were observed. They also demonstrated that the dislocations appeared to interact with the precipitates. This feature was not present in ABC-SiC. Since dislocation glide becomes more prevalent at higher

temperatures during creep of α-SiC,[14] the precipitates may be beneficial in minimizing the steady-state creep rates of ABC-SiC at higher temperatures should dislocation glide become operative. For the temperature range employed in the current experiments, the presence of the precipitates likely would have little effect on the creep rates unless they altered the chemistry of the grain boundaries.

Another interesting feature of the precipitates was the region near the grain boundaries, which was denuded of precipitates, Figure 5-13. For both the tensile and compressive edges, the denuded zone was ~ 100 nm. Since grain boundaries and interfaces possess a more open structure, the solubility limit in these regions is high. Therefore, the Al and the other sintering additives are preferentially deposited into the grain boundaries. Likewise, during the course of the creep experiments the impurities are present above their solubility limit in SiC and there is a driving force for diffusion to the grain boundary which has a higher solubility. The precipitates were ~ 5 nm in diameter, Figure 5-14.

Another feature present at temperatures greater than 1300°C was cavitation. While cavitation was evident at some triple points, a very low density of 2 grain junction cavities was observed for the tensile edge after creep at 1400°C, Figure 5-15 & 5-16. In contrast, the compressive edge of the beam showed little cavitation as expected. The density of triple-junction cavities was slightly higher than hot-pressed ABC-SiC, and cavities at two grain junctions were scarce. This is consistent with Si_3N_4 where similar features were observed.[3] The microstructure was examined with specific attention given to the distribution of two-grain cavities with respect to the stress axis. Two-grain cavities at boundaries perpendicular to the stress axis would be expected to be more prevalent

than randomly distributed cavities, but the low density of these cavities made a definitive assessment difficult.

The cavities at two grain junctions, Figure 5-17, grew into the grains and exhibited a faceted nature. Both of these features are indicative of a solution-precipitation mechanism being operative during the creep of ABC-SiC. These cavities at two-grain junctions likely originate from grain-to-grain contact and subsequent stress enhanced diffusion consistent with a solution-precipitation process; the SiC was removed from these high stress regions, transported through the grain boundary phase, and finally precipitated in a low stress region. Cavitation at multi-grain junctions likely results from the microstructure dilating for grains to slide past each other. Multi-grain junctions cavitated to allow the triple-point materials to flow from cavities to surrounding triple-points. This results in dilation, and sample extension is accommodated by grain boundary sliding.[3]

Creep at 1400°C in advanced Si_3N_4 generates a very high density of cavities at both two-grain and multi-grain junctions.[3,19,20] In contrast, ABC-SiC exhibited very little cavitation. This is supported by the stress exponent of unity determined for ABC-SiC. Both materials are similar since they possess grain boundary intelayers, yet ABC-SiC shows significantly less cavitation. The interlocking and plate-like morphology of the grains may explain this feature. The caviation mechanism requires dilation of the material to allow transport from multi-grain junctions in compression to those in tension, Figure 4-8. However, such dilation is difficult if the grains are interlocked. The interpenetrating microstructure of ABC-SiC minimizes the dilation and subsequent cavity formation. Decreased creep in Si_3N_4/SiC nanocomposites has been attributed to

interlocking of the elongated Si_3N_4 grains.[21] Similarly, transient creep in Si_3N_4 has been attributed to interlocking. After the grains jam a new mechanism, such as cavitiation and diffusion, is required for additional deformation.[19] However, the interlocking described in both cases is different than interlocking in ABC-SiC. In the former two cases, interlocking indicates that grain-to-grain contact is present at various places in the microstructure. In ABC-SiC, grains actually grow into each other.[22] A schematic of this feature is shown in Figure 5-18. Intuitively, the interlocking present in ABC-SiC is a more effective mechanism for preventing dilation deformation, and this is supported by the low cavity density.

5.3.4 ABC-SiC Grain Boundaries After Creep

The intergranular phase in high toughness monolithic ceramics typically limit their high temperature properties. Hence, the grain boundaries were evaluated with special attention given to the properties with respect to the stress axis. The grain boundaries of ABC-SiC after hot-pressing is shown in Figure 5-5. Recall, these boundaries are ~ 1 nm thick and have an amorphous nature; there is no significant long range order in these grain boundary phases prior to the creep process. In contrast, after creep at 1100°C the grain boundaries appeared to crystallize and the thickness was reduced to less than 1 nm, Figure 5-19. Evaluation of the sample obtained from the unstressed region revealed that crystallization resulted from the extended heat treatment during the creep test and was not stress induced. A typical grain boundary from the unstressed region after a creep test is shown in Figure 5-20. Higher magnification of these regions revealed short range order consistent with a 2H structure for an

aluminosilicate phase.[8] The thickness of the grain boundaries was independent of the stress axis; boundaries parallel and perpendicular to the stress axis exhibited similar structural and chemical characteristics.

The crystallization of the grain boundaries likely is a key component of the transient creep regime. As crystallization occurs, the viscosity of the grain boundary phase is likely to change, hence altering the creep response. The viscosity of the intergranular phase can gradually increase as the composition is altered by the crystallization of the amorphous grain boundaries. As the viscosity rises, redistribution of the grain boundary phase and diffusion will both become more difficult. EDS spectra from the grain boundaries before and after creep exhibit similar features. However, the spot size of the probe is ~ 8 nm and a similar spectrum represents enrichment of the Al concentration in the boundaries after crystallization since the grain boundaries are thinner. Despite these changes in the grain boundary phase, no change in the fracture mode was observed for samples that were fractured after a creep experiment, Figure 5-21. This is important since a change in the fracture mode from the predominately intergranular mode to a transgranular mode would compromise the toughness. The toughness actually increases after these long heat treatments, see Chapter 2.[23]

Only the grain boundaries after creep at 1100°C are shown, but they are representative of grain boundaries after creep at all temperatures. The structure of all boundaries was similar. However, the excess amount of Al at the boundaries increased with increasing temperature.[8] This is consistent with Al diffusing towards the grain boundary region during the creep tests. The higher temperatures provided a higher driving force for this process.

Attempts to crystallize the intergranular liquid in Si_3N_4 always results in a residual thin amorphous layer at two-grain junctions. The amorphous grain boundary phase never completely crystallizes.[19,24] Complete crystallization of amorphous interlayers is more difficult than devitrification of the same bulk phase. Since the amorphous interlayers are constrained by the boundary, they may support hydrostatic stresses. Therefore, the volume changes associated with phase transformations will result in a strain energy, which opposes crystallization.[25] In contrast, the grain boundaries in ABC-SiC exhibited no discernable amorphous layer after creep tests, Figure 5-19.

In most boundaries the interlayer appeared to form a coherent interface with one of the grains. Since the adjacent SiC grain possesses either a tilt and/or rotation, the opposite side of the interface is incoherent. The incoherent region is a disordered area with an open structure. This can be visualized by examining a standard grain boundary, Figure 5-22. In the region at the boundary all atoms do not line up and this results in an open structure; the open structure is similar to the incoherent side of the boundary in ABC-SiC. Most of the impurities of the grain boundary phase likely reside at the incoherent interface. Crystallization of the grain boundaries presumably increases their strength, yet intergranular fracture is still predominant on the fracture surfaces after crystallization has occurred. Apparently, the disordered region at the interface provides sufficiently weak bonding that the fracture mode is not completely transgranular. If the bonding between adjacent SiC grains became too strong because the strength of the grain increased, the fracture mode would change to transgranular and the toughness would drop to the inherent value of ~ 2.5 MPa$\sqrt{m}$.

5.4 Conclusions

The microstructure of ABC-SiC exhibited a low density of dislocations, always in isolated grains and without slip bands, and no cavitation at 1300°C and below. The dislocation density increased with increasing temperature. After creep at 1400°C and above, cavitation was observed on the tensile edge of the beam, but caviation was not observed for the compressive edge. Even at higher temperatures, while the dislocation density was higher, slip bands were not a dominant feature. The grain boundaries crystallized during the long holds at the creep temperatures. Additionally, the concentration of impurities is slightly increased compared to hot-pressed ABC-SiC. The amount of Al in the grain boundaries increased as the creep temperature increased.

5.5 References

[1] M. N. Menon, H. T. Fang, D. C. Wu, M. G. Jenkins, and M. K. Ferber, "Creep and Stress Rupture Behavior of an Advanced Silicon Nitride: Part III, Stress Rupture and the Monkman-Grant Relationship," *J. Am. Ceram. Soc.*, **77** [5] 1235-41 (1994).

[2] J. Weertman, " Steady-State Creep Through Dislocation Climb," *J. Appl. Phys.*, **28** [3] 362-4 (1957).

[3] W. E. Luecke, S. M. Wiederhorn, B. J. Hockey, R. F. Drause, Jr., and G.G. Long, "Cavitation Contributes Substantially to Tensile Creep in Silicon Nitride," *J. Am. Ceram. Soc.*, **78** [8] 1085-96 (1995).

[4] J. Ruska, L.J. Gauckler, J.L. Lorenz, and H.U. Rexer, "The Quantitative Calculation of SiC Polytypes from Measurements of X-Ray Diffraction Peak Intensities," *J. Mat. Sci.*, **14** [8] 2013-17 (1979).

[5] P. F. Becher, "Mictrostructural Design of Toughened Ceramics," *J. Am. Ceram. Soc.*, **74** [2] 255-69 (1991).

[6] M. N. Menon, H. T. Fang, D. C. Wu, M. G. Jenkins, M. K. Ferber, K. L. More, C. R. Hubbard, and T. A. Nolan, "Creep and Stress Rupture Behavior of an Advanced Silicon Nitride: Part I, Experimental Observations," *J. Am. Ceram. Soc.*, **77** [5] 1217-27 (1994).

[7] J.J. Cao, W.J. MoberlyChan, L.C. De Jonghe, C.J. Gilbert, and R.O. Ritchie, "*In Situ* Toughened Silicon Carbide with Al-B-C Additions," *J. Am. Ceram. Soc.*, **79** [2] 461-69 (1996).

[8] X.F. Zhang, M.E. Sixta, and L.C. De Jonghe, "The Evolution of Grain Boundaries in SiC," submitted to *J. Am. Ceram. Soc.*, 1999.

[9] W.J. MoberlyChan, J.J. Cao, M.Y. Niu, and L.C. De Jonghe, "Toughened β-SiC Composites with Alumina-Coated α-SiC Platelets," in *High Performance Composites* (edited by K.K. Chawla, P.K. Liaw, and S.G. Fishman), TMS Conference Proceedings (1994).

[10] T.D. Mitchell, L.C. De Jonghe, W.J. MoberlyChan, and R.O. Ritchie, "Silicon Carbide Platelet/Silicon Carbide Composites," *J. Am. Ceram. Soc.*, **78** [1] 97-103 (1995).

[11] J.-L. Ding, K. C. Liu, K. L. More, and C. R. Brinkman, "Creep and Creep Rupture of an Advanced Silicon Nitride Ceramic," *J. Am. Ceram. Soc.*, **77** [4] 867-74 (1994).

[12] M. N. Menon, H. T. Fang, D. C. Wu, M. G. Jenkins, and M. K. Ferber, "Creep and Stress Rupture Behavior of an Advanced Silicon Nitride: Part II, Creep Rate Behavior," *J. Am. Ceram. Soc.*, **77** [5] 1228-34 (1994).

[13] G. S. Corman, "Creep of 6H α-Silicon Carbide Single Crystals," *J. Am. Ceram. Soc.*, **75** [12] 3421-24 (1992).

[14] J. E. Lane, C.H. Carter, and R. F. Davis, "Kinetics and Mechanisms of High Temperature Creep in Silicon Carbide: III, Sintered α-Silicon Carbide," *J. Am. Ceram. Soc.*, **71** [4] 281-95 (1988).

[15] C. H. Carter, Jr., R. F. Davis, and J. Bentley, "Kinetics and Mechanisms of High Temperature Creep in Silicon Carbide: II, Chemically Vapor Deposited," *J. Am. Ceram. Soc.*, **67** [11] 732-40 (1984).

[16] X.F. Zhang, M.E. Sixta, and L.C. De Jonghe, "Precipitates in ABC-SiC," submitted to *J. Am. Ceram. Soc.*, 2000.

[17] kingery paper on al solubility

[18] R. D. Nixon and R. F. Davis, "Diffusion-Accommodated Grain Boundary Sliding and Dislocation Glide in the Creep of Sintered Alpha Silicon Carbide," *J. Am. Ceram. Soc.*, **75** [7] 1786-95 (1992).

[19] S. M. Wiederhorn, B. J. Hockey, D. C. Cranmer, and R. Yeckley, "Transient Creep Behaviour of Hot Isostatically Pressed Silicon Nitride," *J. Mat. Sci.*, **28** [2] 445-53 (1993).

[20] R. F. Krause, W. E. Luecke, J. D. French, B. J. Hockey, and S. M. Wiederhorn, 'Tensile Creep and Rupture of Silicon Nitride," *J. Am. Ceram. Soc.*, **82** [5] 1233-41 (1999).

[21] A. Rendtel, H. Hubner, M. Herrmann, and C. Schubert, "Silicon Nitride/Silicon Carbide Nanocomposites Materials: II, Hot Strength, Creep, and Oxidation Resistance," *J. Am. Ceram. Soc.*, **81** [5] 1109-20 (1998).

[22] J. Cao, "*In Situ* Toughened SiC Ceramics with Al-B-C Additions and Oxide-Coated SiC Platelet/SiC Composites," Ph.D. Thesis, University of California, Berkeley, pp. 22, (1996).

[23] D. Chen, C. J. Gilbert, and R. O. Ritchie, submitted to the *J. Am. Ceram. Soc.*, 1999.

[24] M. K. Cinibulk and G. Thomas, "Fabrication and Secondary-Phase Crystallization of Rare-Earth Disilicate-Silicon Nitride Ceramics," *J. Am. Ceram. Soc.*, **75** [8] 2037-43-45 (1992).

[25] R. Raj and F. F. Lange, "Crystallization of Small Quantities of Glass (or a Liquid) Segregated in Grain Boundaries,"*Acata Metall.*, **29** 1993-2000 (1981).

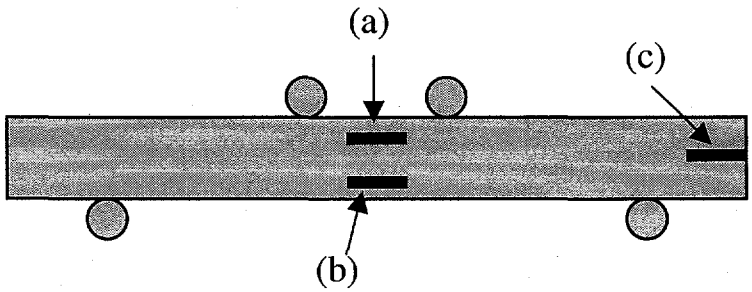

Figure 5-1: Schematic diagram of a beam with the load points. The black lines represent the sections that were cut from the sample for TEM specimen preparation. The sections labeled (a), (b), and (c) represent the tensile edge, compressive edge, and unstressed regions, respectively.

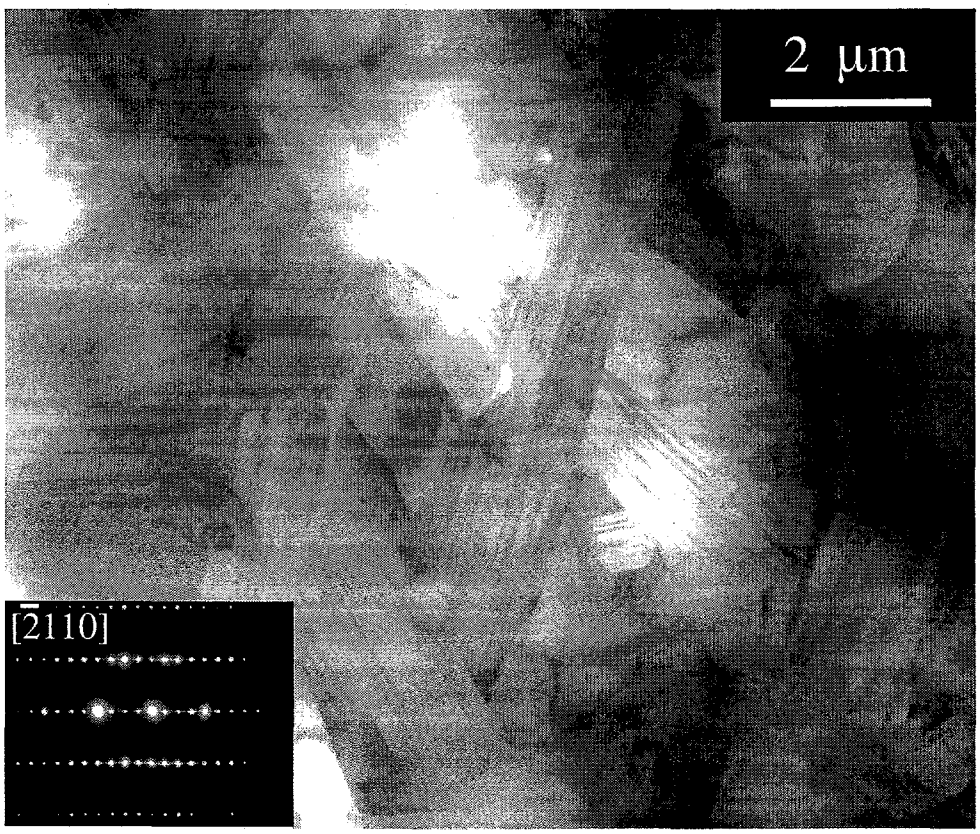

Figure 5-2: TEM micrograph of ABC-SiC prior to creep. Elongated α-SiC grains were the predominant microstructural feature. The inset diffraction is representative of the α-SiC grains. The streaking in the diffraction pattern results from the high stacking fault density.

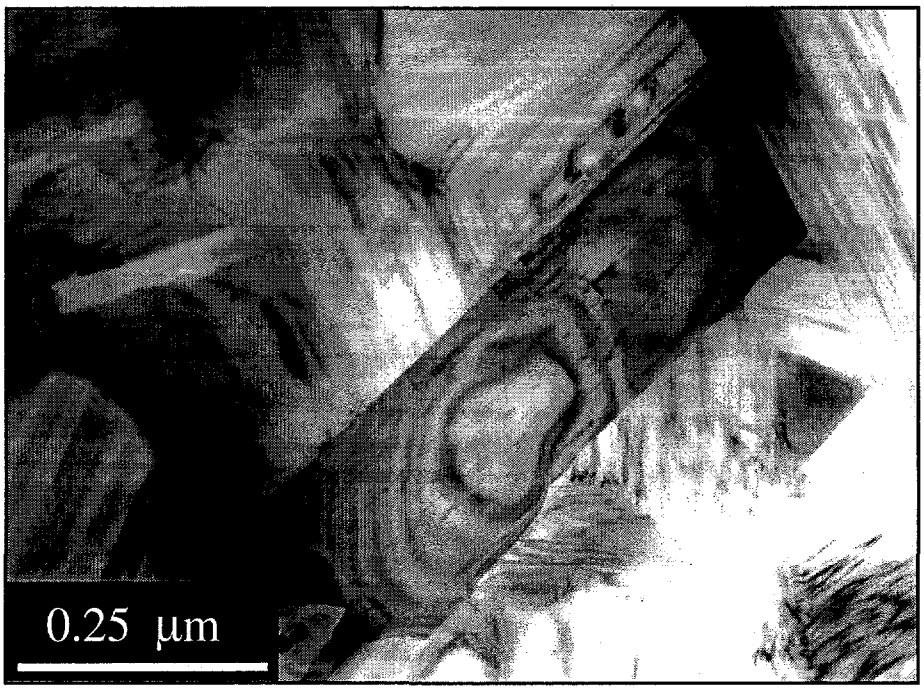

(a)

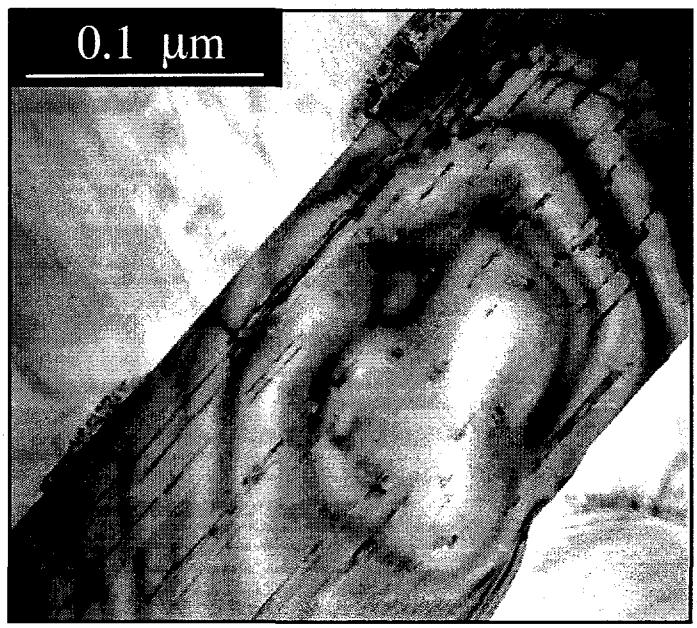

(b)

Figure 5-3: TEM micrograph of ABC-SiC prior to creep. Some small grains exhibit small dislocation features, (a). Higher magnification of the same grain is shown in (b).

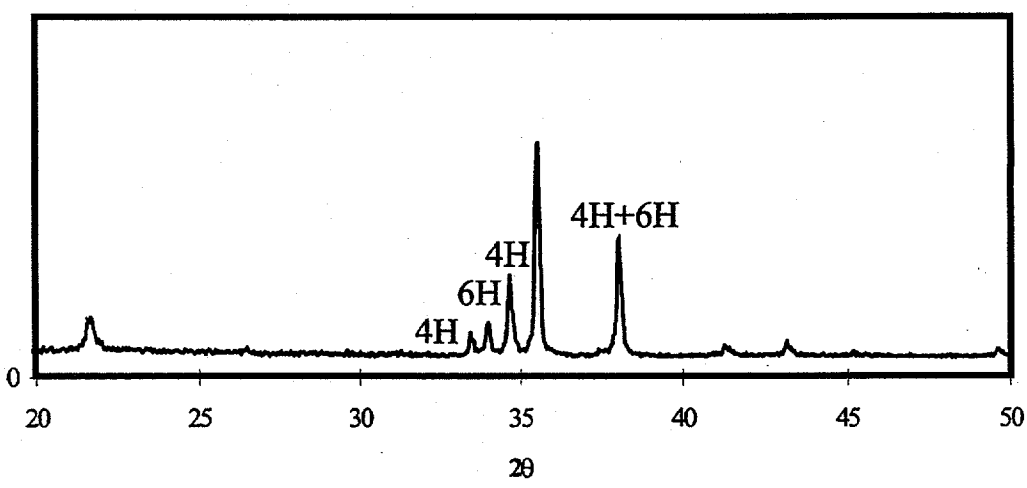

Figure 5-4: X-ray diffraction spectrum of ABC-SiC after hot-pressing.

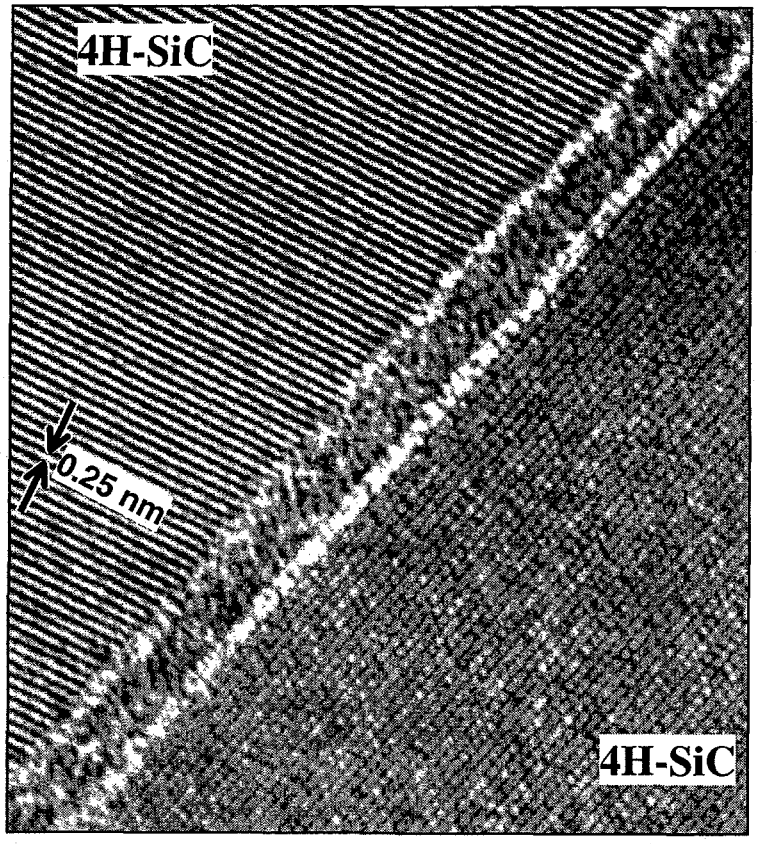

Figure 5-5: High resolution TEM micrograph of an amorphous grain boundary in ABC-SiC prior to creep. (Courtesy of Dr. X. F. Zhang)

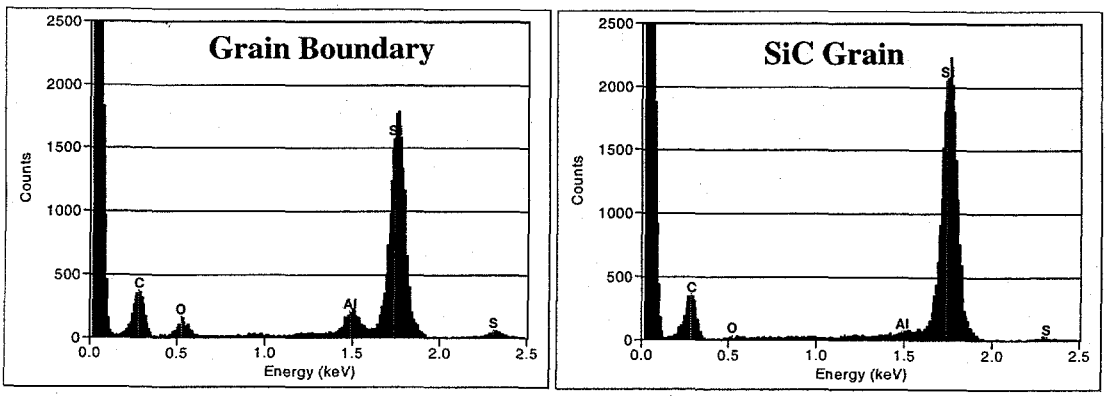

Figure 5-6: EDS spectra for a SiC grain and the grain boundary region. A probe with an ~ 8 nm spot size was utilized to collect the spectra. (Courtesy of Dr. X. F. Zhang)

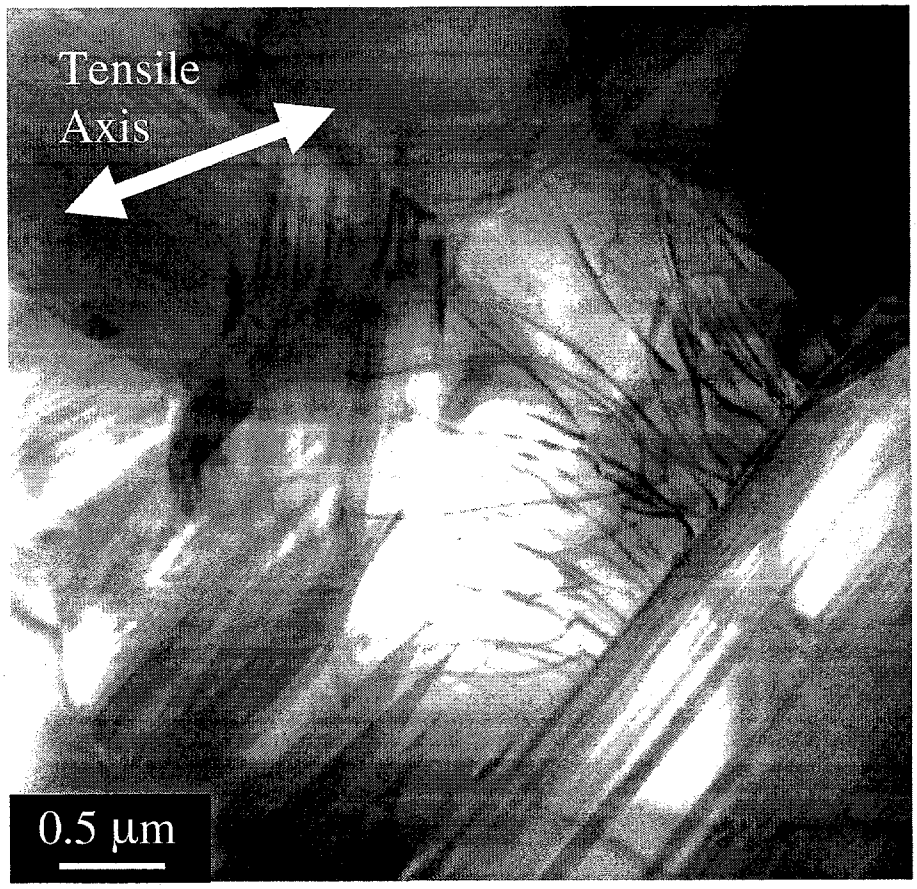

Figure 5-7: TEM micrograph of dislocations on the tensile edge of a sample crept at 1100°C with a stress up to 175 MPa. The dislocations are in a residual β-SiC grain. Courtesy of Dr. X. F. Zhang.

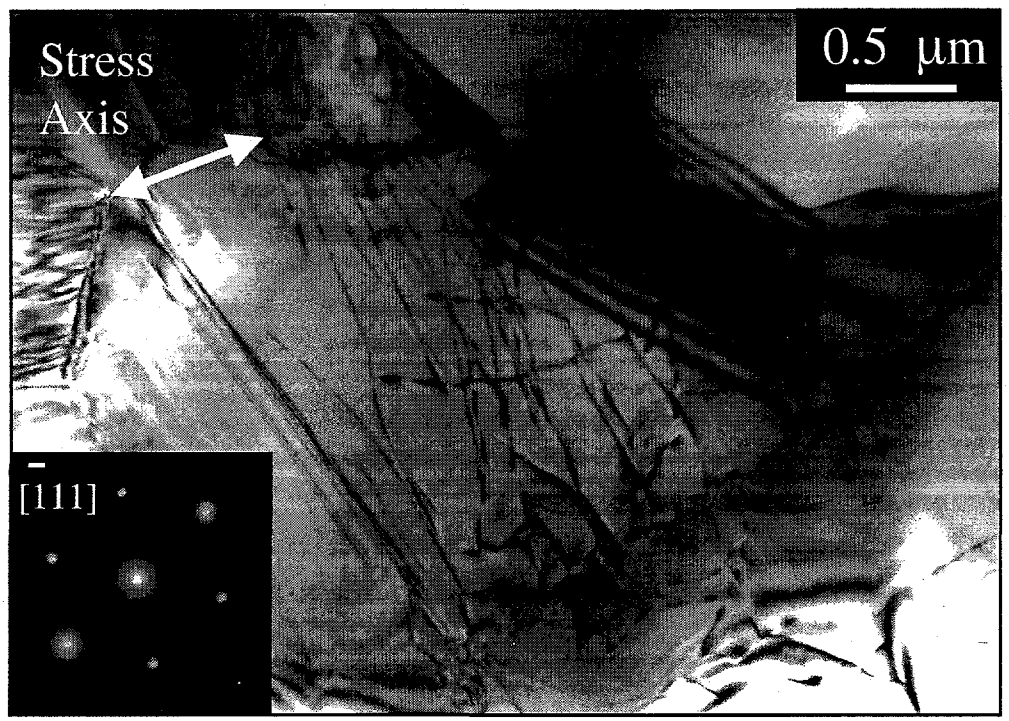

(a)

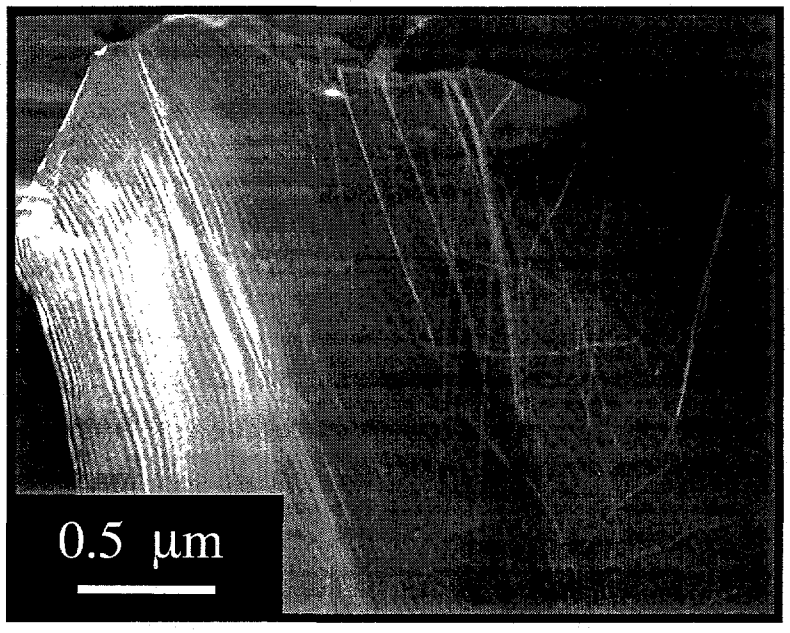

(b)

Figure 5-8: TEM micrograph of dislocations on the tensile edge of a sample crept at 1200°C with a stress up to 150 MPa. A bright field, (a), and dark field, (b), pair is shown to illustrate how the dislocations originate and/or terminate at grain boundaries.

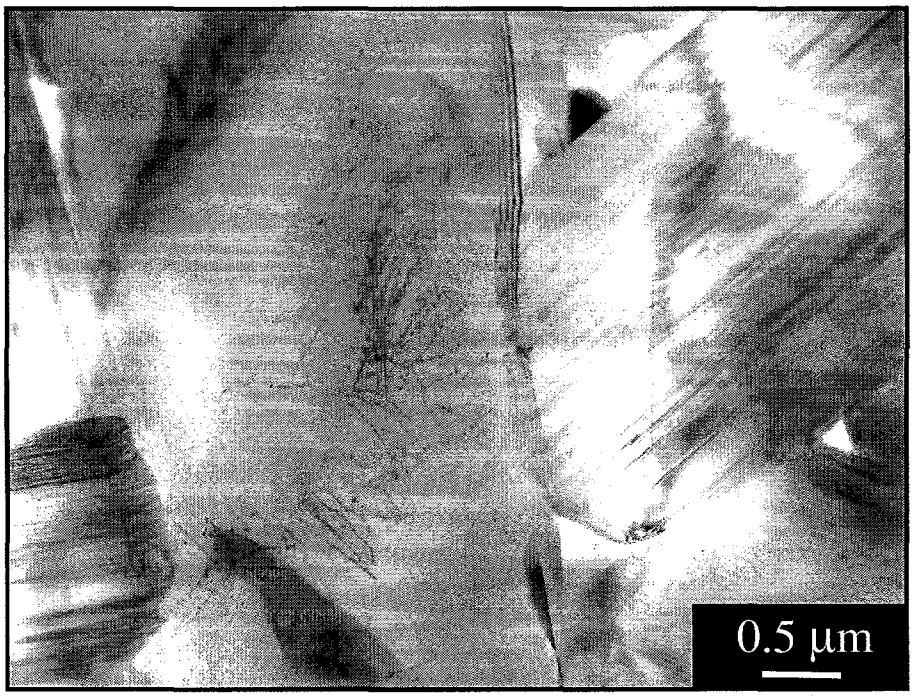

(a)

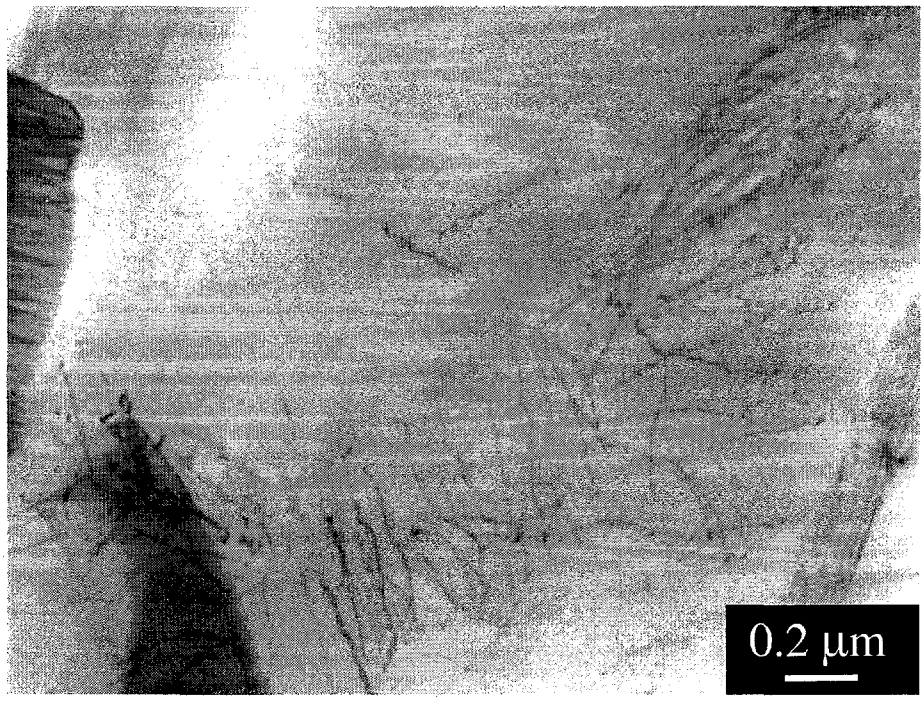

(b)

Figure 5-9: TEM micrograph of dislocations on the tensile edge of a sample crept at 1400°C with a stress up to 200 MPa. A low magnification, (a), and high magnification, (b), of the dislocation structure.

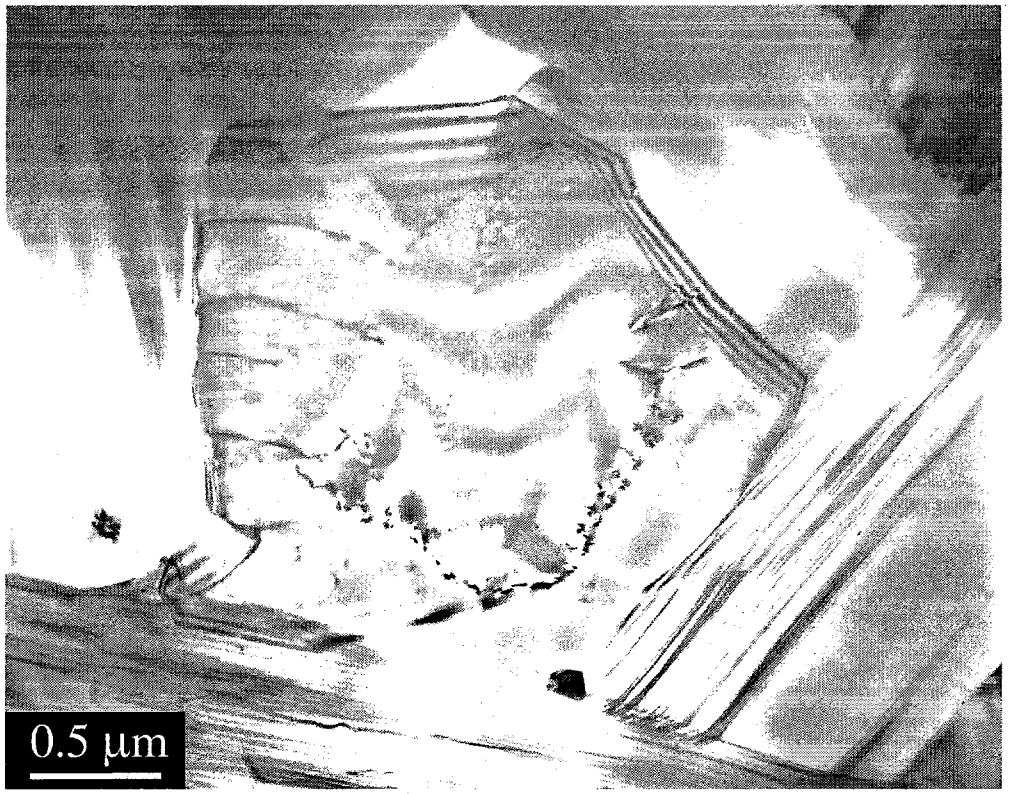

(a)

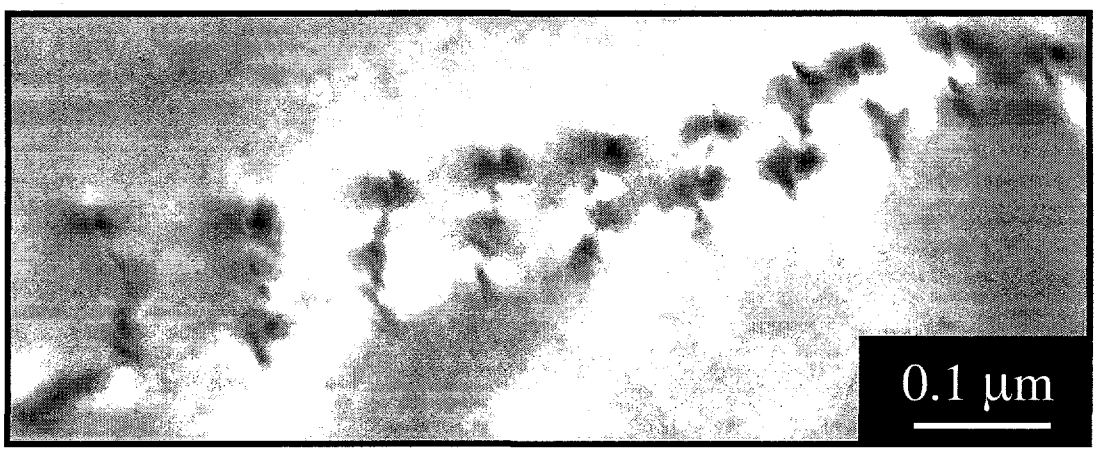

(b)

Figure 5-10: Dislocations on the compressive edge of a crept beam at 1400°C, 200 MPa. The dislocations formed in a residual β-SiC grain, (a), and a higher magnification TEM micrograph of the slip band is shown in (b).

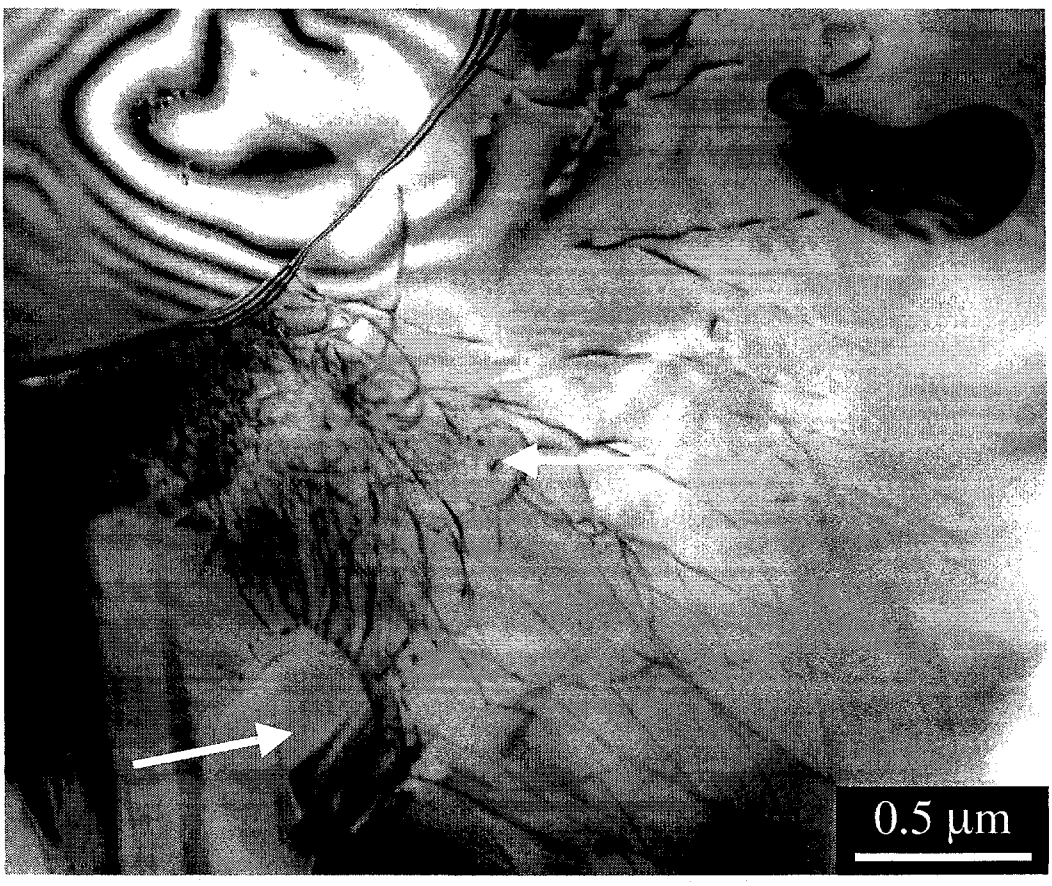

Figure 5-11: TEM micrograph of dislocations in ABC-SiC after creep at 1400°C with a stress of 200 MPa. Dislocations frequently originated at the interface between particles and the SiC grains. Two alumina particles are shown by arrows.

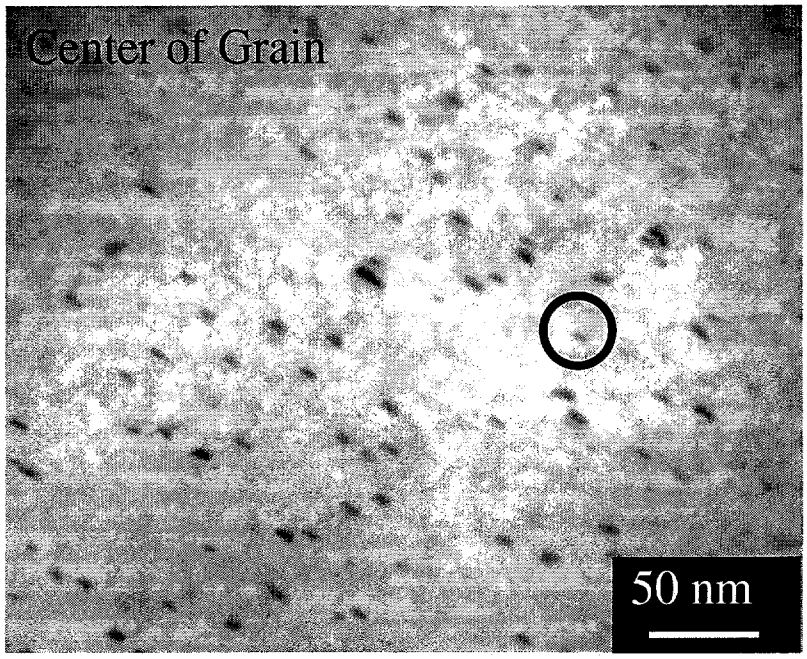

Figure 5-12: TEM micrograph of precipitates in the center of a grain after creep at 1400°C.

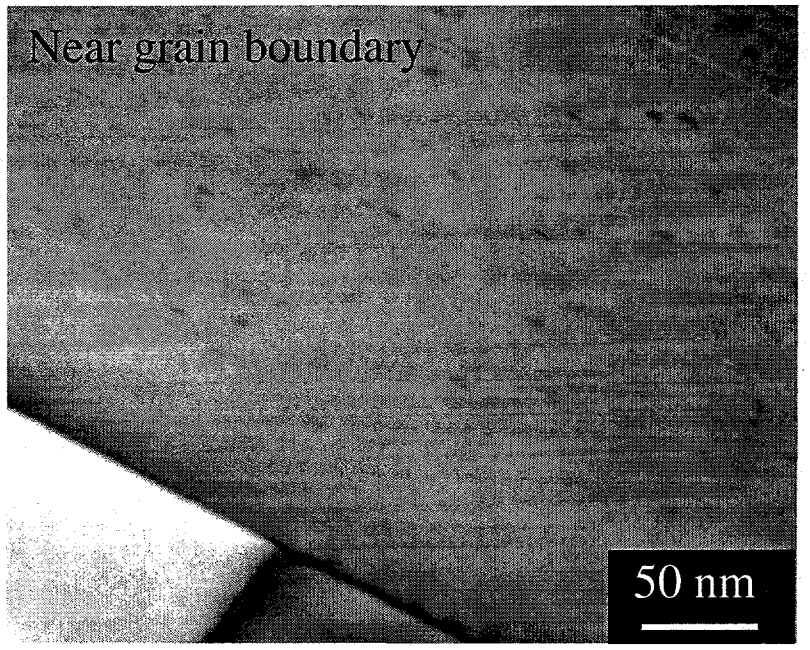

Figure 5-13: TEM micrograph of precipitates near a grain boundary after creep at 1400°C. There is a region ~50-100 nm thick that is denuded of precipitates.

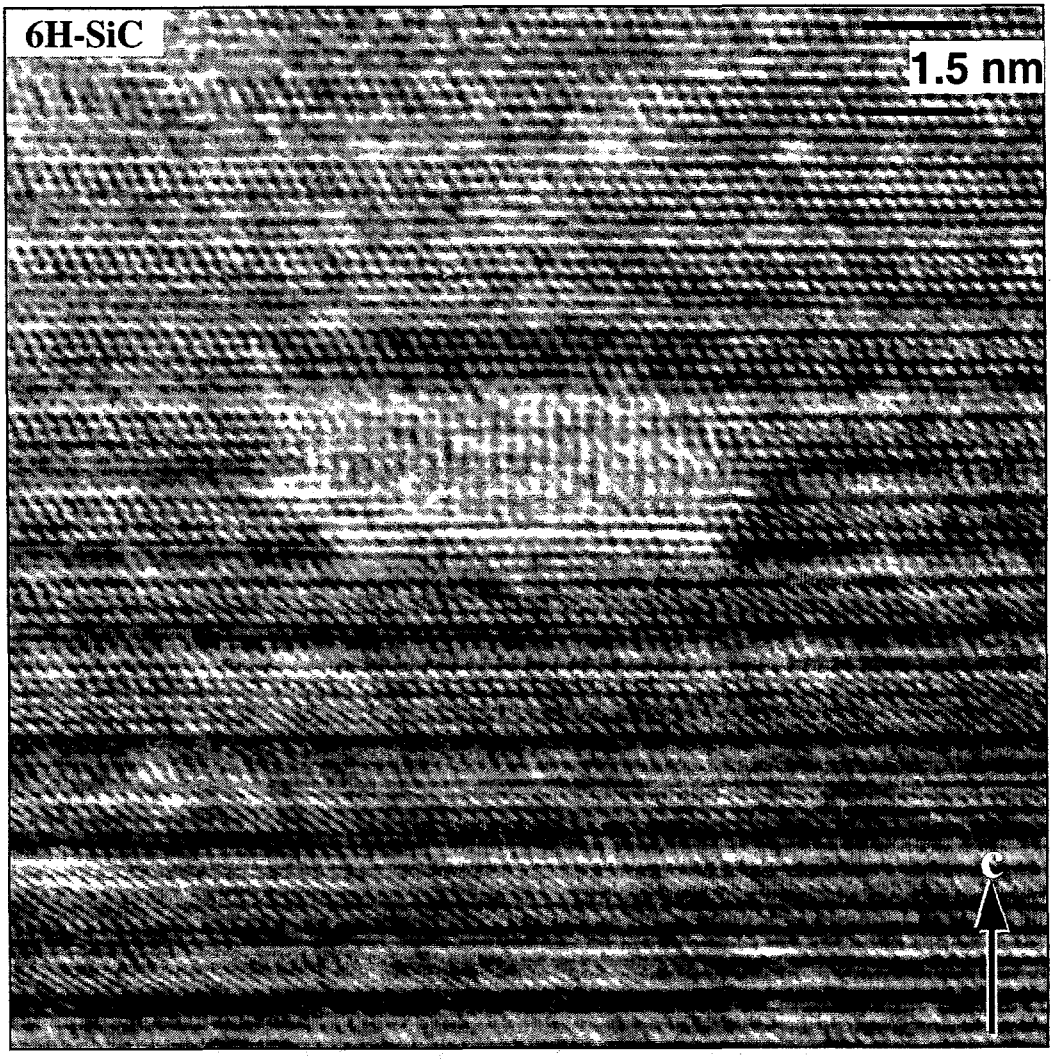

Figure 5-14: High resolution TEM micrograph of a single precipitate. The sample was crept at 1400°C, up to 200 MPa, for 5 weeks. The precipitates were mainly comprised of Al and C. Courtesy of Dr. X. F. Zhang.

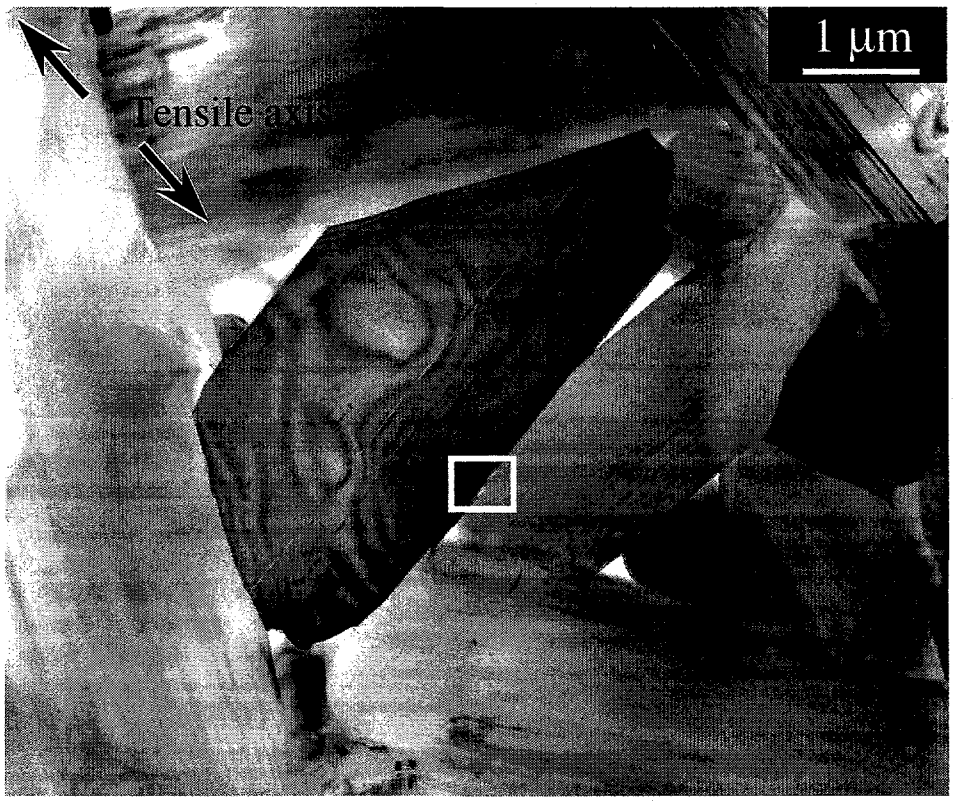

Figure 5-15: TEM micrograph of cavities on the tensile edge of a creep sample. The sample was crept at 1400°C, 200 MPa. Cavities occurred on the tensile edge, but seldom on the compressive edge of the samples after creep. Cavities were observed at two-grain and multi-grain junctions.

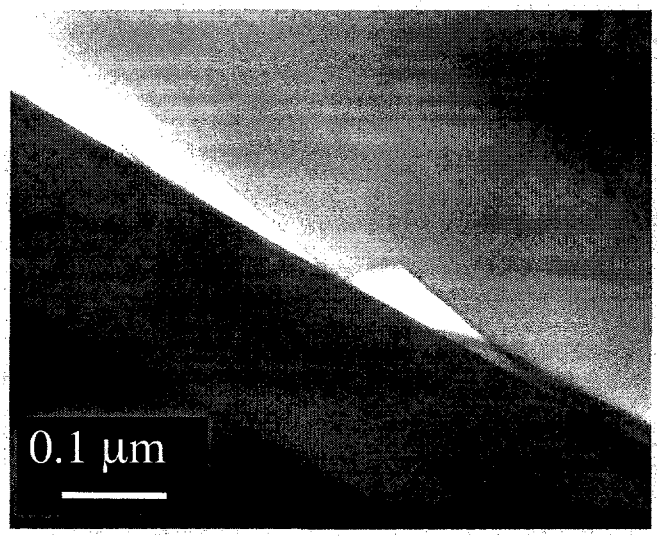

Figure 5-16: TEM micrograph of cavities at a two-grain junction from the region denoted by the box in Figure 5-15.

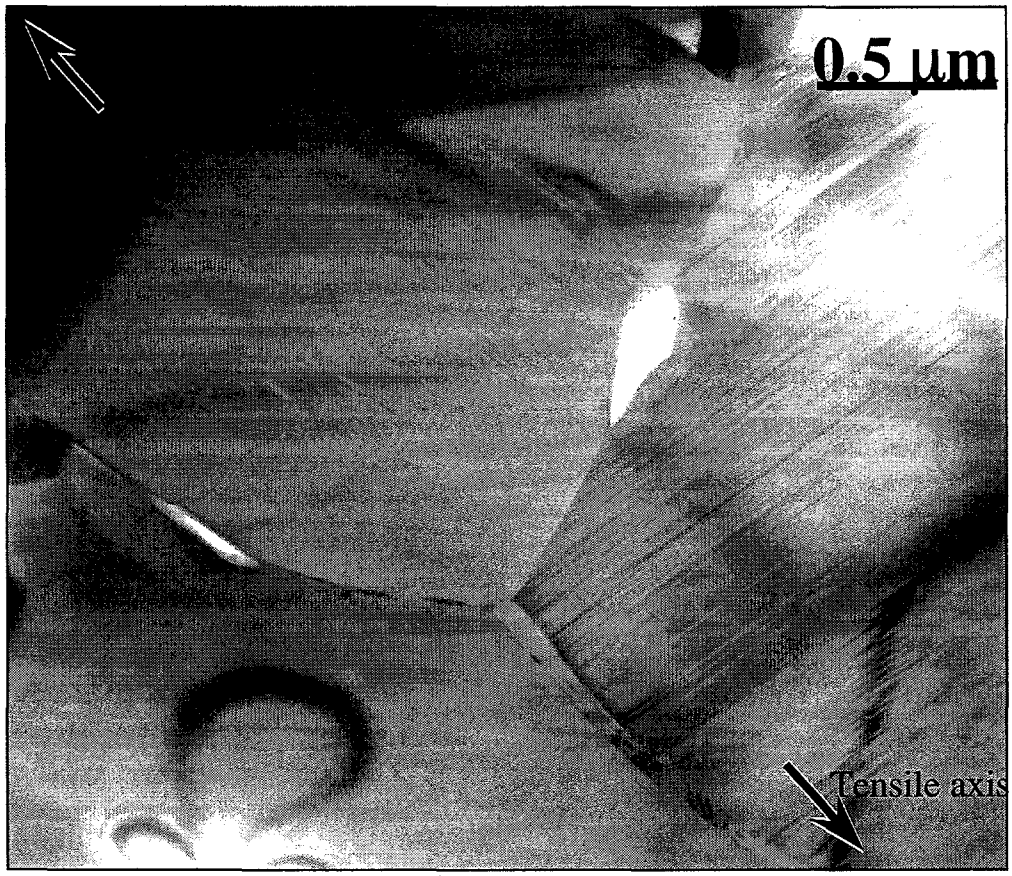

Figure 5-17: TEM micrograph of cavities at two-grain junctions on the tensile edge of a creep sample. The sample was crept at 1400°C, 200 MPa.

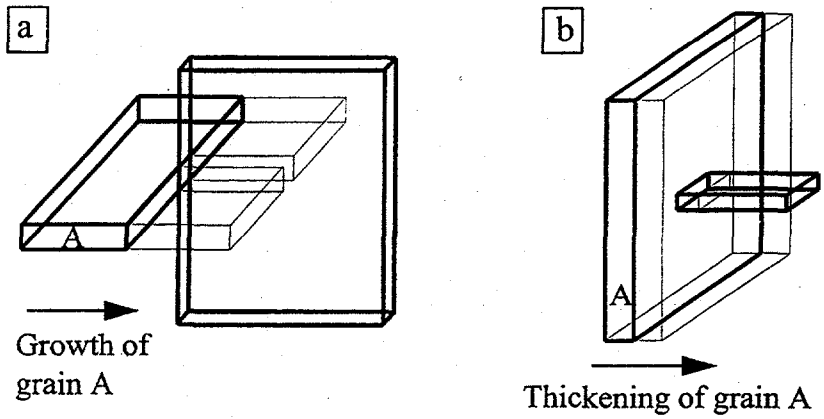

Figure 5-18: Schematic diagram of the interlocking grains in ABC-SiC.

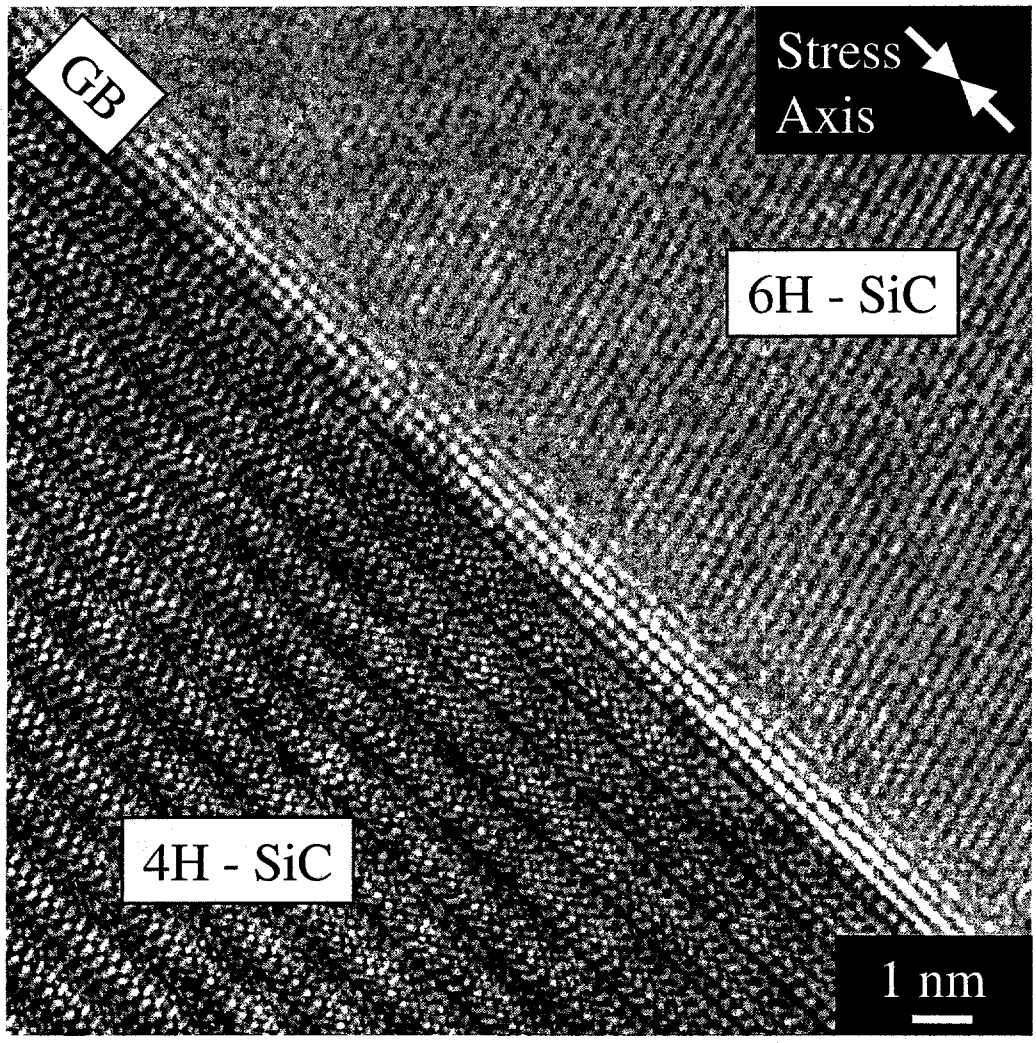

Figure 5-19: High resolution TEM micrograph of a grain boundary after creep at 1100°C, 175 MPa, for ~ 5 weeks. This specimen was cut from the compressive edge of the beam. Courtesy of Dr. X. F. Zhang.

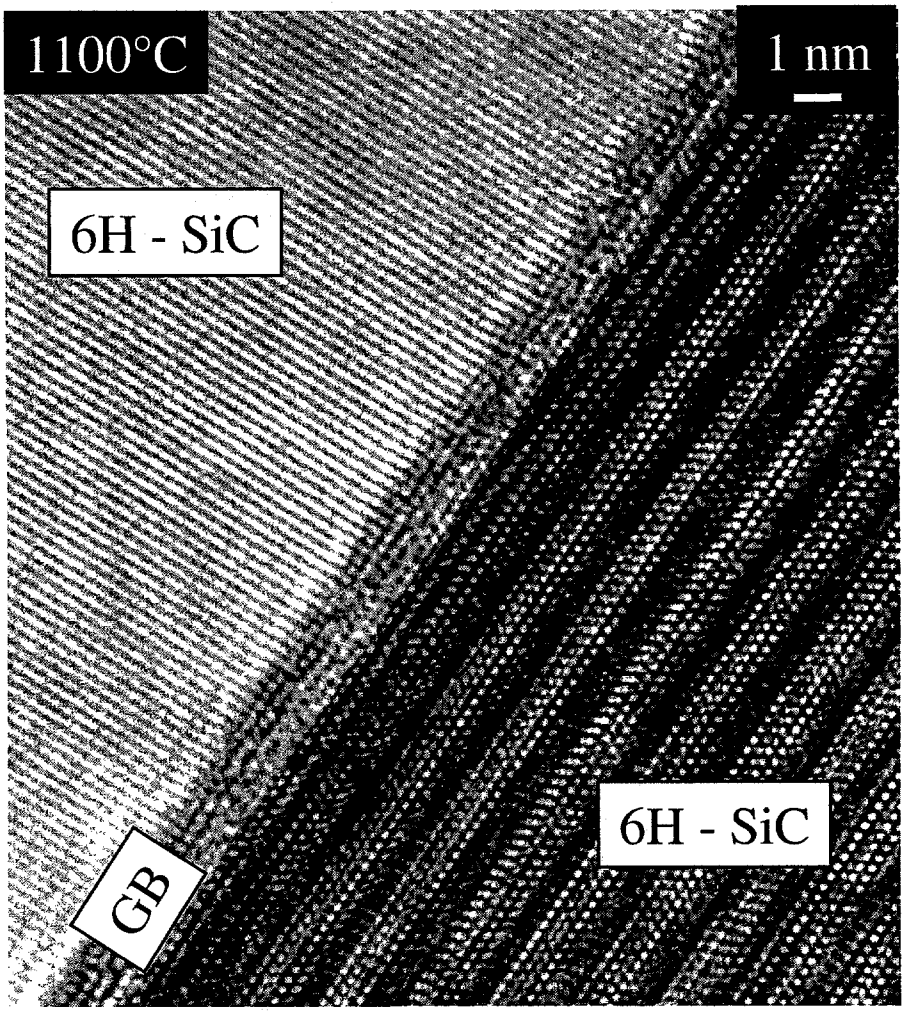

Figure 5-20: High resolution TEM micrograph of a grain boundary after annealing at 1100°C for ~ 5 weeks. This specimen was from the outer edge of the beam and thus experienced no stress. Courtesy of Dr. X. F. Zhang.

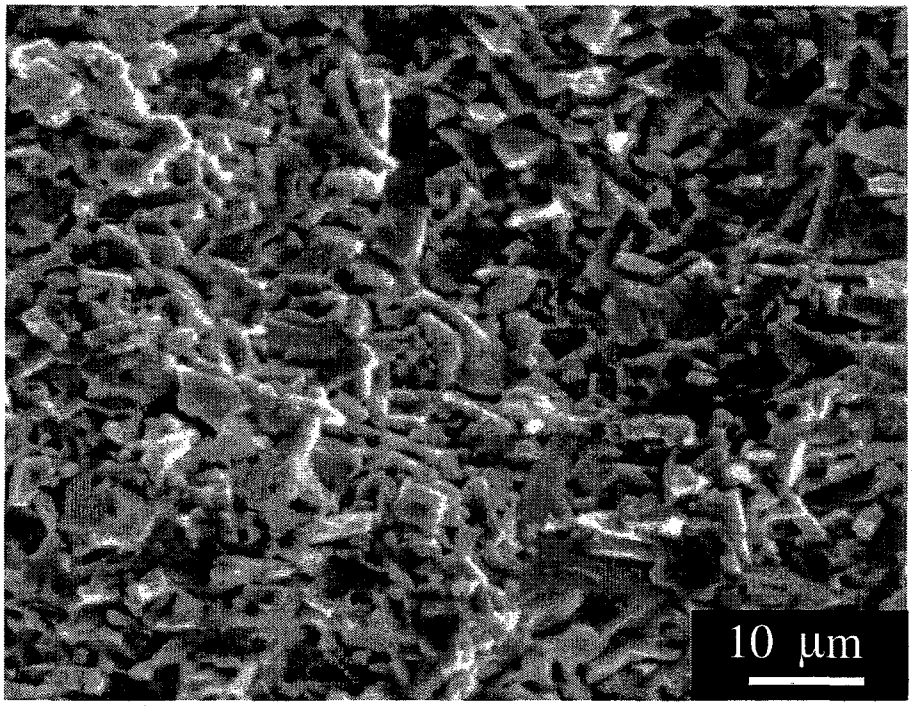

Figure 5-21: Fracture surface for sample loaded to failure at 1300°C after creep at 1200 °C and 1300 °C. The fracture mode is still predominantly intergranular.

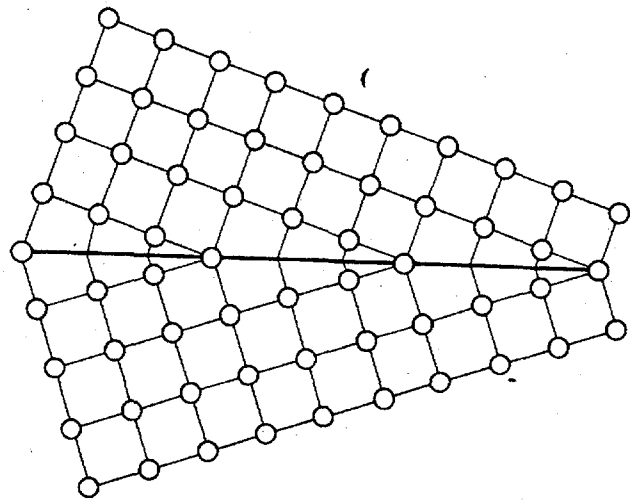

Figure 5-22: Schematic diagram of a grain boundary. This illustrates the relatively open structure at grain boundaries and interfaces compared to the grains. From *Introduction to Ceramics*, 1976.

CHAPTER 6: Controlling Creep Mechanism in ABC-SiC

6.1 Introduction

Understanding the creep mechanism(s) is critical to developing materials that are more resistant to high temperature, time dependent, deformation. For example, development of Ni-based superalloys for high temperature use resulted in present day turbines being single crystal. Since grain boundary diffusion, Coble creep, was identified as the controlling creep mechanism, which is the slowest species moving along the fastest path, the microstructure was originally modified to produce columnar grains instead of equiaxed grains.[1] The columnar grains maximized the distance for mass transport and lowered the creep rates. Finally, single crystal materials were fabricated, and this eliminated the fast diffusion path grain boundaries and yielded excellent creep response.[2]

Numerous creep studies have been conducted on SiC to ascertain the creep mechanisms. Early creep studies were performed over 30 years ago on SiC with no sintering additives.[3] Since the first studies, numerous silicon carbides have been tested for creep response: single crystal SiC,[4] CVD-SiC,[5] SiC with B_4C and C additives,[6] and SiC with Al.[7,8,9] The studies on polycrystalline SiC yielded various creep mechanisms, depending on the test temperature and stress. Table 6.1 shows the proposed creep mechanism for numerous polycrystalline SiC creep tests. Most of the previous tests concluded that diffusional creep mechanisms, either bulk or grain boundary, controlled the high temperature deformation in SiC. However, Wang[10] proposed that Harper-Dorn creep,[11] dislocation climb under saturated conditions, was a more plausible explanation for creep in the tests shown in Table 6.1. While previous creep studies on SiC provide insights about the creep mechanisms in ABC-SiC, the microstructure of ABC-SiC is

distinct from any SiC that has been tested since it possesses a grain boundary phase. In ceramics with glassy grain boundaries, such as silicon nitride, deformation is generally attributed to: solution/precipitation,[12,13] cavitation,[14,15,16,17] and viscous flow of the glass phase.[18,19,20,21,22,23,24]

While the sintering additives for the respective studies are different, all creep tests on SiC were performed on low toughness materials that typically fracture in a transgranular mode. The current creep studies on ABC-SiC are the first creep tests on a high toughness SiC. Understanding the creep mechanisms and the role of the various microstructural features provides useful insights into improving the creep resistance of high toughness ceramics, not just SiC.

The goal of this chapter is to provide an integrated analysis of the data to determine the creep mechanisms in ABC-SiC.

6.2 Experimental Procedure

The data collected for the stress dependence, n, and activation energy, E_a, were presented in Chapter 4. Similarly, the microstructure was characterized and was detailed in Chapter 5. Evaluation of the creep mechanism(s) required comparing the data from the constitutive equation, specifically n and E_a, with microsturcutural features present after creep. Comparing the data with theoretical dependencies and previous creep experiments on SiC and other ceramics allowed the controlling creep mechanism to be determined.

Material	Test Method	T (°C)	Stress (MPa)	n	E_a (kJ/mol)	Mechanism
CVD	Compress.	1300-1750	69-220	2.3-3.7	175	Glide controlled by Peierls stress or climb
Sintered	Compress.	1400-1800	138-414	1.44-1.71	338-434 (<1650°C)	Coble creep
					802-914 (>1650°C)	Nabarro-Herring creep
Sintered	Compress.	1500-1750	35-373	1.4-2.5	387-541 (<1650°C)	Diffusional creep plus glide
				1.0-1.4	838-877 (>1650°C)	
Sintered	Compress.	1620-1760	63-267	1.3-2	735-790	Nabarro-Herring creep
Sintered	Compress.	1300-1500	500-1700	1	170-300	Coble creep
Hot-Press.	Bending	1900-2200	20-200	1	305	Coble creep
Hot-Press.	Bending	1975-2100	5.7-143	1	305	Coble creep
Sintered	Bending	1000-1200	207-496	1-2	230	
Hot-Press.	Compress.	1250-1475	55-344	0.9		
	Bending	1300-1400	34.5-86.2	0.9	145	Coble creep

Table 6.1: Proposed creep mechanisms for various polycrystalline silicon carbides. After Wang.[10]

6.3 Results and Discussion

6.3.1 Stress Exponent, n

The stress exponent data, Figure 4-20, revealed that flexural creep of ABC-SiC proceeded with a linear dependence of the strain rate with increasing stress. A stress exponent of n =1 is indicative of a diffusional creep mechanism. This includes bulk diffusion,[25,26] grain boundary diffusion,[27] and solution-precipitation[28] mechanisms. An additional mechanism, which would result in a stress exponent of n = 1, is grain boundary sliding.[29] Alternatively, a stress exponent of 1 is consistent with Harper-Dorn creep.[11] The steady-state creep of most ceramic materials can be described by Norton power law behavior, Equation 6.1, as described in Chapter 4.

$$\dot{\varepsilon} = A\left(\frac{\sigma}{\sigma_o}\right)^n \exp\left(\frac{-E_a}{RT}\right) \qquad (6.1)$$

In Equation 6.1, $\dot{\varepsilon}$ is the minimum, or steady-state creep rate, A is a constant, σ is the applied stress, σ_o is a normalizing parameter (σ_o = 1 MPa), n is the stress exponent, E_a is the apparent activation energy, R is the universal gas constant, and T is the absolute temperature.

6.3.2 Activation Energy

The temperature dependence of creep for ABC-SiC was obtained by varying the temperature for a fixed outer-fiber stress. Figure 4-23 - 4-25 are plots of strain rate vs. 10^4/T. The apparent activation energy, E_a, was calculated to be ~ 225 kJ/mol for a stress of 100 MPa. For the range of stresses investigated, the activation energy appeared to be independent of the applied stress.

6.3.3 Controlling Creep Mechanism

As previously detailed, a stress exponent of n = 1 is indicative of deformation involving a diffusional process or grain boundary sliding accommodated by either viscous flow or cavitation at triple points or grain boundaries. An additional mechanism that must be considered for cases where n = 1 is Harper-Dorn creep, where creep is controlled by dislocation climb under saturated conditions.[11] Wang[10] proposed that for sintered and hot-pressed SiC, with a stress exponent of unity, creep proceeded in accordance with the mechanism developed by Harper and Dorn.

From the stress exponent data, dislocation glide and climb could be eliminated as the dominant deformation mechanism. Likewise, cavitation creep mechanisms, which generally exhibit $2 < n < 7$,[17] was not the controlling creep mechanism. The current tests were conducted in bending, and these values are for the tensile response. However, an average value of n is obtained in bending, and it is seems unlikely that a cavitation mechanism was dominant since the calculated n is 1 for the current experiments.

Recently, a new model was developed for the tensile creep of Si_3N_4[30] since Equation 6.1 frequently does not fit the data well. The basis of the model is redistribution of the secondary phases from multigrain junctions, where creep is governed by the effective viscosity of the secondary phase and the density of active cavities. The current data was carefully analyzed to confirm the linear dependence between strain rate and stress. The strain rates were compared by doubling and/or tripling the stress and then observing the corresponding increase in strain rates. In all ABC-SiC creep tests a linear dependence between strain rate and stress was observed. Since the overall cavity density,

both at multi-grain junctions and two-grain junctions was low, as well as n =1, creep by cavitation appears to be a parallel process in contrast to the dominant creep mechanism.

The activation energy calculated from Figure 4-24 was ~ 225 kJ/mol. This energy is much lower than the activation energy for lattice self-diffusion of Si and C in α and β SiC, which are both ~ 790 kJ/mol.[31,32] These data preclude Nabarro-Herring creep, where grain boundary sliding is accommodated by bulk diffusion, from being the dominant creep mechanism for tests conducted up to 1500°C. The presence of impurities in the SiC grains undoubtedly alters the diffusion rates and activation energy. However, it likely cannot account for a factor of 3 difference.

The activation energy in the current study, 225 kJ/mol, is very close to the 175 kJ/mol calculated for CVD-SiC, which was determined to be creep by a dislocation glide mechanism.[5] The activation energy was estimated for the formation of a double kink in a dislocation acting against the Peierls stress, and a value of 111 kJ/mol was calculated. While this is reasonably close to the 225 kJ/mol calculated for ABC-SiC, considering the rough approximation, the stress exponent in the CVD-SiC was 2.3 and extensive slip bands were observed in the microstructure. Evaluation of hundreds of grains demonstrated only one case of slip bands in ABC-SiC for tests conducted up to 1500°C. While the activation energy could be consistent with a glide mechanism, the microstructure elucidated the presence of an alternative creep mechanism.

It is difficult to get the activation energy for viscous flow of the grain boundary phase in ABC-SiC since this would require exact reproduction of the grain boundary phase in bulk, which is not practical. However, the activation energy for viscous flow from a Si_3N_4, with an amorphous grain boundary interlayer, was determined to be ~ 125

kJ/mol from 1260-1300°C and increased to ~ 300 kJ/mol between 1300-1350°C.[22] These values are obviously very dependent upon chemistry, but they show, in conjunction with the calculated activation energy for ABC-SiC, that viscous flow the grain boundary phase is a plausible creep mechanism. For a glass exhibiting Newtonian viscous flow, the stress exponent n =1 is consistent with the value calculated in the current study. However, deformation by viscous flow is necessarily a transient process, whereby removal of the glass becomes more difficult as the interlayer thickness decreases. This mechanism cannot account for the steady-state creep observed for all ABC-SiC samples tested. Since the grain boundaries did not exhibit a different thickness, relative to the applied stress axis, it appears that viscous flow of the grain boundaries played only a minimal role in the transient creep of ABC-SiC.

After creep, the microstructure exhibited evidence of solution-precipitation as cavities at two grain junctions grew into the SiC grains, Figure 5-17. The activation energy for solution-precipitation includes two components; heat of solution of the grain into the glass and the activation energy for viscosity. The activation energy for the former value has been calculated to be 333-460 kJ/mol for Si_3N_4.[33] The latter energy varies from 335-1000 kJ/mol for oxynitride glasses.[34] The activation energy for viscosity is very dependent on chemistry, but it can be assumed that this range of energies would be similar to those encountered for the interlayer in ABC-SiC. Given the high degree of covalent bonding in SiC it is unlikely that the heat of solution could be much lower than that of Si_3N_4. Therefore, it appears that the activation energy for a solution/precipitation creep mechanism in SiC is greater than 500 kJ/mol. Again, this is more than double the

calculated activation energy for ABC-SiC. While a solution/precipation process is clearly present in ABC-SiC, this was not the controlling creep mechanism.

The assertion of Wang[10] that creep in hot-pressed and sintered SiC proceeded by a dislocation mechanism, consistent with the model developed by Harper and Dorn,[11] was predicated on the formation of extensive dislocation substructures in these materials.[6] It should be noted that the authors in these studies attributed deformation to Coble creep based on stress exponent and activation energy data. Since Harper-Dorn creep involves the formation of extensive dislocation substructures, it does not appear to be the controlling creep mechanism in ABC-SiC. While dislocations were present in ABC-SiC, the density was low for every test condition and there was little evidence of slip bands or dislocation climb.

An additional mechanism with a stress exponent of unity is creep by grain boundary diffusion, or Coble creep. The activation energy for grain boundary diffusion was calculated for high purity SiC to be 563 kJ/mol[35] and 322 kJ/mol[36] for C and Si, respectively. The activation energy for ABC-SiC is similar to other polycrystalline silicon carbides where creep was attributed to Coble creep, see Table 6.1. The activation energies typically ranged from 170-300 kJ/mol for SiC when Coble creep was identified as the controlling creep mechanism.[37] One test showed an activation energy as high as 400 kJ/mol for Coble creep.[6] However, all of these values were calculated for SiC without an amorphous grain boundary phase. Thus, it is not possible to directly compare published values with the data for ABC-SiC. However, these values provide and indication of the activation energy for disordered regions. The activation energy of ~ 225 kJ/mol calculated for ABC-SiC is significantly lower than the activation energy for bulk

diffusion and solution-precipitation, as previously discussed. Therefore, given n =1 and an activation energy similar to grain boundary diffusion, it is concluded that grain boundary sliding, accommodated by grain boundary diffusion, is the controlling creep mechanism in ABC-SiC.

The mechanism for ABC-SiC creep is slightly different than grain boundary diffusion as described by Coble.[27] ABC-SiC has a grain boundary interlayer present between all grains, hence it is necessary to discuss interfaces as opposed to grain boundaries. The devitrification of the glassy interlayer likely limits the mobility of diffusing species through the grain boundary phase. Therefore, the most likely diffusion path is along the interlayer/SiC interface. This process is illustrated schematically in Figure 6-1. This region is characterized as an area of disorder since the grain boundary appeared to crystallize coherently on one SiC grain; thus, the opposite interface is incoherent, see Chapter 5. Interfaces, like grain boundaries, are high diffusivity paths since the structure is more open due to disorder.

6.3.4 General Creep Mechanisms

While Coble creep appears to be the controlling creep mechanism, more than one creep process was present. The most likely scenario is that grain boundary diffusion was occurring, in conjunction with solution-precipitation and dislocation formation, to accommodate grain boundary sliding at regions of high stress. These various mechanisms occurred in parallel, with interface diffusion being the controlling mechanism.

When more than one creep mechanism is present the processes may occur in parallel or in series. The former represents the case where the creep processes occur simultaneously and independently. Therefore, the total strain rate is a sum of all the individual rates. An example is Coble and Nabarro-Herring creep occuring at the same time. For the latter case, the slowest process dominates the total strain rate, but not necessarily the creep strain.[6] If grain boundary sliding occurs and is accommodated by diffusion, these two processes are in series. One cannot happen without the other and creep is a sequential process.

The cavities that formed during creep are clear evidence that a solution-precipitation mechanism is operating in addition to Coble creep. Evaluation of activation energies can elucidate if the mechanisms are operating in parallel or sequentially. For a parallel process the activation energy will change from a low value to a high value as the temperature is increased. By contrast, the activation energy decreases with increasing temperature if sequential processes are governing creep. For the temperature and stress utilized for ABC-SiC, no change in the activation energy was observed as the temperature increased. However, the most probable mechanism is grain boundary sliding being accommodated by grain boundary diffusion and cavitation, with the two processes acting in parallel. The caviation occurs by a solution-precipitation process, which involves local diffusion to accommodate grain boundary sliding. Cavity formation can occur by solution-precipitation, dilation and subsequent transport of multi-grain junction material, or formation of triple-point folds. This is contrasted with solution-precipitation creep where the material is transported through the glass and precipitated at a low stress region remote from the cavity. However, this diffusional process is independent of the

long range grain boundary diffusion associated with grain shape changes that accommodates grain boundary sliding.

Despite having a higher theoretical activation energy, it is likely that Nabarro-Herring creep is also occurring simultaneously, albeit in a minimal capacity. This process would become more prominent as the temperature is increased since bulk diffusion has a much higher diffusion volume than grain boundary diffusion once the temperature is sufficiently high to activate this mechanism. This was not confirmed for ABC-SiC, but this has been demonstrated for sintered SiC.[6,38] At temperatures less than 1650°C Coble creep accounted for 75-94% of the steady-state creep, while Nabarro-Herring creep contributed 6-25% of the creep. However, Nabarro-Herring creep became prominent above this temperature. The creep tests conducted on ABC-SiC were only up to 1500°C so no change in the activation energy was observed, but a similar transition to Nabarro-Herring creep is anticipated for ABC-SiC at a temperature above 1500°C. Therefore, the constitutive equation describing creep in ABC-SiC is provided in Equation 6.2.

$$\dot{\varepsilon} = A_C\left(\frac{b}{d}\right)^3\left(\frac{\sigma}{\sigma_o}\right)^1 \exp\left(\frac{-225\,kJ/mol}{RT}\right)$$

$$+ A_{N-H}\left(\frac{b}{d}\right)^2\left(\frac{\sigma}{\sigma_o}\right)^1 \exp\left(\frac{-790\,kJ/mol}{RT}\right)$$

$$+ A_{cav}\left(\frac{b}{d}\right)^2\left(\frac{\sigma}{\sigma_o}\right)^{2-7} \exp\left(\frac{-\sim 1000\,kJ/mol}{RT}\right) \qquad (6.2)$$

The subscripts C, N-H, and cav, correspond to Coble creep, Nabarro-Herring creep, and cavitation by solution-precipitation, respectively.

6.3.5 Methods for Improving Creep Resistance in ABC-SiC

Improving the high temperature properties of ceramics possessing a grain boundary phase has generally followed two approaches. The first approach is to modify the grain boundary interlayer. The underlying assumption for this method is that the properties of these ceramics are dictated by the properties of the glass that is present at the grain boundaries from liquid phase sintering. The pertinent glass properties include the amount, chemistry, viscosity, and crystalline nature of the interlayer.

Decreasing the amount of additives reduces the thickness of the grain boundary glass and thus reduces the diffusive flux. One of the most effective methods for improving creep resistance is to improve the refractoriness of the glass. For example, changing the additives to produce a microstructure where the resultant glass has a higher melting temperature will improve the strength and creep resistance at high temperature.[39] Changing the chemistry alters the viscosity of the grain boundary phase. Since deformation mechanisms such as solution-precipitation require diffusion through the glass, increasing the viscosity lowers the diffusivity and improves the creep response. In silicon nitride, elimination of only 2 wt% Al_2O_3 dramatically reduced the creep rates.[40] In the limiting case of no additives, the creep rates in silicon nitride and silicon carbide are very low.[3,41] Crystallization effectively hardens the grain boundary phase and this also improves the high temperature properties. The common theme in these methods is increasing the viscosity, which hardens the grain boundary phase, and minimizes grain boundary sliding and lowers diffusion rates.

An alternative approach to improving the creep properties is to incorporate second-phase reinforcing ceramics. Second-phase particles such as whiskers, fibers, and

platelets failed to show improved creep response since high temperature deformation was still dominated by the intergranular glass.[42] However, incorporating nano-phase SiC particles in Si_3N_4 demonstrated improved high temperature strength and creep resistance.[42,43] The presence of SiC particles at the grain boundaries, where SiC and Si_3N_4 are directly bonded without an interlayer,[44] is believed to minimize grain boundary sliding; hence, improved high temperature strength and creep resistance was observed.

6.4 Conclusions

Creep studies, in four-point bending were performed on SiC sintered with Al, B, and C (ABC-SiC). This material exhibited a stress exponent of n =1 in the temperature range of 1100-1500°C for stresses from 50 to 200 MPa. The corresponding temperature dependence revealed an apparent activation energy of ~ 225 kJ/mol for the above temperature range. After creep, the microstructure was characterized by a low density of cavities and dislocations. The amorphous grain boundary layer devitrified during the long exposure at these elevated temperatures. Evaluation of the stress and temperature dependence, in conjunction with the microstructural changes, revealed the controlling creep mechanism to be grain boundary sliding accommodated by diffusion along the grain boundary interlayer/SiC interface. Parallel mechanisms of solution-precipitation and cavitation were also operative in ABC-SiC for the temperature range that was examined.

6.5 References

[1] R. W. Hertzberg, "Deformation and Fracture Mechanics of Engineering Materials," John Wiley & Sons, New York, 3rd Edition (1989).

[2] P. Lukas, J. Cadek, V. Sustek, and L. Kunz, "Creep of CMSX-4 Single Crystalas of Different Orientations in Tension and Compression," *Mat. Sci. Engr.* **A208** 149-57 (1996).

[3] P. L. Farnsworth and R. L. Coble, "Deformation Behavior of Dense Polycrystalline SiC," *J. Am. Ceram. Soc.*, **49** [5] 264-68 (1966).

[4] G. S. Corman, "Creep of 6H α-Silicon Carbide Single Crystals," *J. Am. Ceram. Soc.*, **75** [12] 3421-24 (1992).

[5] C. H. Carter, Jr., R. F. Davis, and J. Bentley, "Kinetics and Mechanisms of High Temperature Creep in Silicon Carbide: II, Chemically Vapor Deposited," *J. Am. Ceram. Soc.*, **67** [11] 732-40 (1984).

[6] J. E. Lane, C.H. Carter, and R. F. Davis, "Kinetics and Mechanisms of High Temperature Creep in Silicon Carbide: III, Sintered α-Silicon Carbide," *J. Am. Ceram. Soc.*, **71** [4] 281-95 (1988).

[7] G. Grathwohl and T. H. Reets, "Creep of Hot-Pressed and Sintered SiC with different Sintering Additives," *Sci. Ceram.*, **11**, 425-31 (1981).

[8] R. Moussa, J. L. Chermant, and F. Osterstock, "Creep and Creep Rupture of HP-SiC Containing an Amorphous Intergranular Phase";pp. 617-630 in Materials Science Research, Vol. 18, Deformation of Ceramic Materials II. Edited by R. E. Tressler and R. C. Bradt. Plenum Press, New York, 1984.

[9] J. L. Chermant and F. Osterstock, "Creep Behavior of SiC-Al Materials," *Mater. Sci. Eng.*, **71** 147-58 (1985).

[10] J. N. Wang, "Newtonian Flow Process in Polycrystalline Silicon Carbides: Diffusional Creep or Harper-Dorn Creep?" *J. Mat. Sci.*, **29** 6139-46 (1994).

[11] J. Harper and J. E. Dorn, "Viscous Creep of Aluminum Near its Melting Temperature," *Acta Metall.*, **5**, 654-65 (1957).

[12] G.M. Pharr and M.F. Ashby, "On Creep Enhanced by a Liquid Phase," *Acta Metall.*,**31**, 129-38 (1983).

[13] R. Raj, "Creep in Polycrystalline Aggregates by Matter Transport Through a Liquid Phase," *J. Geophys. Res.*, **87**, 4731-39 (1982).

[14] J.-L. Ding, K. C. Liu, K. L. More, and C. R. Brinkman, "Creep and Creep Rupture of an Advanced Silicon Nitride Ceramic," *J. Am. Ceram. Soc.*, **77** [4] 867-74 (1994).

[15] M. N. Menon, H. T. Fang, D. C. Wu, M. G. Jenkins, M. K. Ferber, K. L. More, C. R. Hubbard, and T. A. Nolan, "Creep and Stress Rupture Behavior of an Advanced Silicon Nitride: Part I, Experimental Observations," *J. Am. Ceram. Soc.*, **77** [5] 1217-27 (1994).

[16] M. N. Meno, H. T. Fang, D. C. Wu, M. G. Jenkins, and M. K. Ferber, "Creep and Stress Rupture Behavior of an Advanced Silicon Nitride: Part II, Creep Rate Behavior," *J. Am. Ceram. Soc.*, **77** [5] 1228-34 (1994).

[17] W. E. Luecke, S. M. Wiederhorn, B. J. Hockey, R. F. Drause, Jr., and G.G. Long, "Cavitation Contributes Substantially to Tensile Creep in Silicon Nitride," *J. Am. Ceram. Soc.*, **78** [8] 1085-96 (1995).

[18] D.C. Drucker, "Engineering and Continuum Aspects of Hight-Strength Materials," pp. 795-833 in *High Strength Materials*. Edited by V.F. Zackay. Wiely, New York, 1965.

[19] J.R. Dryden, D. Kucerovshy, D.S. Wilkinson, and D.F. Watt, "Creep Deformation Due to a Viscous Grain Boundary Phase," *Acta Metall.*,**37**, 2007-15 (1989).

[20] M. M. Chadwick, D. S. Wilkinson, and J. R. Dryden, "Creep Due to a Non-Newtonian Grain Boundary Phase," *J. Am. Ceram. Soc.*, **75** [9] 2327-34 (1992).

[21] M. M. Chadwick, R. S. Jupp, and D. S. Wilkinson, "Creep Behavior of a Sintered Silicon Nitride," *J. Am. Ceram. Soc.*, **76** [2] 385-96 (1993).

[22] C. J. Gasdaska, "Tensile Creep in an in Situ Reinforced Silicon Nitride," *J. Am. Ceram. Soc.*, **77** [9] 2408-18 (1994).

[23] J. R. Dryden and D. S. Wilkinson, "Three-Dimensional Analysis of the Creep Due to a Viscous Grain Boundary Phase," *Acta Mater.*, **45** [3] 1259-73 (1997).

[24] Q. Jin, X. -G. Ning, D. S. Wilkinson, and G. C. Weatherly, "Redistribution of a Grain-Boundary Glass Phase during Creep of Silicon Nitride Cermaics," *J. Am. Ceram. Soc.*, **80** [3] 685-91 (1997).

[25] F.R.N. Nabarro, "Deformation of Crystals by the Motion of Single Ions," pp. 75-90 in *Report of a Conference on Strength of Solids* (H.H. Wills Physical Laboratory, University of Bristol, July 7-9, 1947). Physical Society, London, U.K., 1948.

[26] C. Herring, "Diffusional Viscosity of a Polycrystalline Solid," *J. Appl. Phys.*, **21**, 437-45 (1950).

[27] R.L. Coble, "A Model for Boundary Diffusion Controlled Creep in Polycrystalline Materials," *J. Appl. Phys.*, **34** [6], 1679-82 (1963).

[28] R. Raj and C. K. Chyung, "Solution-Precipitation Cree in Glass Ceramics," *Acta Metall.*,**29**, 159-66 (1981).

[29] W.R. Cannon and T.G. Langdon, "Review: Creep of Ceramics," *J. Mat. Sci.*, **18** 1-50 (1983).

[30] W. E. Luecke and S. M. Wiederhorn, "A New Model for Tensile Creep of Silicon Nitride," *J. Am. Ceram. Soc.*, **82** [10] 2769-78 (1999).

[31] J. D. Hong and R. F. Davis, "Self-Diffusion of Carbon-14 in High Purity and N-Doped α-SiC Single Crystals," *J. Am. Ceram. Soc.*, **63** [9-10] 546-52 (1980).

[32] J. D. Hong, D. E. Newberry, and R. F. Davis, "Self-Diffusion of ^{30}Si in α-SiC Single Crystals," *J. Mat. Sci.*, **16** [12] 2485-94 (1981).

[33] R. Raj and P. E. D. Morgan, "Acitvation Energies for Densification, Creep, and Grain-Boundary Sliding in Nitrogen Ceramics," *J. Am. Ceram. Soc.*, **64** [10] C-143-C-145 (1981).

[34] T. Rouxel, J.-L. Besson, C. Gault, P. Goursat, M. Leigh, and S. Hampshire, *J. Mater. Sci. Lett.* **8** 1158 (1989).

[35] M. Hon and R. F. Davis, " Self-Diffusion of ^{14}C in Polycrystalline β-SiC," *J. Mat. Sci.*, **14** [12] 2411-21 (1979).

[36] R. N. Ghoshtagore and R. L. Coble, *Phys. Rev.* NEED MORE INFO

[37] A. Djemel, J. Cadoz, and J. Philibert, "Deformation of Polycrystalline α SiC," pp. 381-94 in Creep and Fracture of Engineering Materials and Structures. Edited by B. Wilshire and D. R. J. Owen. Pineridge Press, Swansea, U.K., 1981.

[38] R. D. Nixon and R. F. Davis, "Diffusion-Accommodated Grain Boundary Sliding and Dislocation Glide in the Creep of Sintered Alpha Silicon Carbide," *J. Am. Ceram. Soc.*, **75** [7] 1786-95 (1992).

[39] M. K. Cinibulk, G. Thomas, and S. M. Johnson, "Strength and Creep Behavior of Rare-Earth Disilicate-Silicon Nitride Ceramics," *J. Am. Ceram. Soc.*, **75** [8] 2050-62 (1992).

[40] A. Rendtel, H. Hubner, and C. Schubert, "Improvements in the Creep Strength of HPSN by Optimization of Additive Content and Thermal Treatment," *Key Eng. Mater.*, **89-91**, 593-98 (1994).

[41] I. Tanaka and G. Pexxotti, "Delayed-Failure Resistance of High-Purity Si_3N_4 at 1400°C," *J. Am. Ceram. Soc.*, **75** [4] 1023-25 (1992).

[42] A. Rendtel, H. Hubner, M. Herrmann, and C. Schubert, "Silicon Nitride/Silicon Carbide Nanocomposites Materials: II, Hot Strength, Creep, and Oxidation Resistance," *J. Am. Ceram. Soc.*, **81** [5] 1109-20 (1998).

[43] K. Niihara, K. Izaki, and T. Kawakami, "Hot-Pressed Si_3N_4-32% SiC Nanocomposite," *J. Mater. Sci. Lett.*, **9**, 598-99 (1990).

[44] D. -S. Cheong, K. -T. Hwang, and C. -S. Kim, "High-Temperature Strength and Microstructural Analysis in Si_3N_4/20-vol%-SiC Nanocomposites," *J. Am. Ceram. Soc.*, **82** [4] 981-86 (1999).

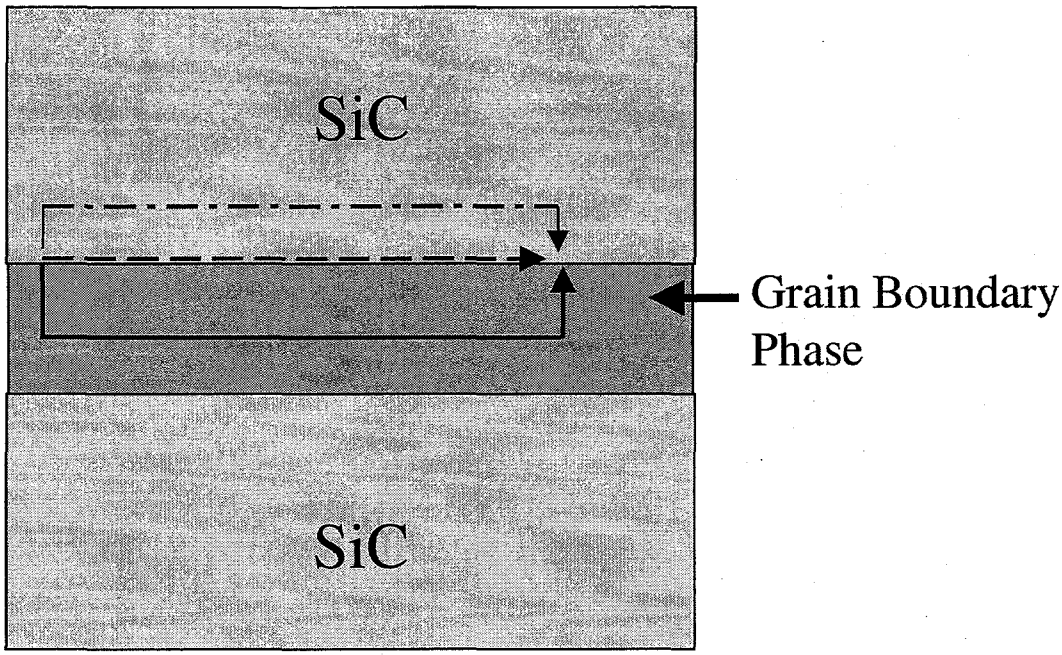

Figure 6-1: Schematic diagram of two SiC grain separated by a grain boundary interlayer. There are three possible paths for mass transport in the above configuration provided no surfaces or defects are present. The dashed line with short and long segments shows bulk diffusion. The solid line illustrates a solution-precipitation process where diffusion occurs through the grain boundary glass. The final diffusion path is along the glass/SiC interface, as shown by a dashed line.

CHAPTER 7: Conclusions

The high temperature properties of SiC, sintered with Al, B, and C, were investigated, ABC-SiC. This is a high strength, high toughness, ceramic that demonstrated promising room temperature properties. Since the applications for such materials are at elevated temperatures to improve the efficiency of engines, etc., the high temperature strength, long oxidation resistance, and creep were evaluated for this material. ABC-SiC is similar to many advanced silicon nitrides since both materials contain an amorphous or crystalline grain boundary phase. However, several aspects of the microstructure are of particular interest in the current study. The elongated, plate-like, grains, which exhibit some interlocking, are anticipated to improve the creep response. Previous SiC creep experiments reported in the literature were all conducted on low toughness silicon carbides. The current study was the first to evaluate the creep response of a high strength, high toughness, silicon carbide.

7.1 High Temperature Strength

The strength of ABC-SiC initially decreased by a factor of five, from 515 MPa to 100 MPa, as the temperature was increased from room temperature to 1300°C. Subcritical crack growth, likely by cavity formation and coalescence, was introduced by grain boundary sliding. A decrease in the toughness at 1300°C resulted in only a minimal amount of the strength degradation. Grain boundary sliding was enhanced at high temperature since softening of the grain boundary phase occurred. The softening results from the inverse dependence of viscosity with temperature.

7.2 Effects of Annealing on High Temperature Strength

The room and high temperature strength were enhanced by annealing ABC-SiC after hot-pressing. The annealing procedure, 1500°C for 7 days, increased the room temperature strength by ~ 20%, and the strength at 1300°C increased by nearly a factor of four. Flaw healing is the most plausible explanation for such a large increase in the high temperature strength. The toughness also increased, but the magnitude cannot account for the entire increase in strength. Also, crystallization of the grain boundary phase, and subsequent viscosity increase, reduced the amount of grain boundary sliding and minimized subcritical crack growth.

7.3 Stability of ABC-SiC in Oxidizing Environments

Oxidation of ABC-SiC follows parabolic kinetics. An oxide of only ~ 2 μm thick was generated after oxidation at 1200°C for 9.5 days. The passivating scale provides excellent resistance to further attack by oxygen. This is in contrast to many advanced silicon nitrides, which exhibit dramatic compositional changes from extensive oxidation in oxygen or air atmospheres. Only small compositional changes were observed during oxidation of ABC-SiC. However, these changes were not severe and did not affect the fracture mode. Therefore, creep experiments in Ar and oxygen should only exhibit minimal differences.

7.4 Transient Creep

Primary creep in ABC-SiC proceeds by a grain boundary sliding mechanism as grains rearrange in response to the applied stress. Grains impinge as strain accumulates, and the microstructure becomes interlocked. Additional contact points are generated, and the load at each point is reduced. Therefore, the strain rate continually decreases during transient creep. Crystallization of the grain boundary interlayer minimizes the amount of strain during the primary regime.

7.5 Steady-State Creep

For the temperatures and stresses used in these creep experiments, the steady-state creep rate varied from less than 1 x 10^{-10}/s at 1200°C, 150 MPa, to 4 x 10^{-9}/s at 1500°C, 100 MPa. The creep rates measured for ABC-SiC were comparable to or better than advanced silicon nitrides and Si_3N_4/SiC nanocomposites reported in the literature. ABC-SiC creep rates were also comparable to high purity, but low toughness, silicon carbides.

The stress exponent, n, was calculated to be 1. The stress exponent was invariant over the temperatures, 1200-1500°C, and stresses, 50-200 MPa, for the creep experiments. An apparent activation energy of ~ 225 kJ/mol was calculated for ABC-SiC.

7.6 Characterization

At temperatures of 1300°C and below the microstructure showed no cavitation and dislocations in isolated grains. However, no evidence of slip bands or dislocation climb was observed. The dislocation density increased with temperature. At 1400°C,

some cavitation was apparent at multi-grain and two-grain junctions in the tensile edge. However, the density was extremely low. Even with the higher density of dislocations, evidence of slip bands, dislocation climb, or dislocation substructures were rarely observed. Cavities were seldom observed on the compressive edge of the crept beam. The grain boundary glass crystallized during the heat treatments of the creep tests. Crystallization was not a stress induced feature as samples from the unstressed region of the beam exhibited identical features to the strained sections. The Al concentration in the grain boundary phase slightly increased during the heat treatments.

7.7 Creep Mechanisms

The controlling creep mechanism for ABC-SiC was grain boundary sliding accommodated by grain boundary diffusion, or Coble creep. Diffusion in ABC-SiC likely proceeded along the SiC/grain boundary interlayer interface. Parallel mechanisms of Nabarro-Herring creep, bulk diffusion, and cavitation, by a solution-precipitation process, were also operative in ABC-SiC. These mechanism accommodate sliding and relieve regions of high stress where grain-to-grain contact was present. Dislocations were also introduced at these high stress regions.